NORTHWESTERN UNIVERSITY

Autophagy Dysfunction in Parkinson's Disease and Related Synucleinopathies

A DISSERTATION

SUBMITTED TO THE GRADUATE SCHOOL

IN PARTIAL FULFILLMENT OF THE REQUIREMENTS

for the degree

DOCTOR OF PHILOSOPHY

Field of Neuroscience

By

Caleb Pitcairn

EVANSTON, ILLINOIS

June 2023

ABSTRACT

Genetic studies have found variants in the protein-degrading autophagy-lysosomal pathway (ALP) to be among the most common risk factors for developing Parkinson's disease (PD). Macroautophagy (MA) is the arm of this pathway which delivers cytosolic components to lysosomes for degradation and is essential for neuronal health. The defining pathological protein of PD, alpha-synuclein (a-syn), has been shown to inhibit MA in cell lines and animal models, but the mechanism of inhibition is not well understood. We previously found that a-syn adversely associates with SNARE protein ykt6 and inhibits its hydrolase trafficking activity (Cuddy et al., 2019). Because ykt6 is regulated by farnesylation, this activity could be rescued by activating ykt6 with farnesyltransferase inhibitor (FTI) treatment. Ykt6 is also required for several steps in MA, and we hypothesized that a similar mechanism may explain a-syn's inhibition of autophagy. We therefore investigated autophagy phenotypes in PD patient-derived human iPSC-derived dopaminergic neurons (iPSn) carrying an endogenous multiplication in the gene encoding a-syn. Mature a-syn-overexpressing iPSn exhibited reduced MA flux and dysfunctional autophagosome-lysosome fusion when compared to CRISPR-corrected isogenic controls. This was accompanied by reduced association of ykt6 with its fusion SNARE binding partner SNAP-29 and increased farnesyltransferase enzyme. Treatment with small molecule FTI LNK-754 restored autophagy to control levels, and this rescue was found to depend on ykt6 activity. Continuing towards clinical translation, we investigated treatment with FDA-approved FTI lonafarnib and found the same effects. Methods were also optimized to explore the use of ykt6 as a treatment biomarker in human erythrocytes. Overall, this work reveals a novel mechanism for a-syn-mediated autophagy inhibition in human neurons and identifies a novel druggable target capable of accelerating the clearance of pathological protein.

ACKNOWLEGEMENTS

I would like to express my sincere gratitude to all those who have helped me throughout the completion of this dissertation.

First and foremost, I would like to thank my advisor Joe Mazzulli for his guidance, support and encouragement throughout the project. His insightful comments, scientific ideas, and suggestions have been invaluable in shaping this work, and his example has helped me become a better scientist. I am so grateful to have had a place in his lab for these years. I would also like to thank my committee members Dr. Bob Kalb, Dr. Congcong He, and Dr. Rajeshwar Awatramani for their valuable feedback and guidance throughout my graduate training.

Next, I would like to express my gratitude to all the past and current members of my lab. I will not name them all here, but each contributed to making the lab a great environment in which to work. They have encouraged me through the difficulties of research, taught me valuable skills, and shared lots of fun times with me. I would particularly like to thank my co-authors for their assistance in the research and for providing valuable feedback on the manuscript.

Additionally, I would like to acknowledge the support of Northwestern, NUIN, and the MSTP for providing the resources and facilities necessary for the successful completion of this work. Special thanks to the Movement Disorders Center (MDC) Biorepository of Northwestern and the investigators therein for collaborating to provide clinical samples for RBC analyses.

I am also grateful to my family and friends, particularly my parents and siblings, who have provided me with encouragement and motivation during the challenging times.

Finally, I would like to express my appreciation to all those who have directly or indirectly contributed to this work. Your support and assistance have been greatly appreciated.

LIST OF ABBREVIATIONS

ALP	Autophagy-lysosomal pathway
a-syn	Alpha-synuclein
Atg	Autophagy related gene
Baf	Bafilomycin
CBE	Conduritol-b-epoxide
CMA	Chaperone mediated autophagy
CRISPR	Clustered regularly interspaced short palindromic repeats
CQ	Chloroquine
CSF	Cerebrospinal fluid
DA	Dopaminergic
DAT	Dopamine transporter
DLB	Dementia with Lewy bodies
DMSO	Dimethyl sulfoxide
Dox	Doxycycline
ER	Endoplasmic reticulum
FTase	Farnesyltransferase
FTI	Farnesyltransferase inhibitor
GCase	Glucocerebrosidase
GD	Gaucher disease
HGPS	Hutchinson-Gilford progeria syndrome
iPD	Idiopathic Parkinson's disease
iPSC	Induced pluripotent stem cell
iPSn	Induced pluripotent stem cell derived neurons
LAMP-2A	Lysosomal associated membrane protein 2
LRRK2	Leucine rich repeat kinase 2
LUHMES	Lund human mesencephalic cell line
MA	Macroautophagy
MPP+	1-methyl-4-phenylpyridinium
mTORC	Mammalian target of rapamycin complex

PBMC	Peripheral blood mononuclear cell
PD	Parkinson's disease
RBC	Red blood cell
SNARE	Soluble NSF attachment protein receptor
SNc	Substantia nigra pars compacta
Syn. 3x	*SNCA* triplication
TFEB	Transcription Factor EB
Vps35	Vacuolar protein sorting 35
WT	Wild-type

TABLE OF CONTENTS

LIST OF FIGURES

CHAPTER 5

CO-AUTHORED PUBLICATIONS

CHAPTER 1: Introduction

Preface: Sections of this chapter have been adapted from a published first-author peer-reviewed review article and a first-author peer-reviewed research article:

- Pitcairn C, Wani WY, Mazzulli JR. Dysregulation of the autophagic-lysosomal pathway in Gaucher and Parkinson's disease. Neurobiol Dis. 2019 Feb;122:72-82. doi: 10.1016/j.nbd.2018.03.008. Epub 2018 Mar 14. PMID: 29550539; PMCID: PMC6138580.

- Pitcairn C, Murata N, Zalon A, Stojkovska I, Mazzulli JR. Impaired autophagic-lysosomal fusion in Parkinson's patient midbrain neurons occurs through loss of ykt6 and is rescued by farnesyltransferase inhibition. J Neurosci. 2023 Feb 13:JN-RM-0610-22. doi: 10.1523/JNEUROSCI.0610-22.2023. Epub ahead of print. PMID: 36788031.

1.1: Parkinson's disease and alpha-synuclein

Parkinson's disease (PD) is the second most common age-related neurodegenerative disorder. Its classical clinical movement symptoms – bradykinesia, resting tremor, rigidity, and postural instability – have been connected to decreased dopaminergic tone from degeneration of the substantia nigra pars compacta (SNc) (Hornykiewicz, 2006; Porritt et al., 2005). Non-motor symptoms such as reduced olfaction, autonomic dysfunction, disordered sleep, depression, and cognitive impairment also often occur early in disease (Kalia and Lang, 2015).

Degenerating regions in PD are characterized pathologically by Lewy bodies, insoluble filamentous accumulations within neurons (Baba et al., 1998). The major component of these Lewy bodies is a presynaptic protein of largely unknown function called alpha-synuclein (a-syn) (Baba et al., 1998; Spillantini et al., 1997). Other elements include structural and cytoskeletal proteins, a-syn binding proteins, and components of the ubiquitin-proteasome system (Beyer et al., 2009). a-Syn is a small acidic protein composed of three domains: an N-terminal alpha-helix that

interacts with lipids, an amyloid binding, aggregation-prone central domain known as NAC, and a C-terminal acidic tail (Emamzadeh, 2016). With this composition, a-syn either takes on a structured conformation following interaction with membrane lipids or remains unstructured in the cytosol (Pfefferkorn et al., 2012; Wang et al., 2010).

Genetics suggest that a-syn accumulation is a primary cause of parkinsonism. While approximately 90% of PD is sporadic, the 10% inherited with known mutations provides insight into its pathogenesis (Tambasco et al., 2016). After the description of a-syn in Lewy bodies, the first missense mutation in the a-syn gene *SNCA* was identified in a family with autosomal dominant PD (Polymeropoulos et al., 1997). The change, A53T, increases a-syn's aggregation propensity (Conway et al., 1998; Li et al., 2001) and alters its lipid binding properties (Wang et al., 2010). Other familial *SNCA* point mutations described since (e.g. A30P, E46K, H50Q) largely cluster around the N-terminal domain and push the pool of intracellular a-syn towards an aggregated state (Villar-Pique et al., 2016). Even without structural change, increased abundance of wild-type (WT) a-syn causes familial autosomal dominant PD. In the "Iowa Kindred," affected family members have a multiplied region of chromosome 4 that includes *SNCA*, leading to early-onset parkinsonism and dementia (Singleton et al., 2003). Age of onset and disease severity correlate with a-syn dosage. Carriers of *SNCA* triplication experience earlier onset and more severe symptoms than those with a duplication (Singleton et al., 2003; Singleton et al., 2013). Because mutations and multiplications of *SNCA* cause early onset autosomal dominant disease while familial mutations in other genes are generally recessive or late onset (Singleton et al., 2013), a-syn accumulation appears a uniquely potent cause of neurodegeneration in PD.

1.2: Lysosomal dysfunction in PD: GBA1 as a case study

Several of these other familial mutations alter protein and mitochondrial degradation, notably affecting the lysosome (Gan-Or et al., 2015). GWAS studies of idiopathic PD (iPD) have similarly found that many of the most significant risk factors connect to the protein-degrading autophagy-lysosomal pathway (ALP) (Chang et al., 2017a; Nalls et al., 2014). Dopaminergic neurons may therefore be particularly sensitive to changes in this pathway, with small alterations producing irrevocably disrupted proteostasis. Several of the notable risk genes directly reduce lysosomal function. *TMEM175*, for example, is a lysosomal potassium channel whose mutation disrupts lysosomal pH (Jinn et al., 2017), and cathepsin B is a cysteine protease that functions in lysosomes (Cavallo-Medved et al., 2011). The most common risk factor for sporadic PD is *GBA1*. This gene encodes B-glucocerebrosidase (GCase), a lysosomal hydrolase whose mutation causes the autosomal recessive lysosomal storage disease Gaucher disease (GD) (Aflaki et al., 2017). GCase hydrolyzes glucosylceramide (GluCer) to ceramide and glucose, and its deficiency causes GluCer to accumulate within lysosomes (Beutler, 1992; Murray and Jin, 1995; Willemsen et al., 1988). Peripheral accumulation of GluCer chronically activates inflammatory pathways as GluCer cannot be digested by mutant macrophages, ultimately leading to variable symptoms of hematopoietic imbalance such as hepatosplenomegaly, pancytopenia, and bone abnormalities (Dandana et al., 2016; Pandey et al., 2017). These features reflect the classical presentation of GD, but variants have been further classified according to disease severity, age-at-onset, and involvement of the nervous system. Adult-onset non-neuronopathic GD is the most common presentation and is classified as Type I. Types II and III are characterized by severe early childhood neurodegeneration and later onset ataxia with myoclonic seizures, respectively (Westbroek et al., 2011).

The connection between GD and PD was first suggested by the observations of a significant proportion of GD patients experiencing parkinsonian symptoms and a high incidence of PD in heterozygous carriers of *GBA1* mutations (Halperin et al., 2006; Neudorfer et al., 1996; Tayebi et al., 2001). Since that time, multiple genetic studies have demonstrated a strong association between mutations in *GBA1* and an increased risk for PD with aging, and mutations at this locus are now understood to be one of the most common genetic risk factors for developing disease (Clark et al., 2007; Goker-Alpan et al., 2006; Goker-Alpan et al., 2004; Sidransky et al., 2009). *GBA1* mutations are commonly analyzed on genetic screenings, and patients with PD and *GBA1* polymorphisms can be subcategorized as having "GBA1-linked parkinsonism" (GBA1-PD). GBA1-PD produces neurodegeneration in a pattern similar to iPD, but has been associated with an earlier age of onset and an increased incidence of neuropsychiatric symptoms (Migdalska-Richards and Schapira, 2016). Studies of human brain pathology have corroborated and extended this connection. Lewy bodies identical to those observed in iPD have been documented in patients with neuronopathic GD (Wong et al., 2004), suggesting that a-syn aggregation is involved in neurotoxicity of GD. Studies of iPD brain have shown that GCase expression and activity are both decreased in the SNc, and reduced GCase is associated with inclusion-bearing regions compared with unaffected brain regions (Alcalay et al., 2015; Gegg et al., 2012; Murphy et al., 2014; Murphy and Halliday, 2014). Together, this demonstrates the similarity of PD and neuronopathic GD at a pathological level, evidenced through the presence of a-syn inclusions as well as reduced GCase activity in synucleinopathy patients expressing wild-type GCase.

The loss-of-function hypothesis proposes that reduced GCase activity and GluCer substrate accumulation leads to cell death by increasing a-syn in a self-reinforcing bidirectional loop. An explanation of this model will be used to illustrate how an ALP dysfunction such as that

investigated in the following chapters may produce self-propagating disease. Our previous studies have shown that GCase depletion reduces lysosomal proteolysis and stabilizes oligomeric intermediates of a-syn in mouse neuronal culture models and patient-derived iPS neurons (Mazzulli et al., 2011). The effect on a-syn oligomers was specific to GCase depletion, since non-specific lysosomal inhibition with leupeptin increased overall a-syn without stabilizing its oligomeric form, indicating that the lysosomal dysfunction alone was not sufficient to produce the same pathology as GCase depletion. Levels of another aggregation-prone protein and lysosomal substrate, tau, were only mildly changed by GCase deficiency, further indicating the specificity of this effect. Using cell-free *in vitro* assays, GluCer was found to directly interact and stabilize soluble oligomeric intermediates of a-syn preferentially under acidic conditions similar to the lysosome (Mazzulli et al., 2011). Other studies supporting the loss-of-function view show that targeted homozygous *GBA1* knockout in mice produces a-syn oligomer aggregation, neuronopathic GD symptoms, and neurodegeneration in brain regions similar to PD (Farfel-Becker et al., 2014; Osellame et al., 2013). Similarly, chemical inhibition of wild-type GCase activity using the inhibitor conduritol-b-epoxide (CBE) increases a-syn accumulation and causes neurotoxicity in SH-SY5Y, mouse primary cortical neurons, and *in vitro* mouse models (Cleeter et al., 2013; Magalhaes et al., 2016; Manning-Boğ et al., 2009).

In addition to mutated GCase leading to loss-of-function, a-syn accumulation alone in the context of wild-type GCase can also reduce GCase activity. Our previous studies indicated that a-syn overexpression decreases maturation of wild-type GCase through the early secretory pathway, leading to a decline of activity in lysosomal enriched fractions of iPD brain (Mazzulli et al., 2011). This effect is consistent with previous observations demonstrating that a-syn inhibits protein trafficking between the ER and Golgi (Cooper et al., 2006). Aggregation of a-syn potentiates this

process, as dysfunction was observed following overexpression of A53T and WT a-syn, but not an aggregation-incompetent form of a-syn (Mazzulli et al., 2011). This suggests that GCase deficiency not only causes an increase in a-syn oligomers, but that a-syn aggregates also inhibit the trafficking of GCase to lysosomes, exacerbating the primary dysfunction. Subsequent studies have likewise verified reduced GCase activity in synucleinopathy animal models and other iPSc models (Mazzulli et al., 2016; Sardi et al., 2013).

Other studies found that a-syn did not selectively affect GCase, but also decreased the maturation and activity of multiple lysosomal hydrolases by inhibiting ER-Golgi trafficking (Mazzulli et al., 2016). Studies in patient-derived PD neurons have shown a decrease in the activity of other hydrolases including cathepsin B, β-galactosidase, and hexosaminidase. Immature (ER) forms of these enzymes were found to accumulate while a-syn aberrantly co-localized with vesicle tethering factor GM130 at fragmented Golgi structures, suggesting that a-syn decreases lysosomal activity by disrupting COPII vesicle fusion early in the secretory pathway. Significantly, accumulation of a-syn altered the staining pattern of the ER trafficking regulator Rab1a, causing it to move from its normal ER-Golgi location into a diffuse cytosolic distribution. Rab1a overexpression was sufficient to completely reverse Golgi pathology, further demonstrating that a-syn-induced lysosomal dysfunction occurs through disrupted trafficking. Overall, this suggests a-syn causes lysosomal hydrolase dysfunction by specifically disrupting trafficking through Rab1a and ER-Golgi pathways. a-Syn-induced trafficking and lysosomal dysfunction may interact with other genetic variants associated with iPD, including *GBA1* mutations, to amplify protein homeostasis imbalance and ultimately lead to Lewy body pathology observed in PD brain.

1.3: Other canonical PD mutations related to autophagic-lysosomal dysfunction

Further suggesting a contribution of autophagic-lysosomal dysfunction to PD pathophysiology, several other familial mutations converge on autophagic mechanisms. Mutations in *LRRK2* encoding leucine-rich repeat kinase 2 have been shown to cause familial PD in an autosomal dominant manner and are also common genetic risk factors for iPD (Zhang et al., 2015). While other mutations may have more straightforward connections to autophagy, we have chosen to focus on LRRK2 as a highly studied mutant that illustrates shared themes of dysregulation. One of the most common LRRK2 mutations, *G2019S* (LRRK2^{G2019S}), has been shown to inhibit chaperone-mediated autophagy in a similar manner as mutant a-syn, through impeding the uptake of substrates by LAMP-2A receptor blockade (Orenstein et al., 2013). Interestingly, LRRK2 has recently been shown to phosphorylate trafficking mediator rab10 (Steger et al., 2016), which may explain LRRK2-mediated effects on vesicular trafficking and autophagic flux (Roosen and Cookson, 2016). While rab10 is known to mediate trafficking between the trans-Golgi network and the plasma membrane, recent studies have also linked its function to autophagic degradation of lipids (Kinghorn et al., 2016). Studies using patient-derived iPS neurons found an increase in LC3 positive puncta and p62 expression by immunofluorescence in both LRRK2-PD (*LRRK2^{G2019S}*) and iPD lines compared to controls. This finding that was reinforced by electron microscopy showing an increase in autophagic vacuoles, lipid accumulation, and dilated ER in PD-derived neurons (Sanchez-Danes et al., 2012).

In addition to LRRK2, other canonical mutations have been tied to autophagic dysfunction through different mechanisms. Autosomal recessive forms of PD caused by loss-of-function PINK1 or Parkin mutations are known to impede mitochondrial turnover through mitophagy (Pickrell and Youle, 2015). *PINK1* was found to be upstream activator of *PARKIN*, a ubiquitin ligase that induces recruitment of factors targeting a mitochondrion for degradation (Geisler et al.,

2010). Studies in iPSC-derived midbrain neurons carrying the PINK1 or Parkin mutations show abnormal mitochondria and elevated oxidant stress, consistent with disrupted mitophagy (Chung et al., 2016). While much less common, several other familial PD mutations are more directly implicated in the autophagic-lysosomal pathway. ATP13A2/PARK9 is a lysosomal ATPase whose loss-of-function causes Kufor-Rakeb syndrome, characterized by early onset parkinsonism (Park et al., 2011; Ramirez et al., 2006). Deficiency in ATP132 observed in patient fibroblasts and primary cortical neurons produces an accumulation of enlarged lysosomes, reduced proteolysis, and decreased LC3 clearance, ultimately increasing a-syn aggregation and neurotoxicity (Usenovic et al., 2012). Autosomal dominant parkinsonism is also associated with mutation of vacuolar protein sorting 35 (Vps35), a component of the retromer system that participates in mediating retrograde transport of endosomes and recycling of cargoes related to the autophagic-lysosomal pathway, including LAMP-2A and soluble N-ethylmaleimide-sensitive factor attachment protein receptors (SNAREs) (Pan and Yue, 2014; Tang et al., 2015b). While its contribution to PD pathogenesis remains incompletely understood, Vps35 mutation has been shown to produce DA neurodegeneration with deficits in mitochondrial function and turnover that may relate to disrupted mitophagy (Tang et al., 2015a; Wang et al., 2016a). While these variants may not be capable of inducing pathogenesis individually, it is possible that a combination of these predisposing factors may culminate to cause autophagic-lysosomal dysfunction in PD, leading to the formation of Lewy bodies.

1.4: Macroautophagy dysfunction in PD

GCase dysfunction illustrates how a-syn accumulation can produce disease by disrupting ALP function in a self-reinforcing loop. The focus of this research is macroautophagy (MA), the

branch of the ALP responsible for degrading bulk cytoplasmic aggregates and damaged organelles (Larsen and Sulzer, 2002). Successful breakdown of MA substrates requires the completion of several distinct stages (Fig. 1-1): the formation of a two-layered autophagosome membrane around the target, closure and trafficking of the autophagosome vesicle to a lysosome, and fusion of autophagosome and lysosome membranes to intermix their contents (autolysosome fusion) (Abounit et al., 2012). Initiation and membrane growth requires a series of Atg (autophagy related) proteins and the formation of the Atg1/ULK kinase complex (Nakatogawa, 2020). Under nutrient rich conditions, active target of rapamycin complex 1 (mTORC1) phosphorylates Atg13 and ULK1 to prevent kinase activity, but inhibition of mTORC1 by starvation or pharmacologic modulation frees the ULK complex to initiate autophagosome biogenesis (Szwed et al., 2021). In the key reaction for membrane formation, MAP1LC3B is conjugated with phosphatidylethanolamine to form LC3-II from the pool of its unconjugated form LC3-I (Tanida et al., 2008). LC3-II provides a specific and distinguishable marker for autophagosomes, and autophagic flux can be evaluated by comparing the accumulation of LC3-II following lysosomal inhibitor treatment (Klionsky et al., 2021). LC3 binding proteins such as p62 are responsible for the delivery of substrates to autophagic vesicles (Komatsu et al., 2007). P62 plays a critical role in the recognition and delivery of ubiquitinated protein aggregates from the cytosol into autophagosomes, and it accumulates within ubiquitinated inclusions of autophagy-deficient mice (Komatsu et al., 2007). Accumulation of p62 is therefore also indicative of autophagic impairment.

Two related pathways for autophagy exist: chaperone-mediated autophagy (CMA) and microautophagy. CMA utilizes chaperones to selectively transfer proteins across a lysosomal membrane. In this process, Hsc70 and its co-chaperones deliver a substrate recognized by its KFERQ-like motif to the translocation complex formed by LAMP-2A (Liao et al., 2021). The

unfolded protein then moves through this multimer into the lysosomal lumen where it can be degraded by proteases (Liao et al., 2021). In microautophagy, a cytoplasmic cargo is directly engulfed by the lysosome, although the factors that mediate this process remain the least understood (Martini-Stoica et al., 2016).
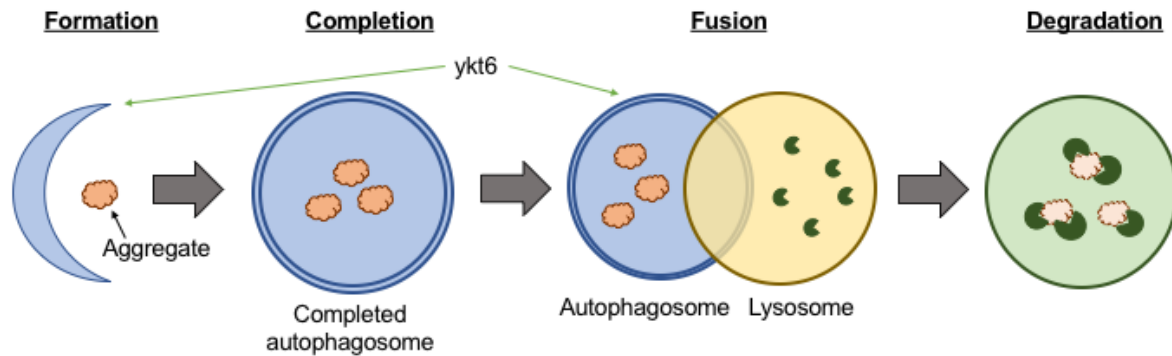
Figure 1-1: Overview of macroautophagy

Macroautophagy proceeds by distinct stages: 1. Formation of double-membraned autophagosome vesicle around a target. 2. Completion and trafficking to a lysosome. 3. Fusion of autophagosome and lysosome membranes. 4. Degradation of target components by lysosomal proteases. SNARE ykt6 is required for formation and fusion steps (Matsui et al., 2018; Nair et al., 2011).

Although clearance of physiological a-syn can occur via the proteasome or CMA, a-syn aggregates developed through transgenic overexpression have been shown to undergo degradation through macroautophagy (Cuervo et al., 2004; Ebrahimi-Fakhari et al., 2011; Tanik et al., 2013; Vogiatzi et al., 2008; Webb et al., 2003). There is also significant crosstalk between these pathways (Klucken et al., 2012; Tanik et al., 2013; Webb et al., 2003). MA's role appears vital, as post-mortem evaluation of synucleinopathy patients' midbrain neuropathology has associated increased a-syn with disrupted MA. Autophagic markers LC3-II, p62, and ULK1 protein levels are increased in SNc neurons of familial and idiopathic PD patients compared to healthy controls, along with the accumulation of incompletely degraded autophagosomes and phospho-ubiquitin that correlate

with age and Braak stage (Dehay et al., 2010; Hou et al., 2018; Mamais et al., 2018). Similarly, human mutations in essential autophagy genes such as Atg5 and Atg7 result in developmental delay and severe neurological dysfunction (Collier et al., 2021; Kim et al., 2016).

Animal studies have shown that a-syn accumulation can be induced by disruptions in autophagic-lysosomal pathways. Inhibiting autophagy in mouse neurons leads to the accumulation of ubiquitinated proteins and produces motor behavioral deficits reminiscent of PD (Friedman et al., 2012; Hara et al., 2006; Sato et al., 2018; Savitt et al., 2012). Conditional deletion of Atg7, an essential factor in autophagosome formation, increased pathogenic a-syn protein levels in neuronal processes in mice (Friedman et al., 2012). In a distinct model, deletion of Atg7 specific to midbrain DA neurons resulted in neurodegeneration with parkinsonian movement abnormalities (Savitt et al., 2012). Neuropathology analyses revealed that such autophagy-deficient DA neurons developed Lewy bodies with accumulated a-syn (Sato et al., 2018). Depleting p62 in a synucleinopathy mouse model further enhanced pathology (Tanji et al., 2015), suggesting this binder contributes to clearance of aggregated a-syn. Other mouse studies have shown that interfering with CMA can produce a-syn accumulation and midbrain neurodegeneration. Depletion of Vps35 mimicking the familial PD mutation disrupts trafficking of LAMP-2A, the receptor for CMA substrates (Tang et al., 2015b). Because a-syn was demonstrated to be degraded through CMA *in vitro* (Cuervo et al., 2004), it is possible that this mutation induces a-syn accumulation through LAMP-2A deficiency. However, Vps35 depletion likely influences multiple trafficking steps, and a-syn accumulation may occur through LAMP-2A independent mechanisms or knock-on effects disrupting connected pathways. Studies in the human brain have further suggested a connection between CMA and a-syn accumulation in PD. The levels of CMA markers are decreased in idiopathic PD brain, an effect that correlates with a-syn accumulation (Alvarez-

Erviti et al., 2010; Murphy and Halliday, 2014). Human genetics, neuropathology, and animal models thus suggest that the autophagic-lysosomal system plays an important role in the degradation of a-syn, and disruptions in this pathway may lead to synucleinopathy.

1.4: a-Syn's effects on MA

Pathologic a-syn itself has been shown to dysregulate autophagic-lysosomal activity. For example, familial-linked mutant forms of a-syn, A53T and A30P, bind with high affinity to LAMP-2A on lysosomes, but fail to translocate, competitively inhibiting a portion of CMA machinery (Cuervo et al., 2004). These a-syn mutants are also degraded at a slower rate compared to the wild-type protein (Li et al., 2004), and mutating the CMA targeting domain of mutant a-syn also impedes a-syn clearance (Xilouri et al., 2009). Dopamine-modified a-syn oligomers generated from wild-type protein can also impede substrate uptake through blocking LAMP-2A, implicating this process in idiopathic PD (Martinez-Vicente et al., 2008).

a-Syn inhibition specific to MA has been shown in cell line and animal models, although the mechanism underlying this effect has remained unclear. Neuroblastoma and primary mouse neurons demonstrate decreased MA flux following WT a-syn overexpression or treatment with preformed fibrils (Tanik et al., 2013; Winslow et al., 2010). From these studies, it was theorized that a-syn may interfere with macroautophagy through impeding the function of rab1a and Atg9, resulting in decreased autophagosome formation (Winslow et al., 2010). More recently, inhibition of autophagosome-lysosome fusion by a-syn was shown in differentiated LUHMES cell cultures (Tang et al., 2021). In rats, midbrain AAV overexpression of a-syn was found to disrupt ALP protein expression, although flux was not evaluated (Decressac et al., 2013). In another synucleinopathy mouse model, conditional overexpression of A53T in dopaminergic neurons

using the dopamine transporter promoter (DAT; DA$_{SYN53}$ mice) demonstrated mitochondrial inclusions that colocalized with the autophagic markers LC3 and p62 (Chen et al., 2015). This pathology notably appears prior to neurodegeneration of DA neurons, suggesting a causative role for neurotoxicity in these mice. Such studies indicate that a-syn can impede protein degradation through autophagy. Since the autophagic process is particularly critical for neuronal health (Komatsu et al., 2006), this suggests a potential toxic mechanism of a-syn-induced neurodegeneration.

Disrupting the potential feedback loop between a-syn and autophagic dysfunction therefore presents a promising approach to counter neurotoxicity, and activating MA indeed has produced neuroprotective effects (Decressac et al., 2013; Ogata et al., 2006; Young et al., 2009; Zhou et al., 2016). In the most relevant example, activating MA at a transcriptional level through AAV-overexpression of the autophagy "master regulator," transcription factor TFEB, rescued rat midbrain neurons from a-syn toxicity, while inhibiting it exacerbated cell death (Decressac et al., 2013). Overexpression and pharmacologic activation of TFEB similarly reduced a-syn aggregates in an a-syn overexpressing human neuroglioma cell line (Kilpatrick et al., 2015). Another pharmacologic MA activator, rapamycin, restored lysosomal clearance and prevented dopaminergic neurodegeneration in MPP+ treated mice (Dehay et al., 2010). Primary mouse neurons expressing polyglutamine repeat proteins could also be rescued by inducing MA through nutrient deprivation (Young et al., 2009). Autophagy was similarly found to protect cell lines from harmful effects of cellular stress induced by sevofluorane (Zhou et al., 2016) or ER-stressors (Ogata et al., 2006). Based on these examples, facilitating MA may be protective in cases of general neuronal stress as well as the case of a-syn.

Although we have presented evidence that pathogenic a-syn and other PD mutants have a primarily inhibitory effect on autophagic clearance because this seems to represent the most comprehensive explanatory model of recent findings, it should be noted that alternative models have been supported. For example, A53T expression has been shown to increase LC3-I to LC3-II conversion, to increase LC3+ puncta, and to reduce association of normal mitochondria with autophagosomes in SH-SY5Y cells and rat cortical neurons (Choubey et al., 2011; Xilouri et al., 2009). Such findings may suggest that autophagic activity is increased by neurotoxic a-syn conformations, potentially leading to digestion of necessary cytosolic proteins and healthy organelles, see (Xilouri et al., 2016). Similarly, LRRK2^{G2019S} expressing SH-SY5Y cells and iPSC DA neurons exhibited increases in autophagic vacuoles with neurite shortening that was reversed by knockdown of autophagy related genes or prevention of aberrant mitochondrial fission (Plowey et al., 2008; Su and Qi, 2013). Variable results therefore argue against a simple first-order induction or inhibition of autophagy in synucleinopathy, favoring instead a complex interaction between autophagy and other degradative pathways that may change as cellular stress increases. For instance, ER stress has been shown to induce autophagy at low levels while inhibiting autophagy at levels high enough to activate apoptotic pathways, likely through mTORC1-dependent feedback loops (Appenzeller-Herzog and Hall, 2012; Kapuy et al., 2014; Ogata et al., 2006). Notably, pharmacologic induction of autophagy through mTORC1 inhibition in this study increased cell survival by promoting resilience to ER stress-induced apoptosis (Kapuy et al., 2014). Thus, while it is clear that GD and PD mutations dysregulate autophagy, further investigation will be needed to resolve conflicting interpretations of the primary pathologic effect of this dysregulation.

1.6: Ykt6

Recently, Soluble NSF Attachment protein REceptor (SNARE) proteins were found to be required for the membrane fusion events that take place in MA (Wang et al., 2016b). Membrane fusion throughout cellular processes requires the mechanical force produced by an assembly of four coiled-coil domains (Daste et al., 2015). Synaptic neurotransmission illustrates the basic paradigm of SNARE assembly. In this scheme, SNARE proteins can be classified as Q-SNAREs or R-SNARES based on whether they contribute a glutamine or arginine to the final layer of the complex, or alternatively as v- (vesicle) and t- (target) SNAREs based on their location (Fig. 1-2) (Fasshauer et al., 1998). The four-coil assembly is composed of one R-SNARE coil and three Q-SNARE coils (Ossig et al., 2000). In synaptic transmission, v-SNARE VAMP2 provides the R-SNARE domain, meeting the Qa coil of cellular membrane syntaxin 1a, sandwiched between Qb and Qc domains of SNAP-25 (Fasshauer et al., 1998).

One SNARE of growing interest in the ALP is synaptobrevin-homolog ykt6, most well characterized for its role in the secretory pathway (Fukasawa et al., 2004; Liu and Barlowe, 2002; McNew et al., 1997). Maturation of synthesized proteins through the ER and Golgi requires vesicle fusion mediated by SNAREs (Hay et al., 1997), and ykt6 plays a role in late stage ER-Golgi maturation where it forms a complex with syntaxin 5, bet1, and GS28 (Fig. 1-2) (McNew et al., 1997; Zhang and Hong, 2001). However, recently ykt6 has also been shown to participate in autophagosome formation (Fig. 1-2). For a phagophore to form, Atg9-containing vesicles must translocate between cytosolic membranes and the phagophore assembly site (Mari et al., 2010). Organization of Atg9 into autophagosomes is abolished in yeast lacking SNARE proteins Sso1 and Sec9 (mammalian homologs are syntaxin 1 and SNAP-25, respectively) (Nair et al., 2011). Ykt6 was found to interact with both Sso1 and Sec9 and produce similar autophagic dysfunction

when knocked out, suggesting that these proteins form a complex required for Atg9-mediated autophagic induction (Nair et al., 2011). Ykt6 also participates in autophagosome-lysosome fusion. Knockdown of ykt6 partially reduces the number of fused autolysosomes, and concurrent knockdown of ykt6 with canonical autophagy SNARE syntaxin 17 completely prevents fusion (Matsui et al., 2018; Takáts et al., 2018). In HeLa cells, this action was found to be mediated by ykt6 binding with lysosomal SNAP-29 and syntaxin 7 (Fig. 1-2) (Matsui et al., 2018), although independent data from *Drosophila* suggest an alternative regulatory role in forming the SNAP-29 complex (Takáts et al., 2018). Together, these data highlight the critical role of ykt6 in MA and suggest that enhancing ykt6 activity may enhance ALP function. In support of this, overexpression of ykt6 can rescue a-syn-induced toxicity in yeast (Cooper et al., 2006) and cell lines (Thayanidhi et al., 2010), although the precise mechanism of rescue remains unknown. Similarly, the contribution of ykt6 to MA in human neurons has not been investigated.

Ykt6 is a neural-enriched R-SNARE of the longin family, composed of a regulatory longin domain and a coiled-coil domain, but lacking a transmembrane anchor (Tochio et al., 2001). Because of this, it has a unique form of regulation in which the protein alternates between an autoinhibited, closed conformation in the cytosol and an active, open conformation anchored in a lipid bilayer (Fig. 1-2) (Hasegawa et al., 2003). This dynamic is regulated by lipid modifications at the C-terminal CCAIM motif typical of prenylated proteins. Palmitoylation occurs at the first cysteine (C194) and is necessary for membrane anchoring (Fukasawa et al., 2004). Meanwhile, farnesylation occurs at the second cysteine (C195) and promotes the closed conformation (Fukasawa et al., 2004). When closed, the longin domain folds back on the coiled coil-domain and prevents SNARE complex participation by making interaction kinetically unfavorable (Tochio et al., 2001). The farnesyl group stabilizes this conformation inside a hydrophobic pocket formed by

the fold that also prevents the molecule from membrane insertion (Wen et al., 2010). This kind of regulation makes ykt6 well suited for a role in the cellular stress response where resources must be quickly activated (Cuddy et al., 2019).
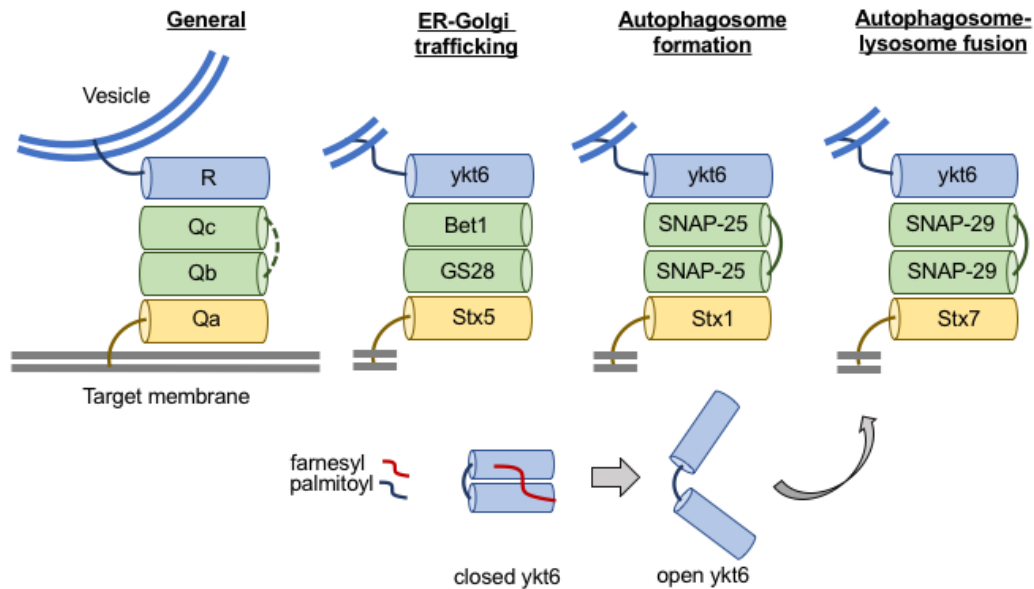
Figure 1-2: SNARE complexes formed by ykt6

Vesicular ykt6 provides the R- coil to SNARE complexes with varied intracellular roles. Farnesylation locks ykt6 into a closed cytosolic conformation while palmitoylation allows anchoring to the necessary membrane.

a-Syn has been shown to produce toxic effects by interacting with SNARE proteins. When overexpressed, pathogenic forms of a-syn can aberrantly bind to synaptic transmission SNARE synaptobrevin-2 in excess, impeding its function and preventing vesicle fusion (Burre et al., 2010; Choi et al., 2013). This was true of toxic oligomeric forms but not physiologic monomers, suggesting this function was pathologic (Choi et al., 2013). A native function of a-syn from these studies appeared to be stabilization of SNARE complexes required for neurotransmission (Burre et al., 2010). Ykt6 has striking sequence homology to synaptobrevin-2, and we recently showed

that a-syn similarly forms a complex with ykt6, but not longin family member Sec22b (Cuddy et al., 2019). This association sequestered ykt6 in its inactive pool away from membranes and reduced participation in SNARE complexes with ER-Golgi trafficking SNAREs bet1 and stx5 (Cuddy et al., 2019). Reduction of ykt6 produced lysosomal and trafficking defects mimicking those observed in PD neurons, but activation rescued diseased neurons from these effects (Cuddy et al., 2019). Given this association and ykt6's other roles in autophagy, a-syn may impede ykt6 function in MA as well, yet no previous work has investigated this question.

In that study, we found that inhibition of farnesylation by small molecule treatment could beneficially increase ykt6 activity. Such farnesylation in mammals is handled by a single enzyme, farnesyltransferase (FTase) (Adjei et al., 2000). Farnesyltransferase inhibitors (FTIs) were first developed to target Ras-driven transformation and proliferation in cancer, but were ultimately found to be ineffective (Wang et al., 2017). One however, lonafarnib, has been repurposed and approved for use in the childhood premature aging disease Hutchinson-Gilford progeria syndrome (HGPS), exerting effects through lamin rather than Ras (Dhillon, 2021). This provides an example of how repurposing an existing drug for a novel target is viable, and we believe ykt6 may also be targeted by FTIs for translation to PD.

1.7: Dissertation overview

Development of disease-modifying therapies for PD will require a deeper understanding of how wild-type a-syn disrupts endogenous protein degradation pathways to ultimately destabilize proteostasis. Intervening in this process could prevent or reverse intracellular protein aggregation and neurodegeneration. While inhibition of autophagy by a-syn has been documented in cell lines and animal models, it has not been shown in human neurons that chronically accumulate WT a-syn, nor has the mechanism of inhibition been established. Because ykt6 is required for successful

autophagy (Matsui et al., 2018; Nair et al., 2011; Takáts et al., 2018) and we found that a-syn inhibits ykt6 trafficking activity (Cuddy et al., 2019), we hypothesized that a similar mechanism might explain a-syn's disruption of MA. If true, then dysfunction could be rescued by activating ykt6 with existing FTIs. To test this hypothesis, we characterized autophagy and ykt6 function in dopaminergic neurons derived from iPSCs (iPSn) of *SNCA* triplication carriers. We then investigated the effects of treatment with FTIs.

In Chapter 2, we describe the phenotype of autophagy dysfunction found in *SNCA* triplication iPSn. When compared to isogenic CRISPR-corrected controls, these cells exhibit reduced autophagy flux with indications of disrupted autolysosome fusion. This was accompanied by reduced ykt6-SNAP-29 SNARE complexes and increased FTase enzyme. Overall, these findings suggest that a-syn inhibits autophagy by reducing ykt6 participation in SNARE complexes required for autolysosome fusion.

In Chapter 3, we describe rescue of this phenotype using FTI LNK-754. This treatment restored LC3-II flux in patient iPSn as well as ykt6 complex formation. Rescue was found to be dependent on ykt6 activity, substantiating the mechanistic findings of Chapter 2.

In Chapter 4, we describe two developments of basic ykt6 findings that may promote clinical translation. First, lonafarnib, an FDA-approved FTI used in progeria, was found to produce similar effects on ykt6 activity and rescued LC3-II flux in patient iPSn. Then, we examined ykt6 membrane localization in red blood cells (RBCs) as a potential biomarker for PD progression and FTI titration. We found that LNK-754 produced a shift in mouse RBCs but observed no difference between PD patients and healthy controls. Further work may pursue either of these directions for clinical use of ykt6 as a target.

Chapter 5 summarizes these findings and expands on their significance considering other literature. Directions for future study and the limitations of the current work are also discussed.

The data in Chapters 2 and 3 are adapted from my original research manuscript: Pitcairn C, Murata N, Zalon A, Stojkovska I, Mazzulli JR. Impaired autophagic-lysosomal fusion in Parkinson's patient midbrain neurons occurs through loss of ykt6 and is rescued by farnesyltransferase inhibition. J Neurosci. 2023 Feb 13:JN-RM-0610-22. doi: 10.1523/JNEUROSCI.0610-22.2023. Epub ahead of print. PMID: 36788031. The introduction to Chapter 3 has been added, and other introduction and discussion sections have been edited and/or expanded to fit the context of this dissertation. Extended data figures are included in the main body of the text with their associated main figures. Chapter 4 is wholly composed of unpublished data.

Contributions

C. Pitcairn designed and analyzed all experiments in the main body of this dissertation. He performed all experiments except Fig. 2-2A, B and Fig. 2-3A. He wrote the original drafts of all the text that appears here. M. Murata took the images that appear in Fig. 2-2A and B. A. Zalon performed the western blot appearing in Fig. 2-5A. I. Stojkovska prepared the EM images that appear in Fig. 2-5E. J.R. Mazzulli mentored in designing and interpreting experiments, and he edited and contributed to the text.

Many investigators contributed to the design and implementation of the MDC Biorepository and/or provided data and collected biospecimens but did not participate in the analysis or writing of this report. MDC Biorepository investigators include Tanya Simuni, MD; Dimitri Krainc, MD PhD; Opal Puneet MD, PhD; Cindy Zadikoff, MD; Onur Melen, MD; Danny Bega, MD; Roneil G. Malkani, MD; Steven Lubbe, PhD; Niccolo Mencacci, MD, PhD; Christina

Zelano, PhD; Joanna Blackburn, MD; Firas Wehbe, MD, PhD; Lisa Kinsley, MS, CGC; Tina

Ward, MS.

CHAPTER 2: a-Syn disrupts autophagy at autolysosome fusion by reducing SNARE

complexes in PD neurons

OVERVIEW

Autophagy is essential for the maintenance of neuronal health, since inhibiting autophagy in mouse neurons leads to the accumulation of ubiquitinated protein aggregates and motor behavioral deficits reminiscent of PD (Friedman et al., 2012; Hara et al., 2006; Sato et al., 2018; Savitt et al., 2012). Similar accumulation of autophagy markers is observed in post mortem neuropathology of synucleinopathy patients (Dehay et al., 2010; Hou et al., 2018; Mamais et al., 2018), and genetic mutations in autophagy genes produce severe developmental delay (Collier et al., 2021; Kim et al., 2016). Autophagy is perturbed by a-syn overexpression in cell lines and animal models, but the mechanism underlying this effect is not completely understood (Decressac et al., 2013; Tang et al., 2021; Tanik et al., 2013; Winslow et al., 2010). Transgenic mice expressing human A53T mutant a-syn in dopaminergic neurons display autophagic defects preceding neurodegeneration (Chen et al., 2015), suggesting a causative role in toxicity. Collectively, such data indicate that autophagy is indispensable for neurons and may play a role in PD pathogenesis, but its relationship to Lewy body formation and neurodegeneration remains unknown. Furthermore, autophagic function in PD patient midbrain models that accumulate endogenously expressed a-syn in an age-dependent chronic manner has not been investigated thoroughly.

Membrane fusion events throughout autophagy require SNARE proteins (Wang et al., 2016b), and recent studies have indicated an important role for synaptobrevin-homolog ykt6. Ykt6 is critical for endoplasmic reticulum (ER)-Golgi trafficking (Fukasawa et al., 2004; Liu and

Barlowe, 2002; McNew et al., 1997), but also interacts with essential autophagy SNAREs to promote autophagosome assembly (Mari et al., 2010; Nair et al., 2011). Late in the autophagic process, ykt6 can mediate the final fusion step with lysosomes by interaction with SNAP-29 and syntaxin 7 (Matsui et al., 2018; Takáts et al., 2018). In this formation, ykt6 is present on the autophagosome and contributes the R-SNARE coil, syntaxin 7 is present on the lysosome and contributes Qa, and SNAP-29 is unlocalized before contributing Qb and Qc (Matsui et al., 2018). Studies in cell lines have shown that syntaxin 17 can independently mediate autophagosome-lysosome fusion in the absence of ykt6, suggesting functional redundancy (Matsui et al., 2018). However, it is unknown if such redundant pathways exist in human neurons and if ykt6 is required for autophagy.

We previously showed that neuronal ykt6 is essential for lysosomal function and that a-syn accumulation in PD patient neurons disrupted trafficking by promoting an auto-inhibited, closed conformation of ykt6 in the cytosol (Cuddy et al., 2019). We hypothesized that this inhibition may also explain a-syn's disruptive effects on autophagy. Therefore, we set out to characterize autophagy for the first time in long-lived *SNCA* triplication midbrain neurons and to assess the function of ykt6. Because of ykt6's dual role, particularly we wanted to distinguish between effects attributable to dysfunction at autophagosome formation versus those at autolysosome fusion. The results of this investigation are presented in Chapter 2. Here, we find that ykt6 is critical for autophagosome-lysosome fusion and is disrupted in PD midbrain neurons. Our data thus indicate that ykt6 controls autophagy by simultaneous coordination of hydrolase trafficking and autophagic-lysosomal fusion.

RESULTS

2.1: Accumulation of wild-type a-syn reduces autophagy flux through impeding autolysosome fusion

To assess autophagy phenotypes in PD patient iPSC-derived midbrain neurons (iPSn), we employed iPSC lines from three different members of the Iowa kindred carrying an *SNCA* triplication and their corresponding isogenic CRISPR-corrected controls as previously described (Stojkovska et al., 2022). These lines differentiate with appropriate midbrain and maturity markers by day 60 and exhibit accumulation of pathogenic insoluble synuclein by day 90 (Mazzulli et al., 2016) (Stojkovska et al., 2022). Autophagic flux was assessed by quantifying LC3-II protein levels in response to an autolysosomal inhibitor chloroquine (CQ) with treatment conditions determined to be non-toxic (Fig. 2-2A). While analysis of day 60 cultures showed no difference (Fig. 2-1A), day 90 iPSn from each triplication carrier showed a ~50% reduction in autophagic flux compared to their isogenic corrected controls and a healthy control line previously published as "2131" (Fig. 2-1B) (Mazzulli et al., 2016). These results were replicated in differentiated SH-SY5Y cells that overexpress a-syn (Fig. 2-2B) (Cuddy et al., 2019). P62/SQSTM1 is a linker between LC3 and ubiquitinated MA substrates that is constantly degraded by MA (Abounit et al., 2012). Although both soluble and insoluble p62 levels increased upon CQ treatment in isogenic control iPSn as expected, *SNCA* triplication lines PD iPSn showed no response to CQ (Fig. 2-1C; Fig. 2-2C). RNA expression of LC3 was increased and p62 unchanged in PD iPSn, suggesting that perturbations in autophagic flux do not occur from decreased transcriptional response (Fig. 2-1D). This is consistent with elevated protein levels of both LC3-II and p62 in untreated (CQ–) PD iPSn (Fig. 2-1E), suggesting a late-stage blockade in autophagy. To assess the effect of a-syn accumulation on autophagy *in vivo*, we measured LC3-II protein in post-mortem cortical samples from patients diagnosed with Dementia with Lewy bodies (DLB). We found that LC3-II was elevated along with

a-syn, similar to our observations in PD iPSn (Fig. 2-1F). These data suggest that a-syn inhibits autophagic flux through post-transcriptional mechanisms at a stage beyond LC3 or autophagosome synthesis.
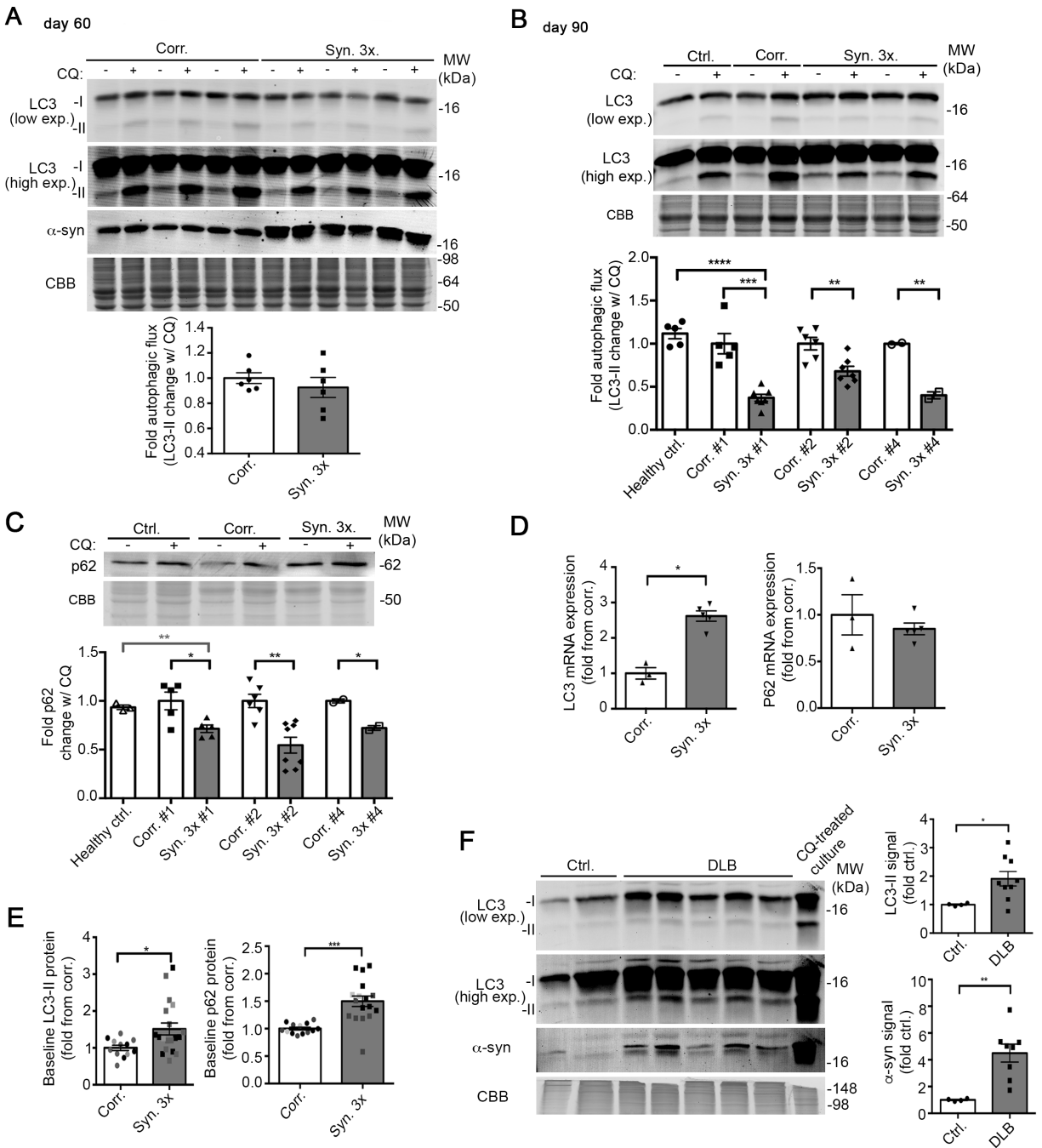
Figure 2-1: Macroautophagy flux is decreased in day 90 *SNCA* triplication neurons that accumulate a-syn.

A) Western blot analysis of day 60 iPSn from patient line #1 (Syn. 3x) and isogenic controls (Corr.) that were treated for 72 hrs with 40 µM chloroquine (CQ). Coomassie brilliant blue (CBB) was used as a loading control. Flux is measured as the ratio of normalized LC3-II levels in inhibitor treated lanes to the average of untreated lanes. Graphs represent fold change compared to controls on the same blot (n=6). **B)** Western blot analysis of day 90 iPSn from 3 patient lines (Syn. 3x) and isogenic controls (Corr.) evaluated as in (A) (Healthy control, Patient 1, and Patient 2: n=5-8; Patient 4: n=2). **C)** Western blot analysis of day 90 iPSn as in (B) showing triton-soluble p62 with and without CQ treatment. Graph shows the increase in p62 with CQ treatment compared to the average of untreated lanes, similar to flux (n=2-8). **D)** RT-PCR analysis of LC3 and P62 mRNA from patient 1 normalized to actin represented as fold change relative to corrected control (n=3-5). **E)** Baseline LC3-II and p62 protein levels measured in untreated (CQ −) lanes of each patient normalized to corresponding controls. Patients are shown as different shaded points (n=12 corrected line; n=19 Syn. 3X). **F)** Representative western blot of LC3 extracted from cortex of DLB patients and controls (n=4 controls; n=9 DLB). For all quantifications, values are the mean +/−SEM. *p<0.05; **p<0.01; ***p<0.001. Student's t-test or ANOVA with Tukey's post-hoc test was used for panel B and C. Student's t-test was used for panels A, D-F.
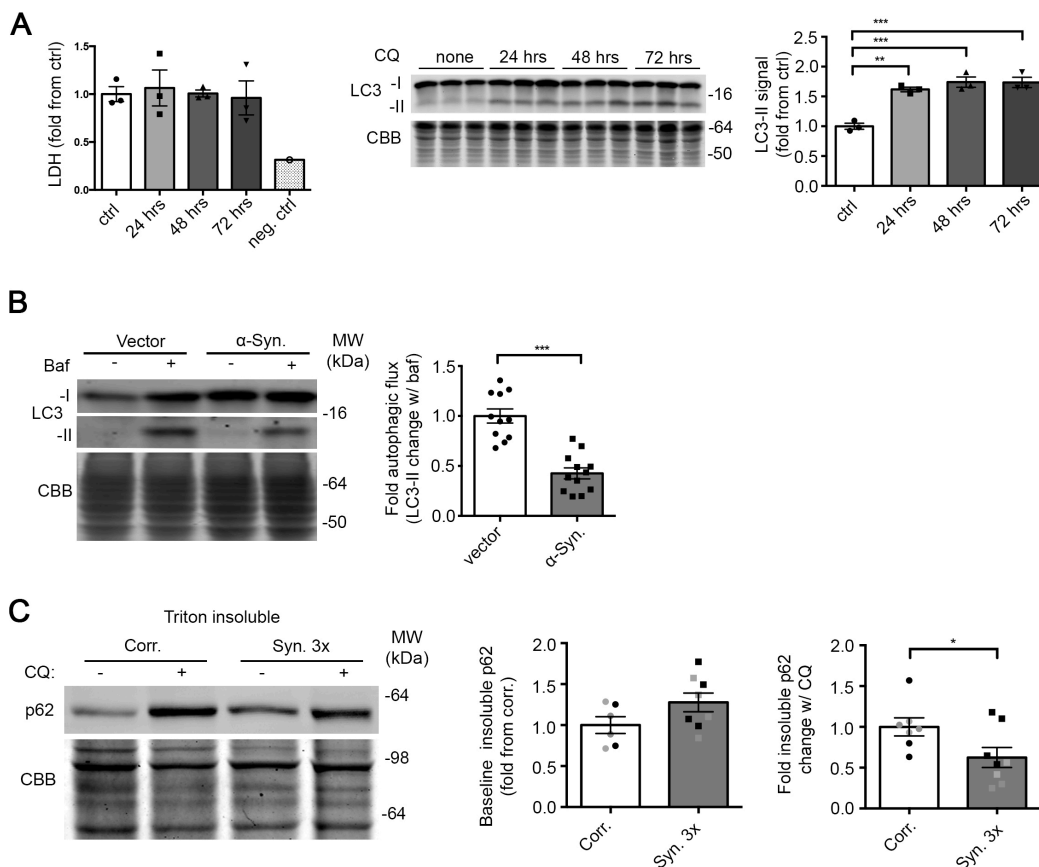
Figure 2-2: Limited chloroquine treatment is non-toxic and macroautophagy flux is decreased by WT a-syn in SH-SY5Y.

A) Triplication iPSn were treated for 24-72 hours with 40 μM CQ and media was analyzed for lactate dehydrogenase (LDH) as an indication of cell death (n=3). Neg. ctrl = media alone sample without cells. Right, CQ efficacy was confirmed by LC3-II increase by western blot analysis. CBB, Coomassie brilliant blue, was used as a loading control from the corresponding gel. **B)** SH-SY5Y stably overexpressing WT a-syn were treated for 2 hrs with 200 nM Bafilomycin A1 (Baf). Autophagic flux was measured by western blot analysis as described in Fig. 2-1. Vector indicates a matched control stable line (n=12). CBB was used as a loading control. **C)** Western blot analysis of triton insoluble (SDS soluble) protein fractions from triplication iPSn CQ flux experiments. Right graph shows fold increase in p62 in CQ treated lanes relative to untreated average, similar to flux calculation. Differently colored points signify different patient lines. (Values are the mean +/−SEM. *p<0.05; **p<0.01; ***p<0.001). ANOVA with Dunnett's test was used for panel A where no CQ treatment was considered the control. Student's t-test was used for panel B and C.

To directly visualize autophagosome puncta by immunofluorescence, we used a previously characterized human neuroglioma H4 model overexpressing wild-type (WT) a-syn under a tet-off system that exhibits lysosomal dysfunction (Mazzulli et al., 2011). We previously established that the degree of a-syn overexpression in this model is similar to *SNCA* triplication neurons (Mazzulli et al., 2016). a-Syn overexpression increased LC3 puncta at baseline, and reduced LC3 response upon inhibitor treatment (Fig. 2-3A). The same pattern was observed for p62 puncta (Fig. 2-3B), suggesting decreased autophagosome degradation. Colocalization between LC3 and the lysosome marker LAMP1 was decreased by a-syn accumulation, consistent with reduced autolysosomal fusion (Fig. 2-3C). Phagophore formation requires movement of Atg9-containing vesicles from the Golgi to provide lipid and scaffolding components (Ohashi and Munro, 2010; Sawa-Makarska et al., 2020). Atg9 movement from the Golgi was assessed in H4 cells by measuring colocalization with the resident Golgi SNARE syntaxin 5 (STX5) following starvation to induce autophagy. We found similar changes in Atg9 / STX5 colocalization after starvation in both high and low expressing a-syn cells (Fig. 2-4), suggesting that autophagic formation is not dramatically perturbed by a-syn. We confirmed immunofluorescence results in *SNCA* triplication iPSn, which showed increased autophagosome puncta within cell bodies and neural extensions of fixed *SNCA* triplication iPSn compared to corrected controls (Fig. 2-3D). As with western blot, LC3 puncta did not increase proportionally with chloroquine treatment in *SNCA* triplication iPSn (Fig. 2-3D), indicating decreased flux through the autophagic pathway.

We next sought to directly examine autophagosomes by electron microscopy analysis of fixed PD iPSn. Qualitative ultrastructural analysis of *SNCA* triplication iPSn revealed unusual vesicles with autophagosome features: double-membraned and completely closed, but abnormally wrapped in multiple layers of lamina (Fig. 2-3E) (Jung et al., 2019; Klionsky et al., 2021). Some

vesicles appeared to contain electron dense, undegraded material (black arrows, Fig. 2-3E). This supports the notion that PD iPSn are capable of autophagosome formation and cargo engulfment, but are compromised in their ability to clear engulfed substrates. Altogether, these data indicate that a-syn disrupts autophagic flux at a stage after autophagosome formation.

Figure 2-3: Immunofluorescence and ultrastructural analysis of autophagy in fixed PD culture models.

A) Representative Z-stack projected confocal images of fixed H4 cells overexpressing a-syn (-dox) treated for 2 hrs with 200 nM inhibitor Bafilomycin (Baf), fixed, and immunostained for LC3. Each point represents intensity measured in a manually selected cell body. Any detectable nuclear signal was excluded. DAPI indicates nuclei and was used for normalization. Upper, graph of flux quantification analyzed by Student's t-test. Lower, graph showing individual LC3 puncta intensity analyzed by ANOVA with Tukey's post-hoc test (n=50-80 cells; 15 fields of view; scale bar=12 μm, N.S., not significant). **B)** Immunofluorescence analyses of H4 cells as in (A) showing p62 staining. Graph shows p62 intensity in individual cells analyzed by ANOVA with Tukey's post-hoc test (n=29-35 cells; 15 fields of view; scale bar=12 μm; N.S., not significant). **C)** Representative confocal images of H4 cells stained for LC3 and LAMP1. Pearson's R calculated in manually selected cell bodies. Each point is one cell (n=65-70 cells; 15 fields of view; scale bar=12 μm). Arrows and white spots illustrate colocalized points. **D)** Immunofluorescence images showing LC3 puncta in fixed day 90 PD iPSn and controls. A 1.6 μm projection is shown. Chloroquine (CQ) was used as before to evaluate flux. Left graph compares LC3 intensity in manually selected cell bodies in untreated wells. Right graph compares LC3 intensity as a response to chloroquine as in Fig. 2-1 and (A) (n=20-33 cells; 20-25 fields of view; scale bar=12 μm) Student's t-test used for panels C and D (Values are the mean +/−SEM. *p<0.05; **p<0.01; ***p<0.001). **E)** Representative electron microscopy images of day 90 *SNCA* triplication and healthy control iPSC-neurons showing autophagic structures. Black arrows label multilamellar vesicles while white arrows label vesicles with traditional autophagosome features. Upper row, scale bar = 2 μm; lower row, zoomed scale bar = 500 nm (6-12 cells per line).
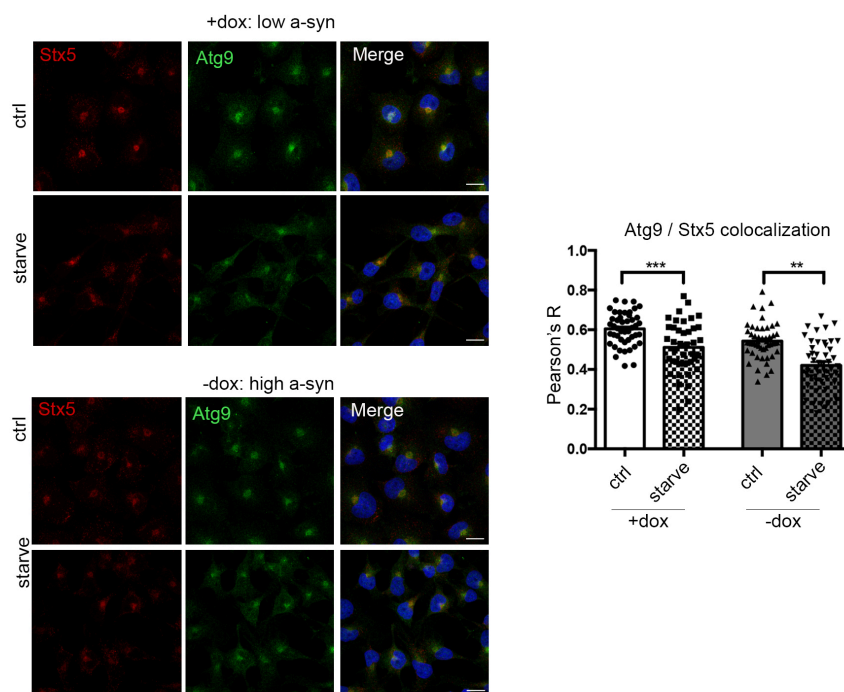
Figure 2-4 Atg9 localization response to starvation is not perturbed by a-syn. H4 were starved for 2 hrs in serum reduced media to induce autophagosome formation, then fixed and immunostained for Golgi marker Stx5 and autophagic protein Atg9. Colocalization was quantified by Pearson's R (n=40-50 cells; scale bar=12 μm). Values are the mean +/- SEM, ***p<0.001; **p<0.01, Student's t-test. Scale bars = 12 m.

2.2: a-Syn decreases the association between ykt6 and autolysosome fusion SNARE SNAP-29

Since previous studies in cell lines showed that ykt6 plays a role in autolysosomal fusion (Matsui et al., 2018), we sought to determine if ykt6 played a similar role in human midbrain cultures. Ykt6 was knocked down (KD) in healthy control iPSn using previously established shRNA constructs (Cuddy et al., 2019), followed by analysis of autophagy by LC3 western blot. Although we only achieved a ~50% KD of ykt6, this was sufficient to cause a dramatic 7-fold accumulation of LC3-II (Fig. 2-5A). Ykt6 KD also abolished the LC3-II response to CQ, indicating a severe impairment in autophagic flux that is similar to the effect induced by a-syn accumulation (Fig. 2-5B). These data suggest that ykt6 is critical for late-stage autophagic flux in midbrain iPSn.

We then examined whether the interaction between ykt6 and its primary SNARE binding partner required for autolysosome fusion, SNAP-29 (Matsui et al., 2018; Takáts et al., 2018) is disrupted in cells that accumulate a-syn. H4 cells were transfected to express Flag-tagged SNAP-29 and GFP-tagged ykt6 to facilitate detection by immunofluorescence analysis. Although the total levels of GFP-ykt6 and Flag-SNAP-29 did not change, colocalization was decreased in a-syn overexpressing cells compared to controls (Fig 2-5C), consistent with a decline in autophagic-lysosomal fusion (Fig 2-2). We verified this finding using antibodies that detect endogenous ykt6 and SNAP-29 in patient iPSn (Fig. 2-5D). We stained endogenous ykt6 and SNAP-29 in fixed *SNCA* triplication iPSn and found that colocalization was also reduced in patient cells (Fig. 2-5D).

To measure SNARE complexes, we immunoprecipitated GFP-ykt6 from stably expressing SH-SY5Y (Cuddy et al., 2019) and probed for V5-tagged SNAP-29 following expression of WT a-syn or empty vector. In this model, the amount of V5-SNAP-29 that pulled down with ykt6 was decreased by a-syn accumulation (Fig. 2-5E). To confirm these findings in PD patient iPSn with a distinct method, we used size exclusion chromatography (SEC) to measure endogenously expressed SNARE complexes in lysates from d90 *SNCA* triplication cultures and isogenic controls. Quantification of the input injected on the SEC column indicated that the total amount of SNAP-29 in *SNCA* triplication iPSn lysates was not different compared to isogenic controls (Fig. 2-5F). SEC analysis indicated that ykt6-SNAP-29 complexes eluted as a 120Å-sized particle, and that the percentage of SNAP-29 co-eluting with ykt6 was dramatically reduced in *SNCA* triplication iPSn compared to corrected controls (Fig. 2-5G). Together, these data indicate that reduced association of SNAP-29 and ykt6 occurs in cells that accumulate a-syn, providing a mechanistic explanation for the inhibition of autophagic flux.
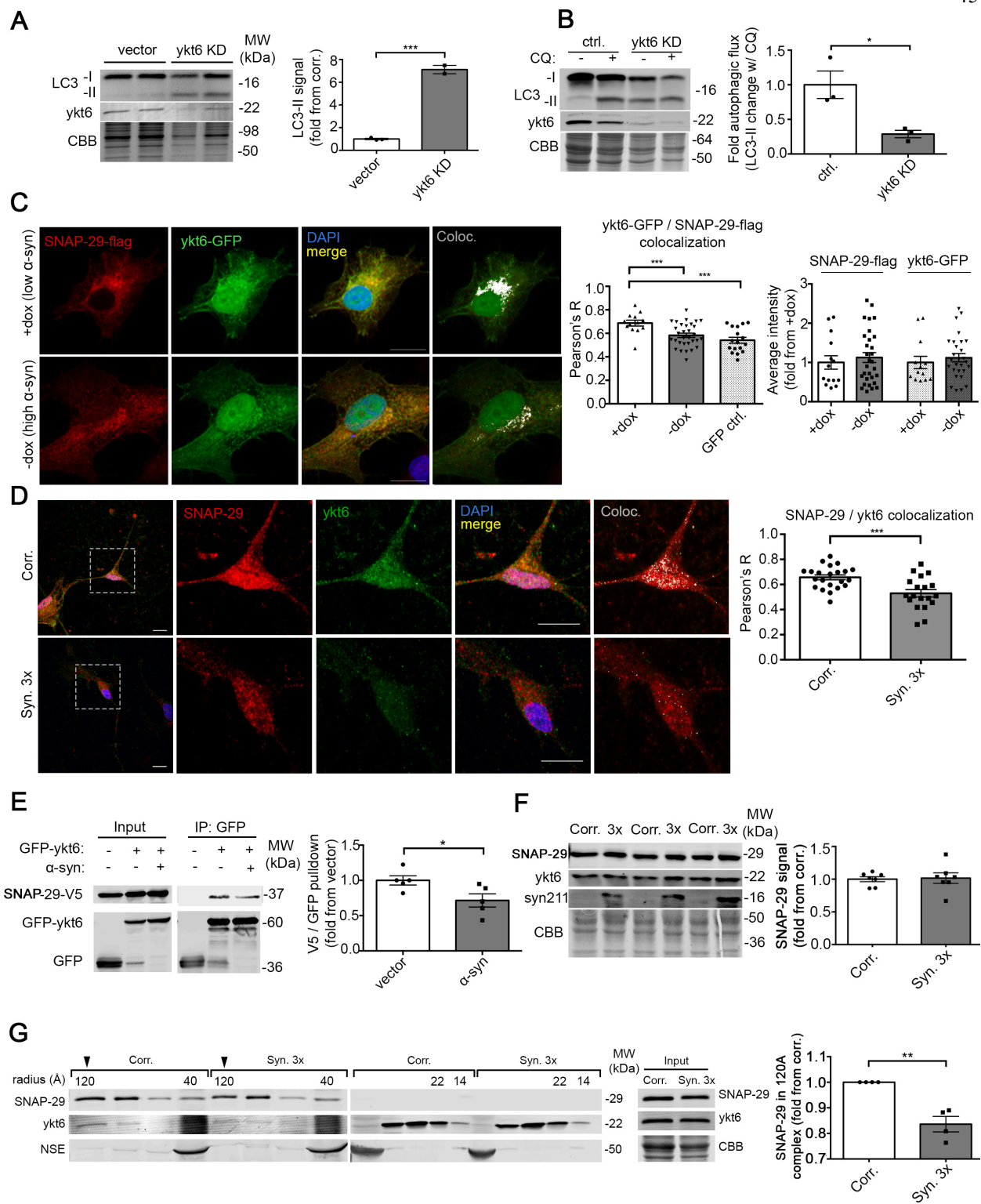
Figure 2-5: a-Syn decreases the association between ykt6 and autolysosome fusion SNARE SNAP-29

A) Ykt6 was knocked down in day 90 iPSn from controls for 5 days by lentiviral infection of shRNA (ykt6 KD) or a scrambled vector, and LC3 and flux measured by western blot (n=2-3). **B)** Control or ykt6 KD iPSn were treated with CQ and analyzed by LC3 western blot analysis (n=3). **C)** Representative zoomed confocal images of H4 cotransfected with SNAP-29-Flag and ykt6-GFP. Pearson's R calculated in cytosol excluding nucleus as before (n=10-20; 15 fields of view; scale bar=12 μm). GFP transfection was used as a negative control. Graph on the right compares relative intensities for each marker across conditions. Each point represents an individual cell. **D)** Representative immunofluorescence projections of fixed day 90 PD iPSn showing colocalization between endogenous SNAP-29 and ykt6 (n=19-22 cells; 18 fields of view per line; scale bar=12 μm). Graph compares Pearson's R in manually selected cell bodies as in (B). **E)** Immunoprecipitation of GFP from SH-SY5Y stably expressing ykt6-GFP infected to express SNAP-29-V5 with a-syn (+) or empty vector (-). V5 signal normalized to ykt6-GFP pulldown (n=5). **F)** SNAP-29 and ykt6 levels from day 90 triplication and corrected iPSn (n=7). **G)** Triton soluble day 90 iPSn lysates separated by size exclusion chromatography (SEC) followed by western blot analysis of collected fractions. NSE was used as control (n=4). Input for column injection is shown to the right. Graph shows the percentage of SNAP-29 signal in the first fraction (120Å) out of the sum of SNAP-29 in all fractions. For all quantifications, values are the mean +/−SEM. *p<0.05; **p<0.01; ***p<0.001. Student's t-test was used in panels A, B, D-G; ANOVA with Dunnett's post-hoc test was used for panel C using + dox as the control condition.

2.3: Farnesyltransferase protein is increased in PD iPSn and DLB brain.

We next wanted to gain mechanistic insight into the cause of reduced ykt6-SNAP-29 complexes and the connection to autophagic dysfunction. Ykt6 is autoinhibited by farnesylation, which promotes a closed, inactive conformation that is incapable of forming SNARE complexes (Tochio et al., 2001; Wen et al., 2010). Our previous study indicated that inactive, cytosolic ykt6 is elevated and interacts with a-syn in PD patient iPSn (Cuddy et al., 2019). To assess the role of farnesylation in *SNCA* triplication iPSn, we first measured the levels of farnesyltransferase (FTase). Western blot analysis showed increased levels of FTase subunit alpha (FT-α) in day 90 *SNCA* triplication iPSn compared to corrected and healthy controls (Fig. 2-6A). This change occurred post-transcriptionally, since mRNA levels were unchanged (Fig. 2-6B). To assess FTase

activity, we quantified the levels of farnesylated and non-farnesylated HDJ-2, an established marker of FTase activity (Adjei et al., 2000; Capell et al., 2008). The proportion of farnesylated HDJ-2 was increased in PD iPSn compared to corrected controls (Fig. 2-6C), suggesting increased FTase activity. To determine FTase levels *in vivo*, we analyzed frontal cortical lysates from DLB brain and found FT-α was increased in DLB patients compared to age-matched healthy controls (Fig. 2-6D). These data indicate that FTase is increased in both iPSC-derived PD patient neurons and DLB brain, and its increased activity may contribute to autophagic dysfunction in PD.
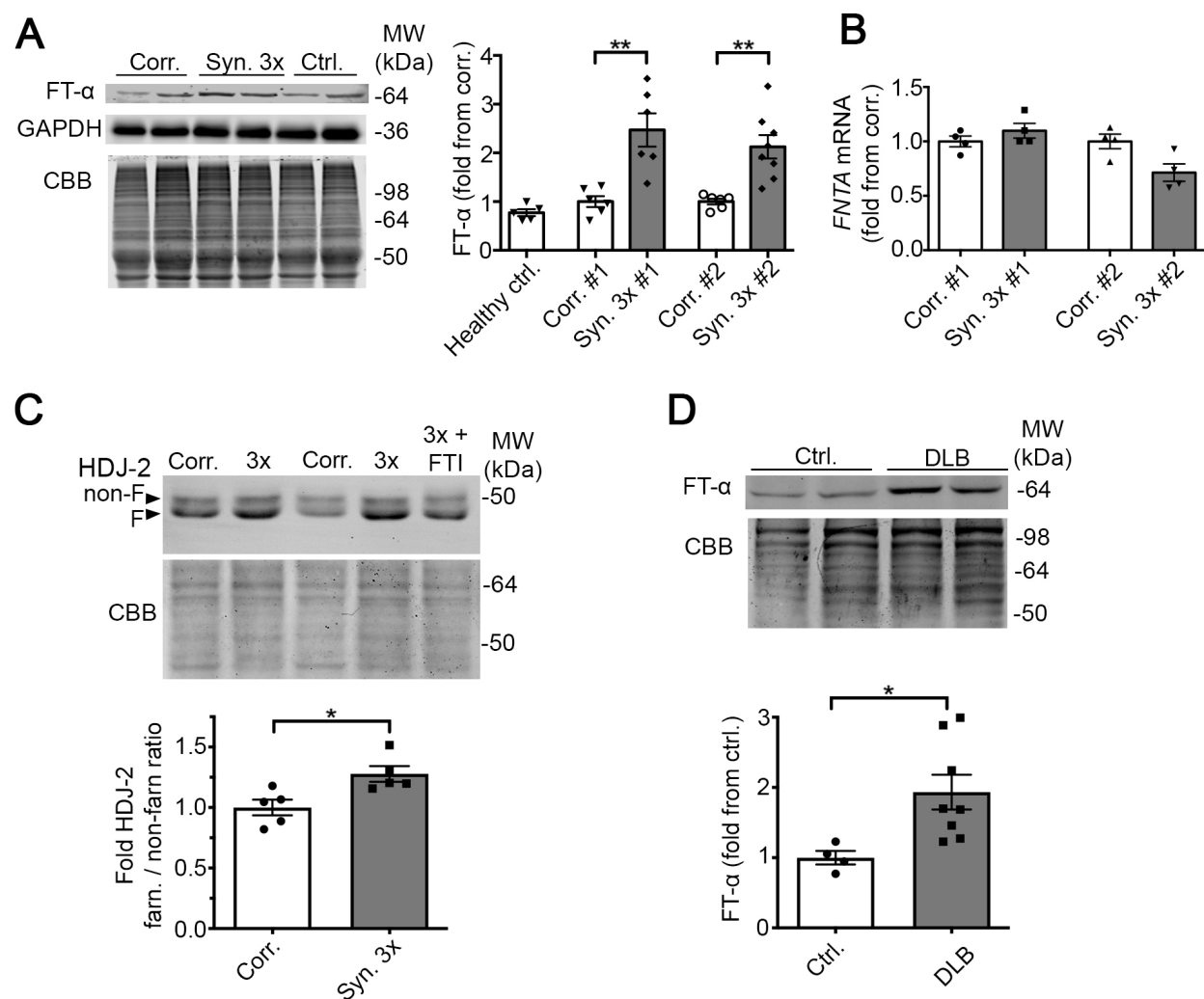
Figure 2-6: Farnesyltransferase protein is increased in PD iPSn and DLB brain.

A) Day 90 iPSn lysates from triplication (3X), corrected (corr), and healthy control (ctrl) showing FT-α (n=5-7). CBB and GAPDH were used as loading controls. **B)** Measurement of mRNA by RT-PCR from matched cultures to quantify *FNTA* expression, normalized to actin (n=4-5). **C)** HDJ-2 from corrected (corr) and triplication (3x) iPSn was separated into farnesylated (lower band: f) and non-farnesylated (upper band: non-f) forms. Fold change ratio of farnesylated to non-farnesylated is shown (n=5). 3X iPSn were treated for 7 days with 10 nM LNK-754 (Ctrl + FTI) and used as a control. **D)** Representative blot of FT-α extracted from cortex of DLB patients and controls (n=4 controls; 9 DLB). For all quantifications, values are the mean +/−SEM. *p<0.05; **p<0.01; ***p<0.001 (Student's t-test).

DISCUSSION

Our data indicate that a-syn disrupts late-stage autophagic flux and highlight a crucial role for ykt6 in autophagosome-lysosome fusion in human midbrain neurons. Previous studies have shown that ykt6-SNAP29 complexes are similarly important for late-stage fusion in HeLa cell lines, although autophagic flux can still occur in the absence of ykt6 through an independent STX17-SNAP-29 complex (Matsui et al., 2018). Our data indicate that midbrain neurons are highly dependent on ykt6 for autophagosome-lysosome fusion, since partial ykt6 KD resulted in a near-complete inhibition of autophagic flux (Fig. 2-5A, B). Ykt6 is a unique SNARE protein since its activity is highly regulatable by post-translational lipidation and phosphorylation (Karuna et al., 2020; McGrath et al., 2021; Wen et al., 2010). Similarly, autophagy is a highly inducible clearance pathway which requires regulated machinery to rapidly sense and respond to various types of cellular stress. Our previous work showed that ykt6 coordinates with TFEB, the master transcriptional regulator of lysosomal biogenesis and MA (Sardiello et al., 2009; Settembre et al., 2011), upon lysosomal stress to enhance hydrolase trafficking between the ER and Golgi (Cuddy et al., 2019). Consistent with previous studies, we show here that ykt6 also regulates autophagy in iPSn models, indicating a critical role in integrating two distinct trafficking pathways to enhance cellular clearance.

Multiple studies have shown that a-syn can bind to SNARE proteins under physiological or pathological conditions, including synaptobrevin-2, which shares sequence homology with ykt6 (Burre et al., 2010; Choi et al., 2013). We previously found that a-syn impedes ykt6 SNARE complex assembly between the ER and Golgi by interacting with a closed, inactive form of ykt6 in the cytosol (Cuddy et al., 2019). Our data here show that a-syn inhibits autophagic flux through a similar mechanism, by impeding ykt6-SNAP-29 complexes during autophagosome-lysosome fusion. Other work in cell lines with viral a-syn overexpression showed that it may inhibit autophagic flux at a similar stage by SNAP-29 depletion (Tang et al., 2021). Although we did not document SNAP-29 depletion in PD patient neurons, we find a reduction in ykt6-SNAP-29 complexes (Fig. 2-5B-E). Ultrastructural analysis suggests that autophagosomes are synthesized in PD neurons and capable of engulfing substrates, which is consistent with the accumulation of LC3-II. The complete multi-lamellar vesicles we observed further suggest that autophagosomes are formed but not processed, perhaps with multiple attempts at engulfment (Fig. 2-2E). Human dopaminergic iPSn with CRISPR-corrected isogenic controls were selected as a primary model for this investigation, to account for relevant differences in autophagic processes of human neurons as compared to other species and cell types such as rapidly dividing cell lines (Benito-Cuesta et al., 2017; Larsen and Sulzer, 2002; Maday and Holzbaur, 2016). Just as age is a primary risk factor for parkinsonism, reduced autophagy only appeared when iPSn were aged to 90 days in culture; no difference was observed at day 60 (Fig. 2-1). Collectively, this indicates that a similar mechanism of chronic endogenously accumulated a-syn simultaneously impedes multiple trafficking pathways required for autophagy. This, in turn, disables essential proteostasis pathways required to remove aggregates, promoting the growth of a-syn aggregates in a self-propagating pathogenic cycle.

We found that increased FTase levels are associated with impaired autophagic flux in PD patient cultures and DLB brain (Fig. 2-6). Other groups have shown that elevated FTase occurs in neurodegenerative disease (Jeong et al., 2021), and that inhibiting FTase can activate proteolytic pathways and reduce protein aggregates (Hernandez et al., 2019; Pan et al., 2008). FTase is the only mammalian enzyme that mediates farnesyl modification of ykt6 and other proteins that harbor the CaaX motif (Casey and Seabra, 1996), and we found it to be increased in disease (Fig. 2-6). The mechanisms leading to increased FTase activity are not fully understood, however elevated FTase proteins levels in the absence mRNA changes suggest that increased FTase protein stability may play a role. Farnesylation of ykt6 is a well-established regulatory mechanism that promotes a closed, inactive conformation in the cytosol (Cuddy et al., 2019; Wen et al., 2010). Our previous work showed that ykt6 activity is decreased in PD (Cuddy et al., 2019), and increased FTase may be a contributing factor. If pathologic, this dysregulation provides a rationale to reduce FTase activity with FTI treatment, as evaluated in the next chapter.

METHODS

Statistical analysis

Each assay was performed with at least 2-3 technical replicates and confirmed with 2-4 individual passages or differentiation sets. Statistical analyses were performed using Prism software. When suspected from graphing, statistical outliers were confirmed and removed using ROUT test (Q=5%). A Student's t-test was used when comparing 2 groups, and 1-way ANOVA with Dunnett's or Tukey's multiple comparisons for selected post-hoc tests was used when comparing more than 2. For ease of representation and comparison across modalities, graphs most often show

fold change in the relevant value compared to each experiment's control. Throughout, *p<0.05; **p<0.01; ***p<0.001.

Culture models

H4 cells

Inducible H4 neuroglioma cells that overexpress WT a-syn under a tetracycline-responsive promoter (tet-off) have been described and authenticated previously(Mazzulli et al., 2011; Mazzulli et al., 2016). Culture media is OptiMem (Gibco) supplemented with 5% heat-inactivated fetal bovine serum (HI-FBS), 1% penicillin/streptomycin (pen/strep), and 200 mg/ml Geneticin (G418) and Hygromycin (both Thermo Fisher). For controls, a-syn expression was suppressed by 72 hours 1 µg/ml doxycycline (+dox) treatment (Sigma).

SH-SY5Y

Generation of pCDNA3.1 (vector), pCDNA3.1-wt-a-syn, pEGFP, and pEGFP-ykt6 stably expressing lines was described previously(Cuddy et al., 2019) (from naïve ATCC # CRL-2266; female). The same approach was taken to generate lines expressing pCDNA3.1-wt-a-syn with pLKO1 or pLKO1-ykt6-shRNA. Briefly, Lipofectamine 2000 transfected cells were exposed to incrementally higher concentrations of G418 over 2 weeks, then remaining colonies were expanded and screened for a-syn and ykt6 expression. Stable lines were maintained in DMEM (Gibco) with 10% HI-FBS, 1% pen/strep, and 200 mg/ml G418. Cells were differentiated for experimental use by addition of 10 µM all trans retinoic acid for 5 days (Sigma).

iPS cells and neuronal differentiation

iPSC maintenance and dopaminergic differentiation has been described previously(Mazzulli et al., 2011; Mazzulli et al., 2016). For these studies, iPSCs were maintained on Cultrex coated plates in mTeSR+ media (Stemcell Technologies). Dopaminergic neuron differentiation followed a well-established dual SMAD inhibition protocol(Kriks et al., 2011). Cells were treated with growth factor cocktail for 40-50 days followed by maintenance in Neurobasal media supplemented with NeuroCult SM1 (Stemcell Technologies), 1% pen/strep, and 1% L-glutamine (Thermo Fisher). Quality of each differentiation set was ensured by monitoring cell body and neurite morphology throughout differentiation and measuring ßIII-tubulin / GAPDH ratio and a-syn after harvesting. Neurons were cultured for 60-120 days before use. Except as stated in results and figure legends, experiments were performed between day 88 and 95. *SNCA* triplication iPSCs, healthy control line (2131), and their differentiated neurons have been extensively characterized in two of our previous papers(Mazzulli et al., 2016; Stojkovska et al., 2021).

Biochemistry and cell biology

Plasmids and lentiviral production

Generation of ykt6-CS, ykt6-GFP, WT a-syn, and ykt6-shRNA plasmids was described previously(Cuddy et al., 2019; Mazzulli et al., 2016). SNAP29 in pLenti6.3/V5-DEST (HsCD00942173) was obtained from DNASU. FLAG-SNAP29 was a gift from Noboru Mizushima (Addgene plasmid # 45915 ; http://n2t.net/addgene:45915 ; RRID:Addgene_45915)(Itakura et al., 2012).

Lentiviral plasmids were packaged as described(Mazzulli et al., 2016) and titer determined using Zeptometrix HIV1-P24 ELISA kit. SH-SY5Y and iPSn were infected at MOI3. Ykt6-CS rescue studies were harvested 7 days post-infection. Ykt6 knockdown, SNAP-29-V5, and a-syn

overexpression were harvested 5 days post-infection. Empty vector or pLKO1-scramble were used as controls. Controls in the right graph of Fig. 2-5A are uninfected.

General western blotting

40 µg of protein lysate or immunoprecipitate was run on a tris-glycine SDS-PAGE gel (time and acrylamide percentage specified in assay section) and transferred onto Millipore immobilon-FL PVDF membranes at 30V for 1 hour. Membranes were post-fixed in 0.4% paraformaldehyde (PFA) for 30 minutes, washed 3 times in pure water, and blocked for 1 hour in 1:1 Odyssey blocking buffer (OBB) and tris-buffered saline (TBS). Primary antibodies were incubated overnight rotating at 4° in 1:1 blocking buffer and TBS with 1% tween (TBS-T). Membranes were then washed three times in TBS-T and secondary antibody in OBB:TBS-T was incubated at room temperature for 1-2 hours (Alexa 680 1:10,000; Alexa 790 and IRDye800 1:5000). Membranes were washed as before and scanned on an Odyssey or Sapphire infrared imaging system. Manual band analysis was performed in Odyssey Image Studio software. Lanes were always normalized to a loading control: total protein using Coomassie stain on gel for most assays (CBB), neuron specific enolase (NSE) for SEC, and GFP for immunoprecipitation. GAPDH and tubulin were also evaluated as additional loading and quality controls.

LC3-II autophagic flux assay and triton soluble protein extraction

40 µM chloroquine (CQ) in water or an equivalent volume in fresh media was added to SH-SY5Y or iPSn, and cells were collected in ice cold PBS 72 hours later. This treatment was found to be non-toxic but caused a significant increase in LC3-II (Fig. 2-2). After spinning down at 400xg, 5 min, 4°C and discarding supernatant, cell pellet was lysed in 1% Triton X-100 buffer (1% Triton

X-100, 20 mM HEPES pH 7.4, 150 mM NaCl, 10% glycerol, 1 mM EDTA, 1.5 mM MgCl2, 1 mM phenylmethanesulfonyl fluoride (PMSF), 50 mM NaF, 2 mM Na orthovanadate, and a protease inhibitor cocktail). Neuron lysates were homogenized ~15 times in a conical glass vessel using a motor driven Teflon homogenizer at 4000 RPM while SH-SY5Y were broken up by vigorous pipetting. Lysates were incubated in ice slurry for 30 minutes then cleared by centrifugation at 100,000 x g, 4°C for 30 min. 40 µg protein determined by BCA assay was run on 15% tris-glycine SDS-PAGE gel for ~1.5 hours, and western blot proceeded as described above (LC3 Sigma L8918 rabbit 1:500).

Signal was normalized to CBB. To calculate flux, LC3-II signal in CQ treated lanes was divided by the average signal in the condition's untreated lanes on the same blot. Fold change in flux compared to control is shown.

qRT-PCR for mRNA measurement

Neuron cell pellet was divided so that one half could be used for mRNA and one half used for protein. PureLink RNA Mini Kit (Thermofisher Scientific) was used to extract total RNA, and RevertAid First Strand cDNA Synthesis Kit (Thermofisher Scientific) was used to synthesize cDNA. Applied Biosytems 7500 Fast system was used for qRT-PCR with the following pre-designed Taqman-primer probes: ACTB (Hs01060665_g1), MAP1LC3 (Hs01076567_g1), SQSTM1 (Hs00177654_m1), and FNTA (Hs00357739_m1). Target mRNA expression was normalized to ACTB and evaluated using delta-delta-CT method (2-3 technical replicates; 3-5 biological replicates).

Immunoprecipitation

Co-IP of GFP-ykt6 from SH-SY5Y was performed using GFP_Trap (Chromotek) beads as described(Cuddy et al., 2019). Briefly, cells from a 10-cm plate were lysed in Co-IP buffer (10mM Tris-HCl pH 7.5, 150mM NaCl, 0.5M EDTA and 0.5% NP-40 containing protease inhibitor cocktail, PMSF and NaF), and 800 – 1000 µg total protein was incubated overnight with 20 µL GFP_trap beads rotating at 4°C. Complexes were washed then eluted by boiling in 50 µL 2X Laemmeli sample buffer, half of which was loaded on the gel. Gel was 12% acrylamide run for ~1 hour.

Size exclusion chromatography

Neurons were lysed in 1% triton buffer as above. 800 µg in 250 µL was injected on a Superdex 200 HR 10/300 gel filtration column using Agilent HPLC 1200 series pumps, injector, UV detector, and fraction collector. PBS pH 7.4 was used as mobile phase: flow rate 0.5 mL/min, collecting 0.5 mL fractions, sample loop max volume 400 µL. Fraction size identity was determined by standard calibration of the column prior to use. Fractions were combined and concentrated using Millipore 10,000 MWCO filters and analyzed by western blot as above. (Snap29 Abcam rabbit 1:500; ykt6 Santa Cruz mouse 1:500). See previous description(Cuddy et al., 2019).

HDJ-2 shift assay

DMSO-treated neuron triton lysates were run as above on an 8% gel for ~1 hour to separate bands (HDJ-2/Hsp40 Santa Cruz mouse 1:500). Along with molecular weight, farnesylated and non-farnesylated bands were ensured by comparison to control FTI treated lane (7 days 10 nM LNK-754).

LDH toxicity assay

40 µM CQ was pipetted into iPSn media 72-24 hours before harvest. Media was collected and cell protein extracted for later analysis. Cytotoxicity was measured using the CyQUANT LDH Cytotoxicity Assay (Invitrogen) according to manufacturer's instructions. Samples included 3 technical replicates and 3 biological replicates. Maximum LDH activity was used as a positive control, and reaction alone was used as a negative control. LC3-II was confirmed to be increased by western blot.

H4 immunofluorescence

Images were acquired using a Leica TCS SPE CTR4000 / DMI4000B microscope. At 63x, a 5 µm Z-section centered on DAPI focus was imaged using 0.5 µm slices and sequential scan. ~15 fields of view were acquired from 2-4 coverglass per condition. Images were analyzed using Fiji software. Slices were stacked in a maximum projection, and individual cell bodies excluding the nucleus were manually selected as ROIs for measurement. Secondary antibody incubation alone was used as a negative control for autofluorescence and background.

Transfection

For experiments requiring transfection, 80 ng of plasmid was transfected per 50,000 cells using X-treme Gene HP transfection reagent (Roche). Non-transfected wells, empty vector, or GFP were used as controls. Cells were fixed 3 days post-transfection.

LC3 flux

Different fixation conditions were optimized for each assay. For LC3 flux assay, cells on coverglass were treated for 2 hours with 200 nM Baf or DMSO then fixed in 100% HPLC grade methanol for 20 minutes at -20°C. Following 3 PBS washes, cells were blocked for 1 hour in triton blocking buffer (0.2% Triton X-100 made in PBS with 5% normal goat serum and 2% bovine serum albumin). Primary incubation with 1:200 LC3 (Sigma L8918 rabbit) was carried out in this same buffer at 4°C for 24 hours. LC3 nuclear stain appeared under these conditions but not others, and we believe it is an artifact.

The following steps were identical for each assay. After washing 3 times in PBS with 0.05% tween, secondary incubation was performed in triton blocking buffer using 1:500 Alexa Fluor 568 and/or Alexa Fluor 488 for 2 hours at room temperature. After washing, coverglass were mounted using DAPI fluoromount G (Southern Biotech), and slides were dried for at least 24 hours before imaging.

Fluorescence was measured as integrated density in each channel. LC3 flux was analyzed by dividing each baf treated cell's intensity by the average of untreated cell intensities.

Colocalization

For lamp1 / LC3 colocalization, cells were fixed in 4% PFA for 15 minutes at room temperature, permeabilized in 0.1% triton for 30 minutes, and blocked in 0.1% triton blocking buffer for 30 minutes. Incubation continued for 48 hours in 1:50 lamp1a (Santa Cruz mouse) and 1:200 LC3 (Sigma L8918 rabbit).

For ykt6 / SNAP-29 colocalization, cells were first permeabilized with 50 µg/mL digitonin for 2 minutes, washed 3X in PBS, then fixed in 4% PFA. Permeabilization and blocking was performed in 0.2% triton blocking buffer as above. Endogenous ykt6 was stained with 1:100 ykt6 (Santa Cruz polyclonal) for 48 hours.

Secondary incubation and imaging as above. "EzColocalization" plugin was used for colocalization analyses(Stauffer et al., 2018), and Pearson's R was compared.

To induce autophagosome formation in Atg9 movement study, media was replaced with Optimem alone 2 hrs before permeabilization in digitonin and fixation in 4% PFA.

Neuron immunofluorescence

Images were acquired as for H4 cells above with the following change: 4.8 μm Z-stacks were imaged in 0.4 μm slices at 12-bit depth resolution.

LC3 flux

Cells were fixed in methanol for 15 minutes at -20°, permeabilized with 0.2% triton for 30 minutes at room temperature, and blocked overnight at 4° with triton blocking buffer described above. Incubation with 1:100 LC3A (Novus Biologicals) was performed overnight in blocking buffer at 4°. Fiji software was used to measure LC3 integrated density in cell bodies of a single slice excluding the nucleus. Autophagic flux was calculated as above.

Colocalization

Cells were permeabilized with 50 μg/mL digitonin for 2 minutes then fixed in 4% PFA for 15 minutes at room temperature. Permeabilization with 0.2% triton and blocking overnight was performed as for LC3 flux. Ykt6 (Santa Cruz monoclonal) and SNAP-29 (Abcam) were both incubated at 1:100 for 48 hours at 4°. Analysis was performed using Fiji software as above.

Electron Microscopy (EM) analysis

Full details of cell preparation can be found previously(Stojkovska et al., 2021). Day 90 neurons were fixed in 2.5% glutaraldehyde, post-fixed in 1% osmium tetroxide (OsO4), and stained with 1% uranyl acetate (Electron Microscopy Sciences). They were finally embedded in LX112 (Ladd Research Industries) resin mix and thin sectioned at ~70 nm width. Imaging was performed on a FEI Tecnai Spirit G2 TEM. For qualitative analysis, blind images were searched for structures with features of immature to mature autophagosomes (double-membraned, roughly circular or crescentiform, medium radiodensity, may include cargo)(Jung et al., 2019; Klionsky et al., 2021) which were labeled for review. A second pass removed questionable structures, images were unblinded, and similarities within conditions assessed with discussion (6-12 cells per line).

Post-mortem synucleinopathy brain tissue analysis

Post-mortem frontal cortex from the Northwestern University Alzheimer's disease pathology core were sequentially extracted for protein as described in detail previously(Stojkovska et al., 2021). Full details regarding control and DLB patient characteristics can be found there as well. Briefly, 5 steps of increasingly harsh detergents were used: high-salt buffer (50 mM Tris-HCl pH 7.4, 750 mM NaCl, 10 mM NaF, 5 mM EDTA), buffer with 1% triton, 1% triton with 30% sucrose, 1% sarkosyl, and remaining sarkosyl-insoluble. LC3 (Sigma L8918 rabbit 1:500) was probed in the 1% sarkosyl fraction, and FT- α (Santa Cruz mouse 1:500) was probed in the high-salt fraction. Samples began blinded.

CHAPTER 3: FTI treatment rescues autophagic flux in PD neurons by activating ykt6

OVERVIEW

Because we observed disrupted ykt6-SNAP-29 complexes and high farnesyltransferase in *SNCA* triplication neurons, we investigated whether reversing these changes could beneficially increase autophagy. Ykt6 is stabilized in its autoinhibited cytosolic conformation by a farnesyl group at cysteine 195 (Fukasawa et al., 2004; Wen et al., 2010). We previously found that a mutation preventing farnesylation at this site increased ykt6 presence in the membrane and could be expressed as a constitutively active form (ykt6-CS) (Cuddy et al., 2019). A similar result could be achieved pharmacologically with small molecule farnesyltransferase inhibitor (FTI) treatment. In our previous study, LNK-754 – a potent yet specific inhibitor of farnesyltransferase – decreased farnesylation of ykt6, increased ER-Golgi trafficking, and reduced a-syn in A53T mutant neurons (Cuddy et al., 2019). It was also shown to be brain penetrant and rescued a-syn and motor deficits in DA_{SYN53} mice (Cuddy et al., 2019). We therefore tested whether activating ykt6 using this method could also rescue autophagy in *SNCA* triplication neurons. We found that LNK-754 treatment was sufficient to return LC3-II flux to normal levels in PD iPSn and increased association between ykt6 and SNAP-29. Rescue was meanwhile prevented when ykt6 was knocked down. This reinforces our finding that ykt6 is a primary contributor to dysfunction and provides proof of concept for repurposing FTIs to clear protein aggregates in PD. These results are presented in Chapter 3.

RESULTS

3.1: Inhibition of farnesyltransferase improves macroautophagy

To determine if increased FTase activity contributes to autophagic failure in PD cultures, we next tested if treatment with a specific farnesyltransferase inhibitor (FTI), LNK-754, could rescue autophagy in PD iPSn. We had previously found that LNK-754 reduces farnesylation of ykt6, promotes its movement from cytosol to membrane, and reduces pathological a-syn levels in A53T mutant iPSn (Cuddy et al., 2019). Here, we find that FTI treatment rescued autophagic flux, as indicated by immunofluorescence analysis of fixed H4 a-syn cells that showed increased LC3 response to lysosomal inhibition (Fig. 3-1A). Western blot analysis of LC3-II corroborated these findings, demonstrating that FTI treatment increased autophagic flux in a-syn overexpressing SH-SYSY (Fig. 3-1B). We verified that reducing FTase activity improves autophagic flux in PD patient cultures since FTI treatment of 2 distinct patient lines completely rescued LC3-II flux to that of isogenic corrected lines (Fig. 3-1C). FTI treatment had no effect on the mRNA of LC3 or p62, suggesting the effect is post-transcriptional (Fig. 3-1D).

Finally, we wanted to determine if FTI treatment can alter autophagy *in vivo*. We used a previously characterized transgenic mouse model that accumulates human A53T a-syn within dopamine neurons, called DA_{SYN53} mice (Chen et al., 2015). These mice were injected for 28 days with LNK-754 or a vehicle, and brainstem lysates were analyzed by LC3 western blot. This treatment not only normalized LC3-II levels, but also significantly reduced a-syn (Fig. 3-1E). This is consistent with our previous findings that showed reduced a-syn pathology and improvement of motor behavior in DA_{SYN53} mice (Cuddy et al., 2019). Collectively, these data indicate that increased FTase activity contributes to autophagic flux inhibition in PD, and that inhibiting FTase in PD patient iPSn or animal models can rescue autophagy and reduce a-syn.
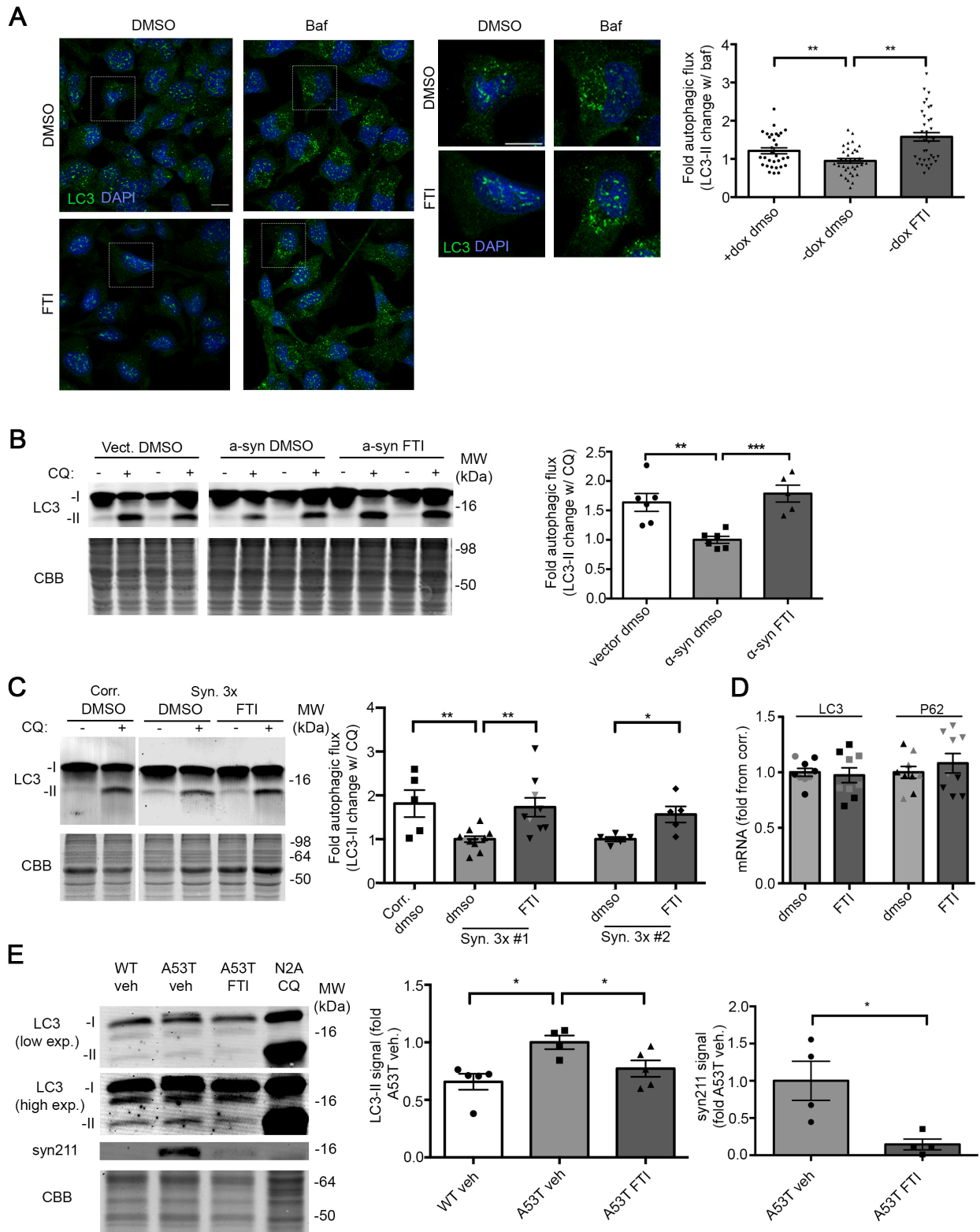
Figure 3-1: Inhibition of farnesyltransferase improves macroautophagy in PD cultures and *in vivo*.

A) Representative images showing LC3 in -dox (high a-syn) H4 cells treated for 3 days with 10 nM FTI and 2 hrs 200 nM Baf (n=30-40; scale bar=12 μm). Nuclear LC3 signal was excluded from quantification. Each point represents a single cell. **B)** Western blot analysis of stably expressing a-syn SH-SY5Y cells treated for 7 days with 10 nM FTI and 72 hrs CQ (n=6). **C)** Western blot analysis of day 90 iPSn to quantify the LC3-II response to CQ following 7 days 10 nM FTI treatment (n=5-11). **D)** RT-PCR analysis of LC3 and P62 mRNA from FTI treated iPSn, normalized to actin (n =4-5). Differently colored points show variation among passages. **E)** Brainstem lysates of 6-month-old DA$_{SYN53}$ mice and littermate controls (WT) receiving 28 days intraperitoneal injections of 0.9 mg/kg FTI or vehicle (n=4-5). N2A cells treated for 24 hrs with 40 μM CQ were included as a positive control to identify LC3-II. Syn211 is a human specific synuclein antibody. For all quantifications, values are the mean +/−SEM. *p<0.05; **p<0.01; ***p<0.001. ANOVA with Dunnett's test was used in panel A, B, C, E (middle graph), using + a-syn / + DMSO as the control condition. Student's t-test was used for panels D and E (right graph).

3.2: FTI rescue depends on ykt6

Since our data indicated that ykt6-SNAP-29 complexes are reduced in PD iPSn leading to reduced autophagic flux (Figure 2-5), we next sought to determine if reducing FTase activity could restore ykt6-SNAP-29 complexes. FTI treatment in *SNCA* triplication iPSn increased the percentage of ykt6-SNAP-29 complexes that co-eluted as a 120Å-sized SEC particle, suggesting increased complex formation (Fig. 3-2A). In fixed a-syn overexpressing H4 cells transfected to express ykt6-GFP and SNAP-29-flag, reducing FTase activity improved the colocalization of ykt6 and SNAP-29, supporting our findings from SEC analysis (Fig. 3-2B). Quantification of immunostained cells for endogenous ykt6 / SNAP-29-flag confirmed increased colocalization with FTI treatment (Fig. 3-3A). Finally, we expressed a ykt6 mutant that resists farnesylation by mutating the farnesyl-modified cysteine residue at position 195 (called ykt6-C195S or CS). Ykt6-CS increased the colocalization with SNAP-29, consistent with increased complex formation (Fig. 3-3B). Ykt6-CS mediated rescue was not further increased by FTI treatment, suggesting that the FTI enhances complex assembly by reducing ykt6 farnesylation rather than reducing the

farnesylation of other proteins (Fig. 3-3B). These data indicate that reducing FTase activity promotes ykt6-SNAP-29 complex assembly and improves autophagic flux in cells that accumulate a-syn.

We further assessed the role of reducing farnesylation on autophagic activity by LC3 western blot analysis. This showed that ykt6-CS rescued autophagic flux in a-syn SH-SY5Y and PD patient iPSn, since the LC3-II response to CQ was more prominent in ykt6-CS expressing cells (Fig. 3-2C, D). We also found that the FTI had no effect on autophagic flux in fixed H4 cells that were transfected with Ykt6 shRNA constructs and immunostained for LC3 (Fig. 3-2E). Western blot analysis of LC3 in both cell lines and PD iPSn models confirmed that ykt6 was required to rescue autophagic flux upon FTI treatment (Fig. 3-2F; Fig. 3-3C). These findings indicate that autophagic flux can be rescued by FTIs through ykt6.

A) Triplication iPSn cultures were treated for 7 days with 10 nM FTI, and lysates were analyzed by SEC / western blot of collected fractions. Percentage SNAP-29 eluting as a complex at 120Å was quantified on the
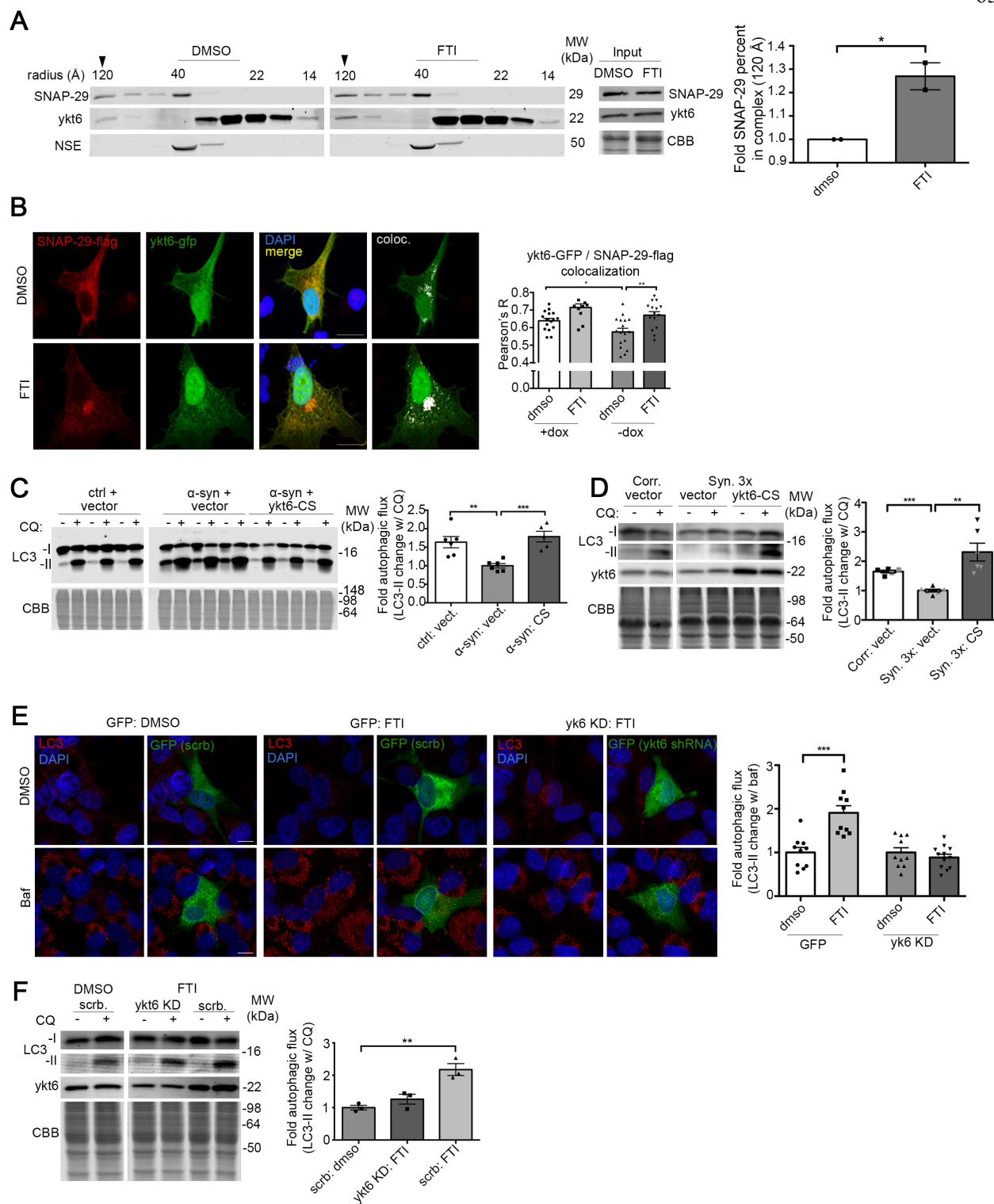
Figure 3-2: FTI rescue of macroautophagy depends on ykt6

right (n=2). **B)** Representative immunofluorescence images of a-syn-overexpressing H4 transfected with SNAP-29-flag and ykt6-GFP treated for 3 days with 10 nM FTI. Quantification of colocalization is shown to the right (n=15-18; scale bar=12 μm). Points represent individual cells. **C)** Stable SH-SY5Y expressing a-syn or empty vector were infected to overexpress constitutively active ykt6-CS for 7 days. Cultures were analyzed by western blot to measure the LC3-II response to CQ. **D)** Triplication iPSn were infected and analyzed as in panel C. Differently colored points illustrate individual passages (n=5-6). **E)** H4 cells cotransfected with ykt6 shRNA and GFP, treated with FTI and Baf as in Fig. 2-5. LC3 intensity was measured in manually selected GFP-positive cells (n=10-12; scale bar=12 μm). **F)** Triplication iPSn infected with ykt6 shRNA (ykt6 KD) or scramble vector (scrb) for 3 days followed by 7 days FTI treatment (n=3). Cultures were extracted and analyzed by western blot to measure LC3-II response. NS, not significant. For all quantifications, values are the mean +/−SEM. *$p<0.05$; **$p<0.01$; ***$p<0.001$). ANOVA with Dunnett's post-hoc test was used for panels B, C, D where the + a-syn / + DMSO or vector condition was considered the control. ANOVA with Tukey's post-hoc test was used for panel F. Student's t-test was used for panels A, E.
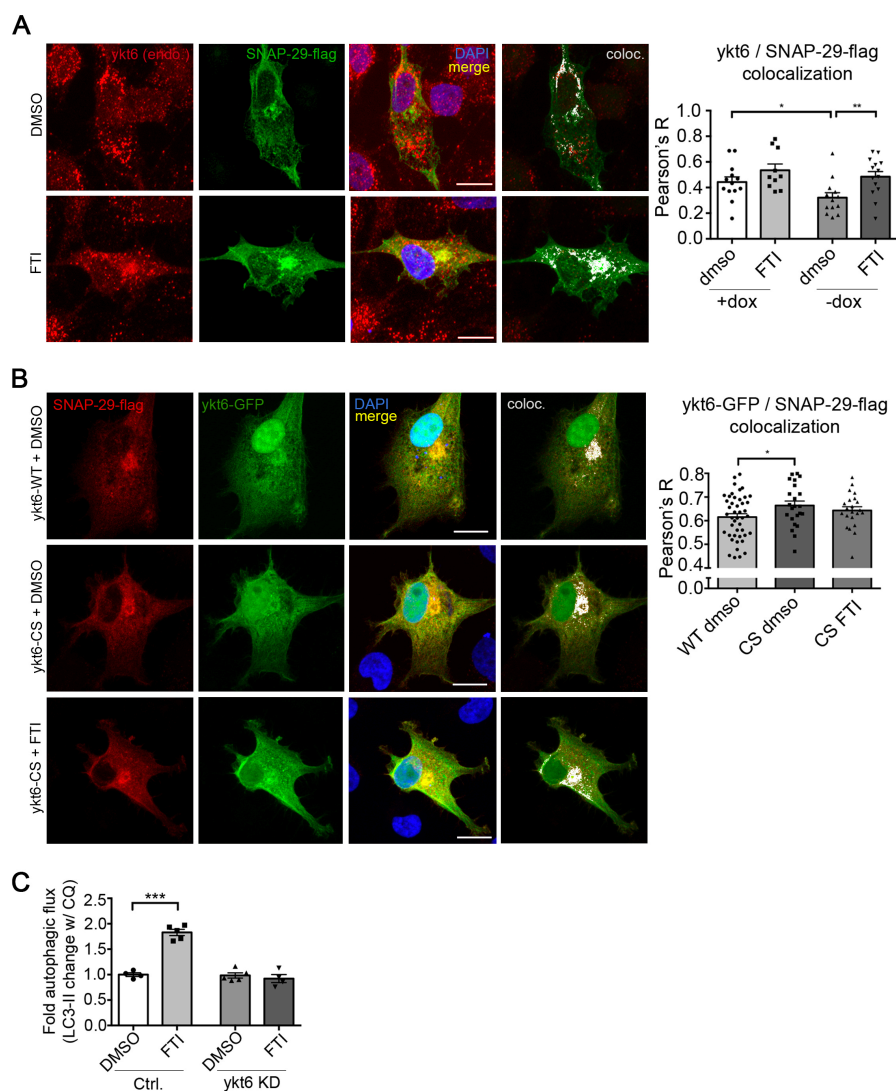
Figure 3-3: Reducing the farnesylation of ykt6 increases ykt6/SNAP-29 colocalization and improves autophagic flux

A) H4 a-syn cells were transfected with SNAP-29-flag and treated with 10nM FTI for 3 days. Cultures were fixed and immunostained to detect endogenous ykt6 and flag, and analyzed for colocalization as in Figure 3-2. **B)** H4 a-syn cells were infected with WT ykt6 or ykt6-CS, with or without FTI. Ykt6 / SNAP-29 colocalization was determined in immunostained cells. **C)** Stable lines of SH-SY5Y cells overexpressing a-syn and either scrambled control (Ctrl) or ykt6 knock-down (KD) were treated with FTI as in figure 3-2. Autophagic flux was determined by measuring the LC3 response to lysosomal inhibitor treatment by western blot (n=5-6). Values are the mean +/- SEM, *p<0.05, **p<0.01, ***p<0.001. ANOVA with Dunnett's post-hoc test where DMSO (-) dox was considered as the control used in panels A and B. Student's t-test used in panel C.

DISCUSSION

Our previous work demonstrated that inactive ykt6 accumulates in the cytosolic fraction of PD patient neurons and that FTase inhibition promotes its active conformation and rescues protein trafficking (Cuddy et al., 2019). Similarly, here we find that inhibiting FTase promotes ykt6-SNAP-29 complexes and restores autophagic flux, suggesting that aberrant FTase activity plays a mechanistic role in autophagy impairment in PD. The dysfunction we describe is attractive for intervention because ykt6 is amenable to pharmacological activation through brain penetrant small molecules, as we demonstrate here with FTI LNK-754. Clinically-validated FTIs are already available for other diseases including progeria (Gordon et al., 2018; Moulder et al., 2004), and it is possible that these agents may be repurposed for the treatment of neurodegenerative disease as ALP activators that function through ykt6. Knocking down ykt6 prevented FTI-mediated rescue of autophagy, and overexpressing ykt6-CS replicated the effect of FTIs (Fig. 3-2), together suggesting that LNK-754 improves autophagy through ykt6. Independently, FTase activity was found to be increased in post-mortem Alzheimer's brain, and its suppression in a mouse model reduced ß-amyloid and neuron loss (Jeong et al., 2021). However, while we found increased FTase in DLB patient cortex, another group reports no difference in this region in PD and decreased FTase in the substantia nigra (Jo et al., 2021). The discrepancy could be due to pathological distinctions between DLB and PD or other technical differences, but developing more robust measures of FTase activity will likely provide clarification beyond protein levels. Increasing farnesylation can also improve phenotypes of PD models induced by loss of Parkin activity through rescuing transcriptional dysregulation (Jo et al., 2021). Therefore, FTI treatment may not be suitable for certain PD sub-types caused by loss of Parkin. Nonetheless, activating ykt6 to stimulate protein clearance by FTIs or other methods may be a viable therapeutic strategy to reduce protein aggregates in multiple types of neurodegenerative diseases including sporadic

synucleinopathies. These therapies may be especially effective in combination with other treatments that synergistically target other elements of the proteostasis pathway (Stojkovska et al., 2021).

While medical and surgical treatments are available to manage PD symptoms, there are currently no disease-modifying therapies capable of reversing its underlying neuropathology. Development of such treatments will likely require a detailed understanding of how basic cellular processes malfunction in response to a-syn accumulation, and one of the most relevant common pathways revealed by genetic studies is the ALP (Chang et al., 2017a; Nalls et al., 2014). Our study highlights the importance of the ALP in PD pathogenesis, and provides a novel therapeutic strategy that simultaneously rescues multiple steps in the autophagic pathway through manipulation of a single SNARE protein.

METHODS

Assays

See Chapter 2 for full details.

FTI treatment in culture

SH-SY5Y and iPSn were treated for 7 days with 10 nM LNK-754 (Link Medicine) in DMSO or DMSO alone. H4 were treated for 3 days. Cell lines had media with fresh compound refreshed daily while iPSn were refreshed every other day. For ykt6 knockdown studies, treatment began 3 days post-infection in iPSn and 1 day post-transfection in H4.

<u>Mouse model</u>

Transgenic a-syn mice

DA$_{SYN53}$ mice expressing human a-syn under the dopamine transporter promoter have been described(Chen et al., 2015) and were graciously provided by the producing lab. Care and genotyping was identical to our previous paper(Cuddy et al., 2019). Housing, breeding, care, and use followed guidelines of Northwestern University's Institutional Animal Care and Use Committee and the US National Institutes of Health Guide to the Care and Use of Laboratory Animals. Standard rodent chow and water were provided ad libitum. Mice were numbered by ear tags and tail samples were collected for genotyping service by Transnetyx at weaning or ~21 days old. Equal numbers of male and females were used for experiments at 6-9 months old. Individuals carrying the A53T transgene were compared with non-transgenic littermates as controls. Animal use was approved by Northwestern IACUC under protocol number IS00011551.

FTI treatment of mice

Mice were injected with LNK-754 (Link Medicine) for 28 days as described previously(Cuddy et al., 2019). They received daily intraperitoneal injections of 0.9mg/kg LNK-754 in 0.5% sodium carboxymethylcellulose (Sigma) or this vehicle alone. After treatment, mice were perfused with PBS, brains rapidly dissected, and brainstem and other regions frozen for analysis. Tissue was lysed in 1% triton buffer and used for western blotting as below. Detection of LC3-II was aided by use of LC3B (Sigma L7543 rabbit 1:500) for 48 hours with CQ-treated mouse cell line N2A used as a positive control.

CHAPTER 4: Developing ykt6 findings towards translation

4.1: FDA-approved FTI lonafarnib activates ykt6 and rescues autophagy flux in PD iPSn

Overview

We have demonstrated that activating ykt6 with FTI LNK-754 rescues autophagy in PD iPSn (Fig. 3-1). The most clinically successful FTI has been lonafarnib, approved by the FDA in 2020 for Hutchinson-Gilford progeria syndrome (HGPS), a childhood pre-mature aging condition characterized by craniofacial abnormalities and fatal vascular disease (Dhillon, 2021). In this rare genetic disorder, mutation of *LMNA* removes a cleavage site from the nuclear membrane protein lamin (De Sandre-Giovannoli et al., 2003). Lamin is normally farnesylated and carboxymethylated before membrane association and subsequently cleaved to remove the modified terminus, but mutant progerin lacks the necessary cleavage site (Gonzalo et al., 2017). Instead it incorporates into the nuclear envelope with modifications still attached and destabilizes the membrane, producing nuclear blebbing and other symptoms of progeria (Gonzalo et al., 2017). Preventing farnesylation of lamin with lonafarnib can reverse some of these effects, lengthening life by reducing cardiovascular complications and strokes (Gordon et al., 2012; Ullrich et al., 2013). Lonafarnib has also been shown to induce autophagy in cancer cell lines but has not been tested in neuronal models (Pan et al., 2008). Stimulating autophagy can rescue cellular phenotypes of cultured fibroblasts derived from HGPS patients by enhancing clearance of progerin protein (Cao et al., 2011). Therefore, the mechanism of lonafarnib may act by both reducing the farnesylation of progerin protein as well as enhancing its clearance through autophagy.

The strategy of targeting farnesylation in PD was prompted in part by the hope that translation could be accelerated by repurposing agents with known safety profiles, and lonafarnib is an ideal case. FTIs were originally designed to treat bladder cancer by inhibiting ras genes, the primary regulators of the MAPK pathway, controlling cell cycling, proliferation, and differentiation (Molina and Adjei, 2006). They are frequently mutated in cancer, particularly lung, colorectal, and genitourinary carcinomas (Prior et al., 2020). This family of small GTPases requires farnesylation at the C-terminus to incorporate into membranes and take on an active GTP-bound conformation (Molina and Adjei, 2006), and compounds were thus designed to prevent farnesylation as an indirect means of reducing oncogenic ras activity (Wang et al., 2017). However, clinical results were disappointing due to the unanticipated functional redundancy of geranylgeranyltransferase on K-ras (Moore et al., 2020), and following studies have focused on more specific mutations. Clinical trials for malignancy (Khuri et al., 2004) and HGPS (Kieran et al., 2007) have found a consistent toxicity profile for lonafarnib. In children, a range of dosages below the adult maximum tolerable dose of 200 mg/m^2 produced no more than mild side effects (Kieran et al., 2007), and effective doses for HGPS were significantly lower at 115 mg/m^2 and 150 mg/m^2 (Gordon et al., 2016; Gordon et al., 2012). When they did appear, the most common side effects were nausea, vomiting, diarrhea, and fatigue and could be relieved with standard supportive treatments (Gordon et al., 2016; Gordon et al., 2012; Kieran et al., 2007). As the furthest clinically developed FTI, we hypothesized lonafarnib could be repurposed for PD treatment. We therefore began testing whether lonafarnib treatment had the same effects on ykt6 and autophagy as LNK-754, as the compounds belong to different chemical classes. LNK-754 is defined by one bicyclic ring and three monocyclic rings, including an imidazole group, while lonafarnib is a non-imidazole compound characterized by a tricyclic core (Shen et al., 2015). These preliminary results are

presented in section 4.1. We found that lonafarnib treatment causes ykt6 to localize to membranes similar to LNK-754 and is also capable of rescuing reduced autophagy in PD iPSn.

Results

We first sought to assess lonafarnib's ability to target ykt6 with our established method of ykt6 membrane localization (Cuddy et al., 2019). Protein lysates from two a-syn overexpressing SH-SY5Y lines treated with lonafarnib were fractionated into their cytosolic and membrane-localized components. Lonafarnib treatment increased ykt6 in the membrane to a similar extent as previously found using ykt6-CS and LNK-754 (Fig. 4-1A) (Cuddy et al., 2019). Different concentrations were used because of the different binding efficiencies of each compound (IC_{50} LNK-754=0.86, IC_{50} lonafarnib=1.9) (Shen et al., 2015). We then compared the effects of lonafarnib and LNK-754 on HDJ-2 farnesylation at the doses used for ykt6 shift and found that lonafarnib produced a greater reduction in the farnesylated form (Fig. 4-1B). Finally, lonafarnib treatment rescued autophagic flux in multiple *SNCA* triplication iPSn lines, similar to LNK-754 (Fig. 4-1C). Repeated findings with two chemically distinct compounds substantiate FTase inhibition as the primary driver of autophagy rescue, and these results in sum suggest that lonafarnib is well-suited to repurpose for therapeutically targeting ykt6.
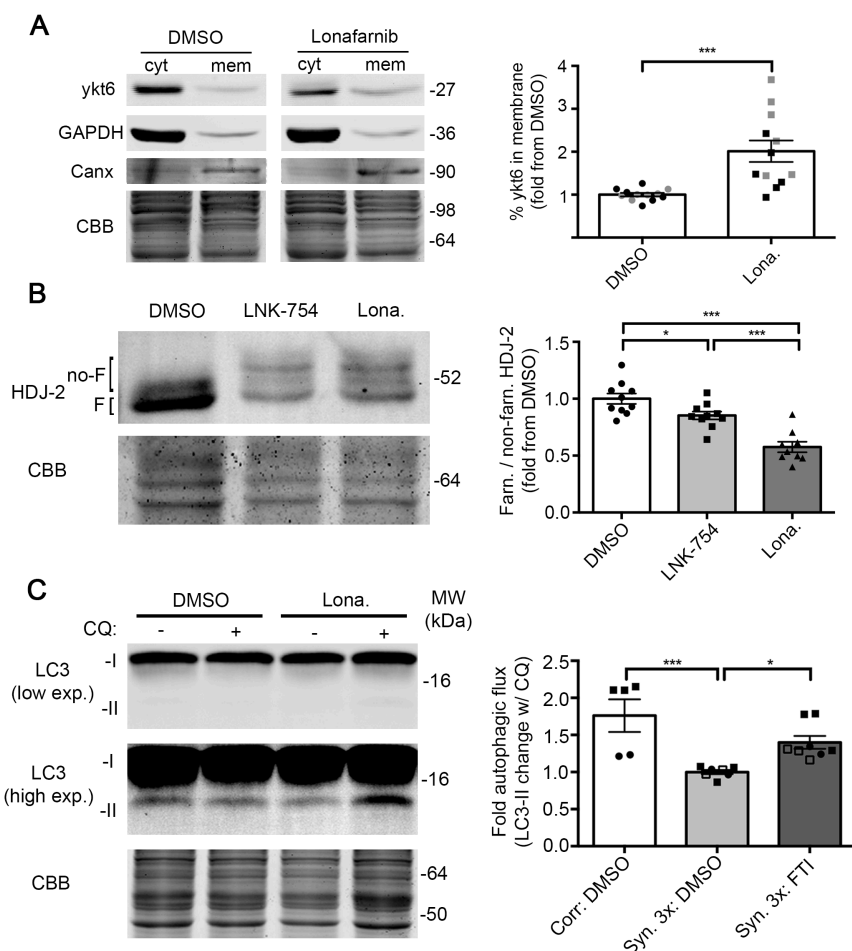
Figure 4-1: Lonafarnib increases ykt6 membrane localization and rescues autophagic flux in PD iPSn.

A) Representative western blot showing fractionated protein lysates from a-syn overexpressing SH-SY5Y cells treated for 7 days with 240 nM lonafarnib. CBB was used as a loading control, GAPDH was used as a marker of cytosolic (cyt) fractionation, and calnexin (canx) was used as a marker of the membrane bound (mem) fraction. Graph shows fold percentage of ykt6 in the membrane fraction out of the total in both fractions. Differently shaded points represent two distinct a-syn overexpressing lines (n=12). Student's t-test was used. **B)** WT a-syn overexpressing SH-SY5Y were treated for 7 days with 10 nM LNK-754 or 240 nM lonafarnib. Western blot shows HDJ-2 separated into farnesylated (F) and non-farnesylated (no-F) forms. Graph compares the ratio of farnesylated to non-farnesylated HDJ-2 for each condition (n=9-10). Results analyzed with one-way ANOVA using Tukey's multiple comparisons test. **C)** Western blot flux analysis of day 90 – 120 PD iPSn treated for 7 days with 240 nM lonafarnib. Flux measured with LC3-II response to chloroquine (CQ) as previously. Data point shapes represent different patient Syn. 3x lines (n=2-4). Results analyzed with ANOVA and Dunnet's post-hoc test using Syn. 3x DMSO as control. Values are the mean +/−SEM. *p<0.05; **p<0.01; ***p<0.001

4.2: Developing ykt6 membrane localization as a blood biomarker

Overview

Another challenge in developing effective disease-modifying therapy is the need to treat early in disease and with optimized individual dosages. Because significant neuron loss has occurred by the time traditional motor symptoms (e.g. tremor, bradykinesia) of PD become obvious, earlier predictors are needed to provide time for intervention. Markers that have been evaluated fall into three broad categories: clinical, imaging, and biochemical (Lotankar et al., 2017). Clinical markers include non-motor symptoms of the prodromal syndrome such as olfactory dysfunction, constipation, and mood disorders, although they generally lack the specificity necessary for useful prediction of PD conversion without other tests (Li and Le, 2020). Among these, one of the most useful currently is REM sleep behavior disorder (RBD). This disorder is characterized by complex motor behaviors and acting out dreams during REM sleep (St Louis and Boeve, 2017). Five years after diagnosis, about $15 - 35\%$ of patients will be diagnosed with a synucleinopathy, and after 12 years a reported $40 - 80\%$ of patients phenoconvert (Iranzo et al., 2013; Jozwiak et al., 2017; Postuma et al., 2009; St Louis and Boeve, 2017). Imaging techniques allow more sensitivity and include MRI, transcranial sonography, and PET focused on SNc changes and dopamine metabolism (Lotankar et al., 2017). While sensitive, these tests are expensive, require specialized equipment, and may expose patients to radiation (Parnetti et al., 2019).

Biochemical markers have been studied in the cerebrospinal fluid (CSF) and the blood. While CSF has the benefit of physically interacting with the brain, its collection by lumbar puncture carries some risk and requires a skilled technician. For a measure that may be repeated to follow treatment efficacy, cost and availability make blood an ideal marker. Much interest has

focused on the predictive value of a-syn levels in CSF and blood, and such studies showed that red blood cells (RBCs) contain the large majority of a-syn in the circulation (Barbour et al., 2008). When overall abundance proved insufficient for prognostication, focus shifted to pathogenic forms such as oligomeric and misfolded a-syn (Daniele et al., 2018; Shahnawaz et al., 2017). While these studies have shown promise, further validation and optimization will be needed before widespread use (Parnetti et al., 2019). Lysosomal enzyme function has also been investigated as a biochemical marker, but similarly requires more development (Parnetti et al., 2017). Given the benefits and drawbacks of each test, optimal early prediction will likely include some combination of these modalities.

Ykt6 could be used as an additional marker given its measurable shift from the cytosol to membranes (Fig. 4-1A). We somewhat unexpectedly found that ykt6 could be measured in fractionated mouse RBCs and that it was shifted to membranes following LNK-754 treatment (Fig. 4-2A). This prompted us to explore the use of ykt6 as a blood biomarker in humans with two goals: first, to measure and predict progression of disease, and second, to measure FTI activity throughout treatment. Preliminary results are presented in section 4.2. While consistent methods were developed, preliminary data show no difference between PD patients, RBD patients, and healthy controls.

Results

DA$_{SYN53}$ mice were injected intraperitoneally with LNK-754 or a vehicle for 28 days as described previously (Chapter 3). RBCs extracted from the treatment group at sacrifice and fractionated into cytosolic and membrane proteins exhibited a higher proportion of ykt6 present in membranes (Fig. 4-2A). Methods were then optimized for use in human samples. First, fresh RBCs

extracted from finger prick samples were lysed using different mechanical methods, and it was found that freeze/thaw cycling produced the clearest separation between cytosolic marker GAPDH and RBC-specific membrane marker Band3 (Fig. 4-2B). Then collection was tested using standard phlebotomy and evacuated collection tubes designed to stratify peripheral mononuclear blood cells from RBCs (BD Vacutainer CPT). This method produced consistent measures of ykt6 localization from one collection to another for a single patient (Fig. 4-2C) and similar values between three healthy patients (Fig. 4-2D). Overnight refrigerated storage did not affect values (Fig. 4-2E), expanding practical clinical application. Using this protocol, RBCs were collected with other matched biological samples from idiopathic PD patients and patients exhibiting RBD alone. No difference in ykt6 localization was observed between either of these groups compared with healthy controls, nor was membrane ykt6 significantly correlated with age (Fig. 4-2F).
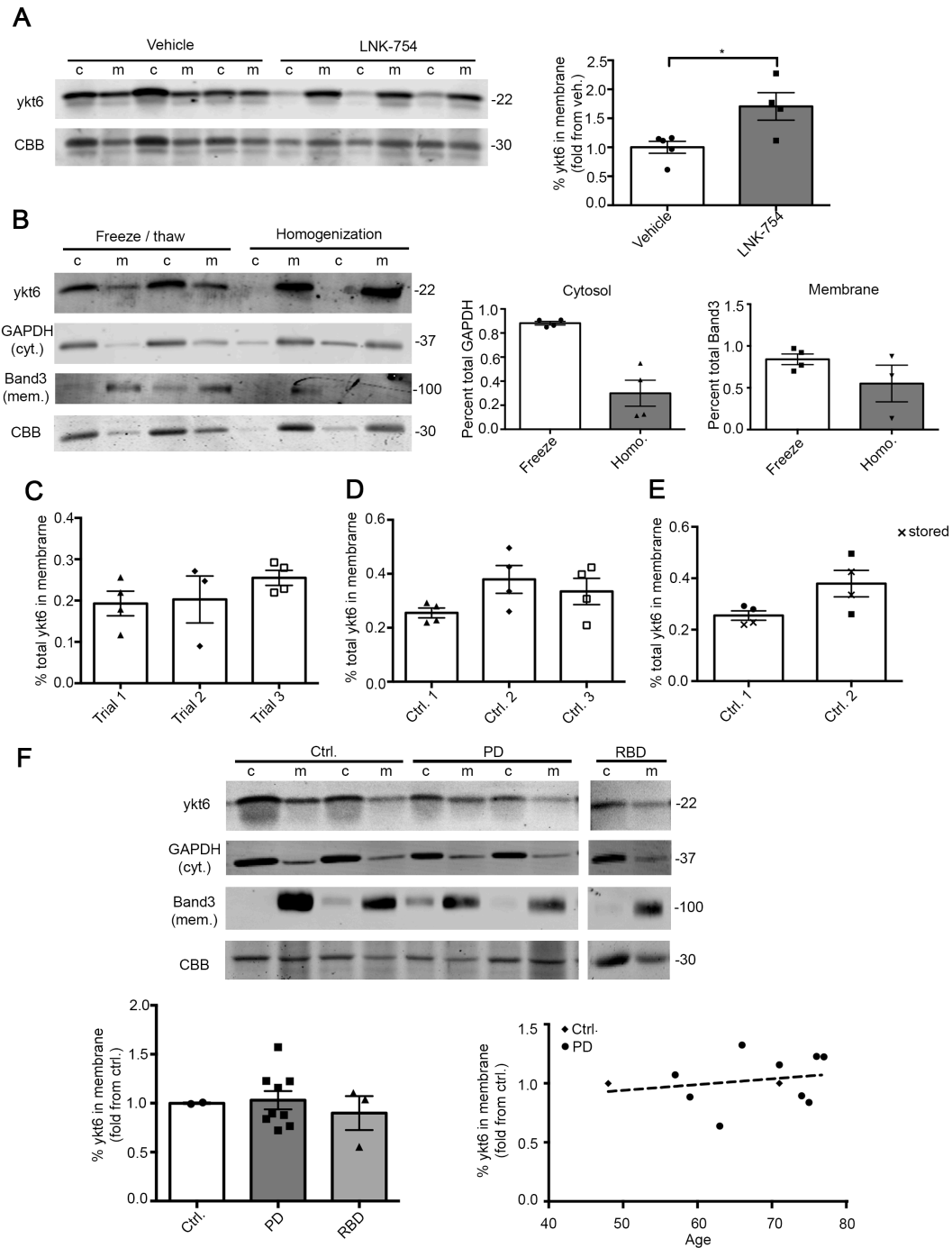
Figure 4-2: Development of ykt6 membrane localization as a marker in human red blood cells (RBCs)

A) Western blot analysis of cytosolic (c) and membrane (m) extracts of DA$_{SYN53T}$ mice treated for 28 days with 0.9 mg/kg LNK-754. Percent membrane ykt6 was analyzed as in Fig. 4-1 (n=4-5; Student's t-test). **B)** Western blot showing RBCs of healthy control patients fractionated with either 3 freeze / thaw cycles or homogenization.

GAPDH is a cytosolic marker, and Band3 is a membrane marker. Percent of each marker in their respective fractions is shown in the graphs. **C)** Quantification of ykt6 localization in RBCs collected from one healthy control on three separate dates. **D)** Quantification of ykt6 localization measured by western blot from three healthy controls. **E)** Quantification of ykt6 localization from 2 healthy controls collected in BD Vacutainer CPT tubes and processed immediately or stored overnight at 4°C (x=stored). **F)** Representative western blot showing ykt6 fractionation as in (A) in patients diagnosed with PD or REM sleep behavior disorder (RBD). Left graph shows ykt6 percentage in membrane as previously (Control n=2; PD n=9; RBD n=3). ANOVA with Tukey's post-hoc test was used. Right graph represents ykt6 membrane percentage as a function of age. Controls are represented by diamond points. Linear regression analysis was performed. Values are the mean +/−SEM. *p<0.05.

DISCUSSION

Here we show two ways in which our basic ykt6 farnesylation findings may be developed for clinical use. First, we found that FDA-approved FTI lonafarnib produced the same effects as LNK-754, both increasing ykt6 membrane localization and rescuing a-syn-induced autophagy flux defects. This suggests that FTase inhibition may be a general strategy for enhancing autophagy with lonafarnib as a prime candidate for application. Second, we show that ykt6 localization can be reliably measured in human RBCs. Although we found no differences in PD and RBD patients compared to controls, mouse data suggest that FTI treatment may produce an effect that allows treatment monitoring.

With LNK-754 as proof of concept for the beneficial effects of decreasing ykt6 farnesylation, our approach to developing lonafarnib was to test its action in several of our established assays. Lonafarnib was able to target ykt6 as measured by increased localization to membranes of differentiated a-syn-overexpressing SH-SY5Y. The effect was similar to our previously published findings with LNK-754 (Cuddy et al., 2019), in the range of a 1.5- to 2-fold increase in membrane ykt6. HDJ-2 shift was used as an indirect measure of FTase activity to test

whether similar inhibition was achieved at the doses of LNK-754 (10 nM) and lonafarnib (240 nM) used for ykt6 experiments. Lonafarnib had previously been shown to reduce HDJ-2 farnesylation in an ovarian cancer cell line (Taylor et al., 2008) and peripheral blood samples (Kieran et al., 2007) and produced the same shift in a-syn overexpressing SH-SY5Y. However, despite a similar range of effects on ykt6 shift, lonafarnib appeared a more potent effector of HDJ-2. From these preliminary results, it is unclear if the distinction is due to a true difference on global FTase activity, farnesylation specific to ykt6 or HDJ-2, or a difference in relative dosages of each drug. These drugs are chemically distinct and have different enzyme binding affinities that may affect FTase activity (Shen et al., 2015), so determining an explanation may require a more direct assay evaluating purified FTase activity *in vitro* (Cassidy et al., 1995; Hougland et al., 2010). LNK-754 is a generally more potent inhibitor with an IC_{50} of 0.86, while that of lonafarnib is 1.9 (Shen et al., 2015). Lonafarnib finally successfully rescued decreased LC3-II flux in *SNCA* triplication iPSn. Induction of autophagy has been demonstrated in osteosarcoma and pancreatic cancer cell lines using a 10-fold higher dose (Pan et al., 2008), but this is the first evidence in human neurons. Similar rescue using two distinct FTIs suggests that it results primarily from the effect of FTase inhibition rather than other unknown mechanisms. Further work will be necessary to determine lonafarnib's effects on other ykt6 functions such as ER-Golgi trafficking, as well as therapeutic endpoints such as a-syn reduction and neuron viability. These findings remain limited by their small scale but show that lonafarnib can be developed further using insights from LNK-754 treatment.

We found that ykt6 localization could be reliably measured in human RBCs sampled with standard clinical phlebotomy. LNK-754 treatment produced a shift in mouse blood in tandem with brain changes (Cuddy et al., 2019), although this finding is limited by its small sample size. For

applications like flow cytometry, RBC contamination is removed by osmotic lysis. However, we opted for mechanical disruption to maintain some membrane integrity and match our established methods. Freeze / thaw cycling appeared optimal for lysing cytosolic components while maintaining separation of membrane markers. While cell type and plasma fractionation of whole blood is commonly practiced, sequential extraction of intracellular fractions has not been, so this represents a step forward in optimizing the methodology. As mature erythrocytes lack secretory pathway organelles (Moras et al., 2017), the function of ykt6 in the remaining cell membranes is unclear. Ykt6 may play a role at the plasma membrane in cells generally, or its trafficking functions may be adapted non-traditionally in the unique erythrocyte environment. In *Drosophila* oocytes, ykt6 disruption produced changes at the plasma membrane consistent with altered endo- and exocytosis (Pokrywka et al., 2022), so perhaps ykt6 is retained in RBCs for similar functions. Our pilot study has yet found no difference in membrane localization between healthy controls and PD or RBD patients. The data is limited by the small number of controls and RBD patients, so it may be that higher power will provide more informative data. Toxic forms of a-syn may also not reach the threshold in RBCs necessary to affect ykt6, or other sources of variation may have a larger impact in peripheral circulation. In neurons, a-syn associates with ykt6 near the cis-Golgi and autolysosomes, neither of which are present in RBCs. a-Syn in RBCs may not have the opportunity to interact with ykt6 without such structures. Ykt6 might also be an early victim of dysfunction that only appears in uniquely vulnerable DA neurons. Any of these explanations decreases the potential of ykt6 as a peripheral biomarker, but future studies may investigate predictive shifts in PBMCs or CSF. It may still be a useful measure of FTI treatment efficacy (Fig. 4-2A), and experiments assessing the effects of lonafarnib in mice are ongoing.

METHODS

Lonafarnib treatments

For membrane shift experiments, SH-SY5Y overexpressing WT or myc-tagged a-syn as described were differentiated with 20 uM retinoic acid and treated with 240 nM lonafarnib for 7 days. Cytosolic and membrane bound proteins were fractionated by sequential extraction as described previously (Cuddy et al., 2019). For HDJ-2 assay, WT a-syn SH-SY5Y were treated for 3 days with 240 nM lonafarnib or 10 nM LNK-754. HDJ-2 forms were separated by western as described in Chapter 2. iPSn were treated with 240 nM lonafarnib for 14 days replaced every other day. Wells were treated with chloroquine and LC3 flux assessed as in Chapter 2.

Sample requisition

Biospecimens used in the analyses presented in this article were obtained from the Movement Disorders Center (MDC) Biorepository (Northwestern Medicine). As such, the investigators within MDC Biorepository contributed to the design and implementation of the MDC Biorepository and/or provided data and collected biospecimens but did not participate in the analysis or writing of this report. MDC Biorepository investigators include Tanya Simuni, MD; Dimitri Krainc, MD PhD; Opal Puneet MD, PhD; Cindy Zadikoff, MD; Onur Melen, MD; Danny Bega, MD; Roneil G. Malkani, MD; Steven Lubbe, PhD; Niccolo Mencacci, MD, PhD; Christina Zelano, PhD; Joanna Blackburn, MD; Firas Wehbe, MD, PhD; Lisa Kinsley, MS, CGC; Tina Ward, MS.

RBC fractionation

Prior to perfusion, blood was collected from treated DA_{SYN53T} mice by cardiac puncture in microcentrifuge tubes with 10 uM EDTA. RBCs were separated by centrifugation at 2200x g 4°C for 10 minutes and plasma and buffy coat removed by pipet. RBCs were washed three times in

cold 1X PBS with 5-minute centrifugation. The RBC pellet was resuspended in one volume of 1X PBS with PIC, NaF, NaVO4, and PMSF using extensive pipetting. Samples were frozen and thawed 3 times to lyse cells and ultracentrifuged at 100,000 g for 30 minutes 4°C. The supernatant was collected as the cytosolic fraction and the remaining pellet was resuspended in one volume of 1% triton buffer with PIC, NaF, NaVO4, and PMSF. Samples were incubated in ice slurry for 30 minutes, ultracentrifuged as before, and supernatant was collected as the membrane fraction.

For initial human samples, ~200 ul of blood was collected from healthy volunteers by finger prick. Blood was collected in EDTA containing microcentrifuge tubes and RBC pellet washed as with mouse samples. This was processed by sequential extraction as described with the following addition: for selected samples, freeze / thaw was replaced with homogenization using a motor driven Teflon homogenizer at 4000 RPM ~20 times in a conical glass vessel. PBS extraction volume was also increased to 2 volumes going forward.

For phlebotomy samples, 5-7 mL of blood was collected in BD Vacutainer CPT tubes with sodium heparin following manufacturer's directions. Tubes were centrifuged at 25°C 1500 g for 30 minutes. Supernatant was removed and RBCs under membrane were collected and washed as above.

To calculate ykt6 percent localization, ykt6 signal was first normalized to CBB and the triton lane signal was divided by the sum of PBS and triton signals.

CHAPTER 5: Summary and Discussion

The ALP is one of the most important common pathways implicated in PD pathogenesis by genetic studies (Chang et al., 2017a; Nalls et al., 2014). Cell line and animal models have previously demonstrated that WT a-syn can dysregulate MA (Chen et al., 2015; Tanik et al., 2013; Winslow et al., 2010), but the mechanism of inhibition and specific autophagic processes affected have been uncertain. Identifying a mechanism in human neurons may provide one access point to intervene in the vicious loop a-syn promulgates to collapse proteostasis (Mazzulli et al., 2011). Given recent descriptions of SNARE ykt6 as a key player in autophagy (Bas et al., 2018; Gao et al., 2018; Matsui et al., 2018; Takáts et al., 2018) and our finding that a-syn disrupts ykt6 activation (Cuddy et al., 2019), we hypothesized that this association may also explain a-syn's inhibition of MA and that flux could be rescued by targeting ykt6. Because protein aggregation and disrupted ALP are common features of age-related neurodegeneration, understanding this mechanism should promote new approaches for other diseases as well.

5.1: Ykt6 and autophagy in PD neurons

Our results indicate that efficient MA degradation is reduced in PD neurons through decreased activity of ykt6 in autolysosome fusion. MA regulation is especially vital in the specialized environment of the neuron compared to a rapidly dividing cell line (Benito-Cuesta et al., 2017; Larsen and Sulzer, 2002; Maday and Holzbaur, 2016), so we set out to investigate the effects of endogenous a-syn overexpression in dopaminergic human iPSn with CRISPR-corrected controls. Previous assessments of a-syn's effects on autophagy have focused on cell lines and primary mouse cultures (Tanik et al., 2013; Winslow et al., 2010), but we show for the first time that endogenous synuclein similarly inhibits flux in human iPSC-derived neurons (Fig. 2-1). Inhibition occurred through chronically accumulating WT a-syn, implicating this process in the

pathogenesis of idiopathic PD. Reduced MA significantly only appeared when iPSn were matured to 90 days in culture; no difference was observed at day 60 (Fig. 2-1). This mirrors aging as a risk factor for PD as well as findings of a general age-related decline in autophagy (Chang et al., 2017b; Fernandez et al., 2018; Lipinski et al., 2010). A previous study reports increased autophagy in day 30 PD iPSn (Oliveira et al., 2015), so it may be that the ALP is activated before the burden of disease reaches a threshold and gradually fails as a-syn increases. Because a-syn is processed by MA (Vogiatzi et al., 2008), its inhibition may set up a feedback loop that reinforces further a-syn accumulation, as with GCase maturation.

Like us, another group recently located a-syn's inhibition of MA to reduced autolysosome fusion using LUHMES cells, although they attribute this to decreased SNAP-29 abundance (Tang et al., 2021) which we did not observe in iPSn (Fig. 2-5F). We expected autophagosome synthesis to be disrupted as well based on ykt6's role in yeast (Nair et al., 2011), but were surprised to find this process appeared non-contributory in our models. It may be that ykt6 is uninvolved in formation in human neurons or that dysfunction at this stage was masked by more significant disruption at autolysosome fusion. The complete multi-lamellar vesicles we observed with electron microscopy may suggest that autophagosomes are being formed but incorrectly recognized or processed with multiple attempts at engulfment (Fig. 2-3E). Future work could investigate necessary targeting mechanisms and the activity of selective autophagosome-lysosome tethers (Kirkin and Rogov, 2019; Lorincz and Juhasz, 2020). While discrepancies remain to be resolved, zeroing in on the SNAP-29 / ykt6 fusion SNARE complex as a target is a substantial step toward preventing a-syn's harmful effects on the ALP.

Built on the description of this complex in yeast (Bas et al., 2018; Gao et al., 2018), HeLa cells (Matsui et al., 2018), and *Drosophila* (Takáts et al., 2018), our results confirm its importance

in human neurons and relate biochemical insights to a disease mechanism. We found the same association between ykt6 and SNAP-29 but also show that this is reduced with high a-syn (Fig. 2-5). This matches our previous finding that a-syn exerts pathogenic effects by interfering with ykt6 SNARE complexes necessary for hydrolase trafficking (Cuddy et al., 2019). For the first time in human neurons, we found that knocking down ykt6 reduced MA flux (Fig. 2-5A-B) while overexpressing ykt6-CS increased flux (Fig. 3-2E); i.e. ykt6 activity is both necessary and sufficient for driving autophagy. Ykt6 appears particularly vital for neurons as knockdown produced a large effect in iPSn (Fig. 2-5A) with little change in H4 (Fig. 3-2D). It remains unclear how the redundant role of Stx17 described in HeLa (Matsui et al., 2018) may compensate for ykt6 in various cell types. These SNAREs alternatively might be used preferentially under specific cellular conditions, for example basal autophagy versus the stress response, or used selectively for autophagosomes matching specific sizes and cargoes (Lorincz and Juhasz, 2020). Future work to address this may study the effects of knocking down each factor individually and in combination in iPSn. Our findings thus extend knowledge of a unique SNARE's conserved role in cell biology and indicate a mechanism for a long-observed phenomenon in PD.

5.2: FTase and inhibition

Disruption of autolysosomal fusion represents an intervention point for therapy because ykt6 activity can be increased with small molecules, as we demonstrate here with LNK-754 and lonafarnib. We found FTase to be increased in disease (Fig. 2-6), perhaps aberrantly locking a greater proportion of ykt6 in its closed, farnesylated form. This matches findings of increased FTase activity in post-mortem Alzheimer's brain and rescue of pathology in a mouse model through its suppression (Jeong et al., 2021). However, while we found increased FTase in DLB patient cortex, another group reports FTase to be unchanged in this region in PD (Jo et al., 2021).

As of now, it remains unclear if this represents a true pathologic distinction or the result of technical variability. Because activating FTase was found to be beneficial in a reduced Parkin model (Jo et al., 2021), it may be that FTI treatment is not suitable for all PD subtypes, but further work will be necessary to determine the effects of individual mutations.

Lonafarnib has already been clinically validated in progeria (Moulder et al., 2004), and inhibitors of FTase may also be repurposed for PD as ALP activators that function through ykt6. The fact that knocking down ykt6 prevented FTI effectiveness and overexpressing ykt6-CS replicated its rescue strongly suggests that LNK-754 works through this SNARE (Fig. 3-2). Lonafarnib's similar effect on autophagy (Fig. 4-1) suggests that FTase inhibition rather than off-target activity is the primary mechanism of rescue. High dose lonafarnib was previously shown to induce autophagy in cancer lines (Pan et al., 2008), but this is the first evidence in human neurons. Other work suggests phosphorylation is a primary driver of ykt6 activity through promotion of its open form (McGrath et al., 2021). We selected our approach mainly for the availability of drugs targeting farnesylation and found benefits here as previously (Cuddy et al., 2019), but this does not exclude other possibilities. Activating ykt6 by these and other methods should be investigated for therapeutic use in PD, especially in combination with synergistic treatments targeting other elements of the early secretory pathway (Stojkovska et al., 2022).

Our findings indicate that targeting ykt6 has the benefit of amplifying two processes perturbed in PD: both ER-Golgi trafficking and autolysosomal fusion (Fig. 5-1). We previously found that a-syn's inhibition of ykt6 SNARE complexes disrupts trafficking of lysosomal hydrolases and reduces lysosomal activity (Cuddy et al., 2019). Here we find that a-syn's inhibition of the ykt6-SNAP-29 complex similarly reduces autophagy by preventing autophagosome fusion with lysosomes. Ykt6 activity in these roles could be increased by expression of the ALP master

regulator TFEB (Cuddy et al., 2019). Under healthy conditions, this system may be intended to coordinate delivery of lysosomal enzymes with the arrival of autophagy substrates in response to cellular stress. TFEB regulates the ALP by directing transcription of a suite of genes related to lysosomal function, termed the Coordinated Lysosomal Expression and Regulation (CLEAR) network (Napolitano and Ballabio, 2016; Sardiello et al., 2009). When TFEB is overexpressed, cells increase their number of lysosomes and capability to degrade protein aggregates (Sardiello et al., 2009). This is accompanied by increased numbers of autophagosomes and fused autolysosomes, indicating coordination of substrate delivery with lysosomal function (Settembre et al., 2011). Our findings are among the first to identify ykt6 as an important factor in this coordination. Total ykt6 levels were not changed by TFEB overexpression, but its membrane localization was increased (Cuddy et al., 2019), so it is likely indirectly regulated by an effector in the CLEAR network. Future studies may investigate whether FTase activity is regulated by TFEB or search for other CLEAR factors that increase ykt6 localization.

Evidence suggests that lysosomal stress promotes CLEAR network and ykt6 activation. For example, sucrose treatment as a model of lysosomal stress increased TFEB nuclear localization (Song et al., 2013) as well as ykt6 in membranes (Cuddy et al., 2019). Ykt6 was similarly activated by other sources of lysosomal inhibition through Baf, NH_4Cl, and GCase inhibitor CBE (Cuddy et al., 2019). TFEB expression in turn was sufficient to increase GCase trafficking and lysosomal activity (Cuddy et al., 2019). In disease, the cell may chronically activate this response to cope with intracellular aggregates, but the inhibitory effects of a-syn may prevent the system from working effectively. Considering mechanisms of activation, mTORC1 is the most well-studied regulator of TFEB, although mTORC1-independent mechanisms also exist (Napolitano and Ballabio, 2016). Under normal conditions, amino acids activate mTORC1 at the lysosomal

membrane to phosphorylate TFEB (Sancak et al., 2010), which is then sequestered in an inactive cytosolic state. Stressors such as starvation and hypoxia inhibit mTORC1's kinase activity (Sengupta et al., 2010), and release of lysosomal calcium activates phosphatase calcineurin, allowing dephosphorylated TFEB to enter the nucleus and promote transcription (Medina et al., 2015). Similar mechanisms using the lysosome as a central hub may transduce stress signals to activate ykt6 coordination when needed, and a future more in-depth pathway analysis may reveal further elements of a ykt6-coordinated stress response pathway. FTIs such as lonafarnib could take advantage of this system by targeting a single protein to simultaneously drive two arms of the endogenous ALP and reduce aggregates (see Fig. 5-1).
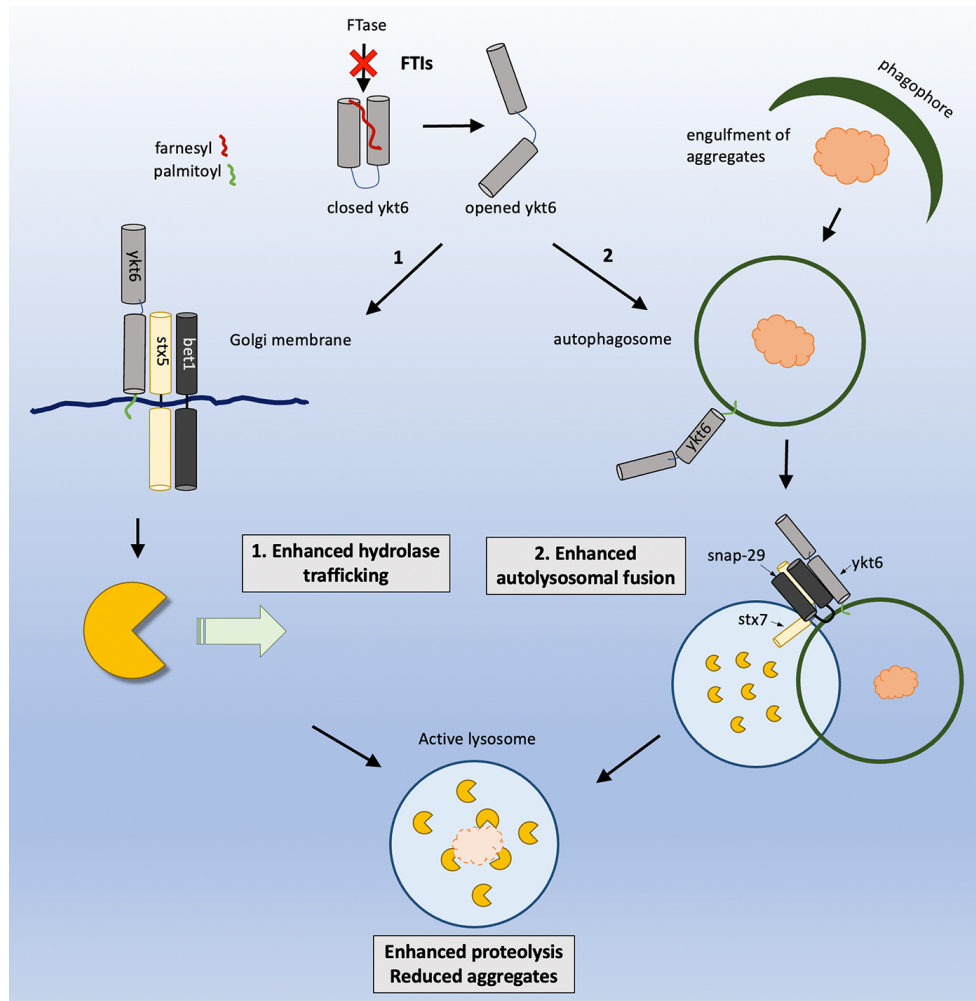
Figure 5-1: a-Synuclein perturbs the autophagic-lysosomal system through ykt6 and simultaneous blockade of lysosomal hydrolase trafficking and autophagic cargo delivery into lysosomes.

5.3: Limitations

There are limitations to our work. The multiplied region in *SNCA* triplication carriers includes other genes of largely unknown function that may contribute to disease, although our isogenic correction of a-syn should eliminate this variable. A trade-off of neural specificity in 2D iPSn culture findings is their inability to model the role of other cell types in neurodegeneration. While we have made efforts to match findings from iPSn with *in vivo* studies, the number of mice

tested remains small, and a full analysis of autophagy phenotypes in DLB brain was not performed. Particularly, we did not extend our investigation in any model to upstream regulators of MA such as mTORC activity. The number of subjects used for RBC studies was similarly limited. Mice were our only model to express mutant A53T a-syn instead of wild type, and each subtype may challenge the ALP in unique ways (Cuervo et al., 2004; Tanik et al., 2013; Vogiatzi et al., 2008). In any such study, it is difficult to isolate a primary dysfunction while accounting for compensatory upregulation of other processes. As well as MA, pathogenic a-syn is handled by chaperone-mediated autophagy, the proteasome, and exosome secretion (Burbidge et al., 2021; Cuervo et al., 2004; Klucken et al., 2012; Tanik et al., 2013; Vogiatzi et al., 2008; Webb et al., 2003), and crosstalk between these pathways further complicates the picture (Appenzeller-Herzog and Hall, 2012; Tanida et al., 2004; Wu et al., 2015). In turn, a-syn has been shown to disrupt the ALP at multiple steps beyond autolysosome fusion, for instance through direct interaction with essential lysosomal machinery (Cuervo et al., 2004; Freeman et al., 2013; Yap et al., 2013) and prevention of hydrolase maturation through the early secretory pathway (Cuddy et al., 2019; Mazzulli et al., 2011; Mazzulli et al., 2016; Stojkovska et al., 2022).

Perhaps the most pressing limitation is the possibility for unanticipated effects of LNK-754 or lonafarnib FTase inhibition. We have shown that rescue depends on ykt6, does not affect transcription of autophagy markers, and is effective in nanomolar-range doses designed to avoid unwanted activity, but we cannot rule out all off-target effects. This includes potential negative effects in other cellular processes regulated through farnesylation, notably Ras-driven signaling and growth (Casey and Seabra, 1996). However as noted, the safety profile of lonafarnib is well-documented, so the adverse effects appear minimal if multiple targets are affected. The variability of LNK-754 and lonafarnib on HDJ-2 farnesylation may become important here, especially in

determining optimal dosing for each compound to affect ykt6 without hitting other targets. Development of RBC membrane localization as an indicator of ykt6 activity may prove useful in achieving this balance.

5.4: Future directions

Further work will be necessary to address such limitations and the broader implications of our findings. Despite the importance of ykt6 in vesicular processes, many fundamental questions remain regarding its regulation and interactions. The factors that signal its opening for activation and targeting to specific membranes have still not been identified. If one wishes to disrupt the ykt6 / a-syn association, investigation may also determine which domains and amino acids are required. *In vitro* studies and expression of binding-deficient mutants may be used to demonstrate the interaction and its contribution to pathogenesis more directly. We have focused on WT a-syn here, but further work may investigate if the same MA phenotypes occur with mutant a-syn and other PD mutations such as LRRK2, particularly to distinguish if this represents a primary insult or common disease endpoint. We report increased FTase protein without increased transcription, so contributors to FTase stability and degradation may be investigated further. As interest in this enzyme's relationship to neurodegenerative disease grows, it would be valuable to develop measures of FTase activity suitable for different models and to explore the factors regulating its activity. a-Syn's contribution to this process may also be investigated.

The end goal of investigating FTase and the autolysosomal function of ykt6 is to develop effective disease-modifying therapies for PD. The use of LNK-754 as a potent FTI may serve as proof of concept that FTase inhibition and ykt6 activation are beneficial in PD. While we have focused on repurposing FTIs for their known profiles, an alternative might be the development of small-molecule ykt6-specific activators that directly target the hydrophobic farnesyl-binding

pocket. This would avoid the potential limitation of inadvertently reducing farnesylation of other substrates, although FTI side effects appear minimal at nanomolar doses. Further development of lonafarnib will require determining its ideal dosage, screening the effects on other important FTase targets, and verifying rescue in a larger set of mice. Culture and *in vivo* studies might investigate its downstream effects on a-syn, lysosomal function, and neuron viability. A "Go/No Go" decision for clinically investigating lonafarnib may be made based on its ability to affect ykt6 in the brain at relevant doses (Potter, 2015). Moving forward will require that mouse studies indicate ykt6 activity is increased in brain along with functional rescue of a-syn and behavior. If the doses necessary to reach this threshold adversely affect other farnesylation targets in the periphery, study may be halted. Phase II decisions regarding efficacy may be made similarly, based on improvement of primary motor symptoms paired with a readout of ykt6 activity corresponding to human brain. Following more positive results of ykt6 membrane localization in mouse RBCs after treatment, this technique could be used to monitor dosage in future clinical studies. Further development of ykt6 as a biomarker will require a larger sample set and would be aided by establishment of a positive control. This work may also investigate the native functions of ykt6 within the simple intracellular setting of RBCs for a deeper understanding of its pathophysiology.

Because a-syn may disrupt interacting processes throughout the ALP, we conclude by reiterating that complete neuroprotection is unlikely to result from modifying single targets but will instead require testing approaches in combination for their greatest benefit (Stojkovska et al., 2022). This may be an alternative course if clinical trials for FTI treatment alone cannot move forward. We previously found that easing ER stress with diltiazem in combination with FTI treatment improved lysosomal function and reduced a-syn more than the sum of each treatment alone (Stojkovska et al., 2022). Future studies may investigate this approach and other

combinations targeting the ALP along with upstream proteostatic elements disrupted in PD, for example the unfolded protein response, protein folding, and chaperone activity (Mullin and Schapira, 2015).

Here we show for the first time that WT a-syn disrupts MA in mature iPSC-derived dopaminergic neurons by inhibiting the process of autolysosome fusion. We narrow the mechanism to a reduction of SNARE ykt6 participation in its autolysosome fusion complex with SNAP-29. a-Syn-mediated MA dysfunction can then be rescued by increasing ykt6 activity through inhibition of overabundant FTase. This represents not only a novel toxic mechanism for a-syn in proteostasis but also a practical therapeutic target that promotes clearance of protein aggregates in patient neurons.

<div align="center">**CO-AUTHORED PUBLICATIONS**</div>

1. Stress-Induced Cellular Clearance Is Mediated by the SNARE Protein ykt6 and Disrupted by α-Synuclein.

ABSTRACT

Age-related neurodegenerative disorders are characterized by a slow, persistent accumulation of aggregated proteins. Although cells can elicit physiological responses to enhance cellular clearance and counteract accumulation, it is unclear how pathogenic proteins evade this process in disease. We find that Parkinson's disease α-synuclein perturbs the physiological response to lysosomal stress by impeding the SNARE protein ykt6. Cytosolic ykt6 is normally autoinhibited by a unique farnesyl-mediated regulatory mechanism; however, during lysosomal stress, it activates and redistributes into membranes to preferentially promote hydrolase trafficking and enhance cellular clearance. α-Synuclein aberrantly binds and deactivates ykt6 in patient-derived neurons, thereby disabling the lysosomal stress response and facilitating protein accumulation. Activating ykt6 by small-molecule farnesyltransferase inhibitors restores lysosomal activity and reduces α-synuclein in patient-derived neurons and mice. Our findings indicate that α-synuclein creates a permissive environment for aggregate persistence by inhibiting regulated cellular

clearance and provide a therapeutic strategy to restore protein homeostasis by harnessing SNARE activity.

CONTRIBUTIONS

- Contributed by performing membrane fractionation experiment that appears in Fig. 3G (here termed Fig. S1-1G), showing that TFEB overexpression causes ykt6 to localize to membranes.

- Contributed by treating mouse cohort with LNK-754 used throughout figures 7-8 (here termed Fig. S1-2 and S1-3). Assisted in image analysis shown in Fig. 7A (Fig. S1-2A). Performed weight and behavioral experiments appearing in Fig. 8E, F (Fig. S1-3E, F). These experiments show that LNK-754 treatment rescues weight and motor deficits observed in a mouse PD model.

- Contributed by developing the method and performing the GFP-ykt6 IP experiment shown in Supplemental Fig. 6A (Fig. S1-4A). This experiment gave direct evidence that LNK-754 decreases farnesylation specific to ykt6. Wrote the methods section pertaining to this experiment.

FIGURES
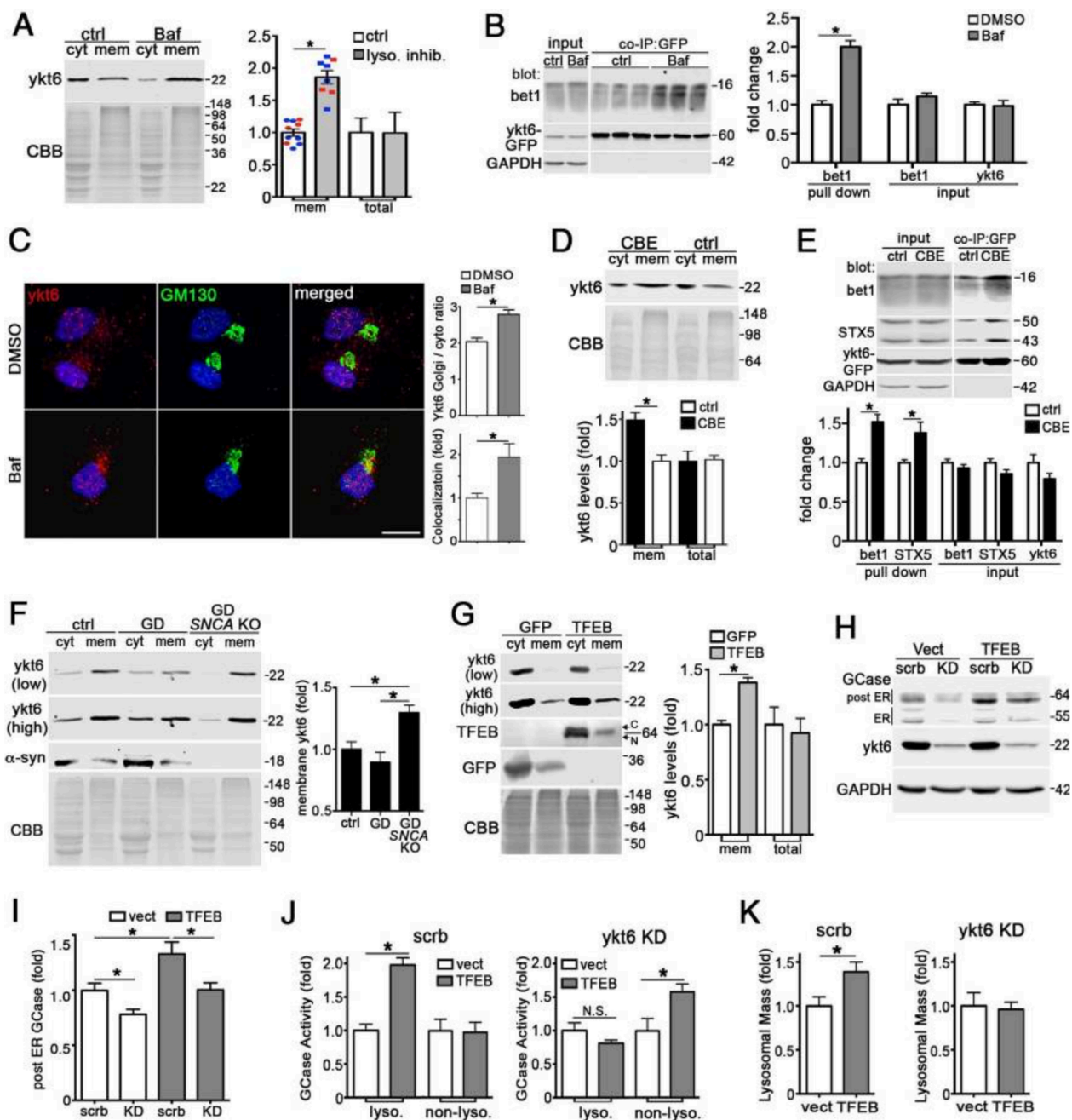
Fig. S1-1: Ykt6 is activated in response to lysosomal stress.

A) Ykt6 membrane shift analysis in bafA1 (200nM, 2 hrs) or NH4Cl (1M, 12 hrs) treated iPSn (d60). CBB, coomassie brilliant blue, (red=BafA1; blue= NH$_4$Cl, n=7–10). **B)** Co-IP of GFP-ykt6 and bet1 in control iPSn (d60) treated with bafA1 (n=3). **C)** Ykt6 and GM130 immunofluorescence analysis of baf A1-treated H4 cells (n=9). Scale bars=10um. **D)** Ykt6 membrane shift analysis in

CBE-treated SH-SY5Y cells (50mM, 2d, n=3). **E**) Co-IP of GFP-ykt6, bet1 and STX5 in CBE-treated SH-SY5Y cells (n=5). **F**) Ykt6 membrane shift analysis in control or Gaucher disease (GD) iPSn (d100). a-Syn was knocked-out (*SNCA* KO) in GD lines by CRISPR/Cas9. Two exposures are included to better visualize cyt and mem ykt6 (n=4). **G**) Ykt6 membrane shift analysis in lenti-infected SH-SY5Y cells (moi3, dpi 10) (n=3). C, cytosolic; N, nuclear. **H**) GCase maturation was assessed by endo H digest in lenti-infected SH-SY5Y cells. Empty vector (vect), scrambled (scrb). **I**) Control iPSn were infected as in H and analyzed for GCase maturation (n=3). **J**) Live cell GCase activity in lenti-infected iPSn (n=4). **K**) Lysosomal mass measurement in control iPSn (n=4). Values are the mean +/− SEM, *p<0.05.
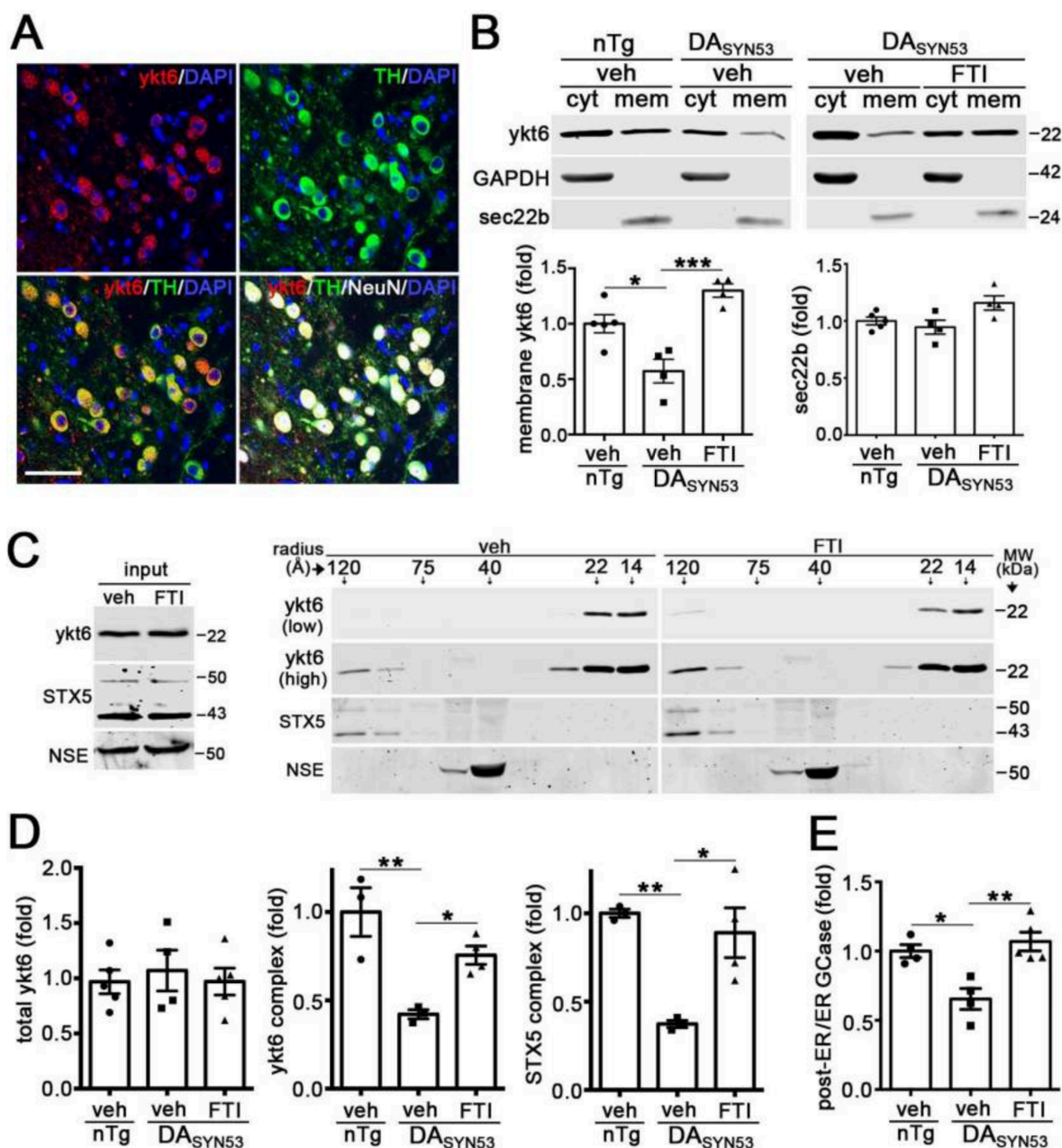
Fig. S1-2: FTI treatment restores functional membrane-associated ykt6 complexes in DA_SYN53 mice.

A) Immunohistochemistry in the midbrain of mice showing ykt6 (red), tyrosine hydroxylase (TH, green), NeuN (white), and nuclei (DAPI, blue). Scale bar, 50mm. **B)** Ykt6 membrane shift analysis in olfactory bulbs of FTI (LNK-754)-injected DA_SYN53 mice (12–14 months, i.p. 26d, 0.9mg/kg) (n=5, non-transgenic (nTg) +veh; n=4, DA_SYN53 + veh; n=4 DA_SYN53 + FTI). GAPDH and sec22b are loading controls. **C)** SEC / western blot analysis of midbrains of FTI-treated DA_SYN53 mice.

Inputs are shown on the left. NSE is a loading control. Low exposure of ykt6 shows changes in monomers (22–14A); high exposures shows changes in complexes (120A). (n=3, nTg + veh; n=4, DA_{SYN53} + veh; n=4 DA_{SYN53} + FTI). **D**) Quantification of complexes from SEC in C. **E**) GCase maturation was assessed in midbrain lysates by endo H resistance (n=4, nTg + veh; n=4, DA_{SYN53} + veh; n=4 DA_{SYN53} + FTI). For all quantifications, each point represents a measurement from an individual animal. Values are the mean +/− SEM, *p<0.05; **p<0.01, ***p<0.001, ANOVA with Tukey's post-hoc test.
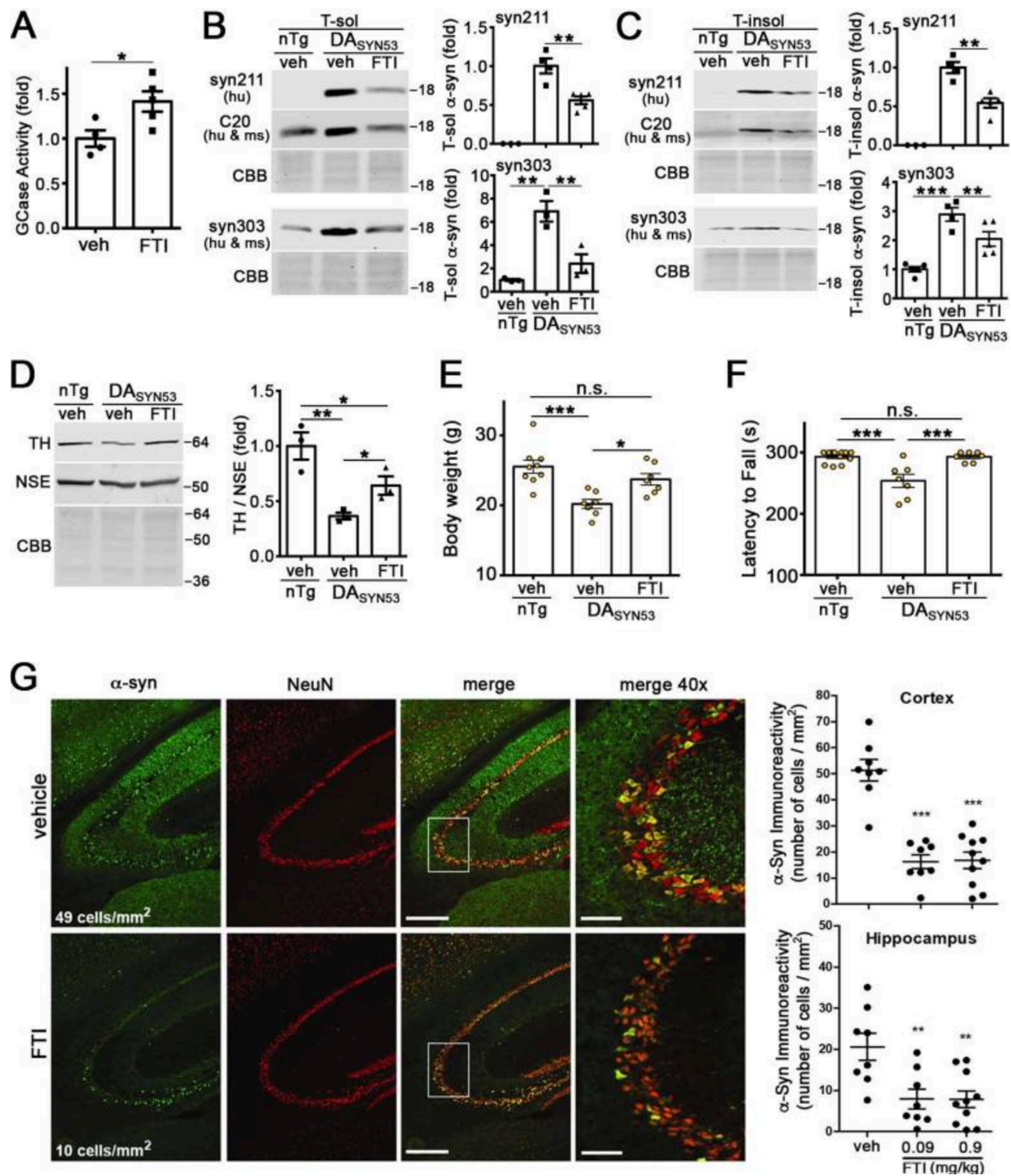
Fig. S1-3: FTI treatment enhances GCase activity and reduces pathological a-syn in transgenic mice.

A) GCase activity in the midbrain of FTI (LNK-754)-treated DA$_{SYN53}$ mice (treated as in fig. 7) (n=4, veh; n=5, FTI). **B & C)** Quantification of soluble and insoluble a-syn from midbrains of FTI-treated DA$_{SYN53}$ mice normalized to total protein (CBB). Syn211 is selective for human (hu) a-

syn; C20 and syn303 detect mouse (ms) and hu a-syn, (n=3, nTg +Veh; n=4, DA_{SYN53} + veh; n=5 DA_{SYN53} + FTI). **D**) Midbrain TH levels were quantified by western blot of FTI-treated DA_{SYN53} mice (n=3). **E**) Body weight of FTI-treated DA_{SYN53} mice (n=9, nTg +Veh; n=7, DA_{SYN53} + veh; n=7 DA_{SYN53} + FTI). **F**) Rotarod test of FTI-treated DA_{SYN53} mice (n=12, nTg +Veh; n=7, DA_{SYN53} + veh; n=7 DA_{SYN53} + FTI). **G**) Immunohistochemistry of a-syn in the hippocampus of PDGF-b wt-a-syn mice treated for 3 months (between 6 and 9 months) via oral gavage at 0.09 mg/kg (n=8) and 0.9 mg/kg (n=10). (0.9 mg/kg). a-Syn, green; NeuN, red. Scales bars = 0.6mm and 0.15mm (40X). Each point represents a measurement from an individual animal. Values are the mean +/−SEM. *$p<0.05$, **$p<0.01$, and *** $p<0.001$. Student's t-test, panel A; ANOVA with Tukey's post-hoc test, panels B-F; ANOVA with Newman-Kuels post hoc test compared to vehicle, panel G.
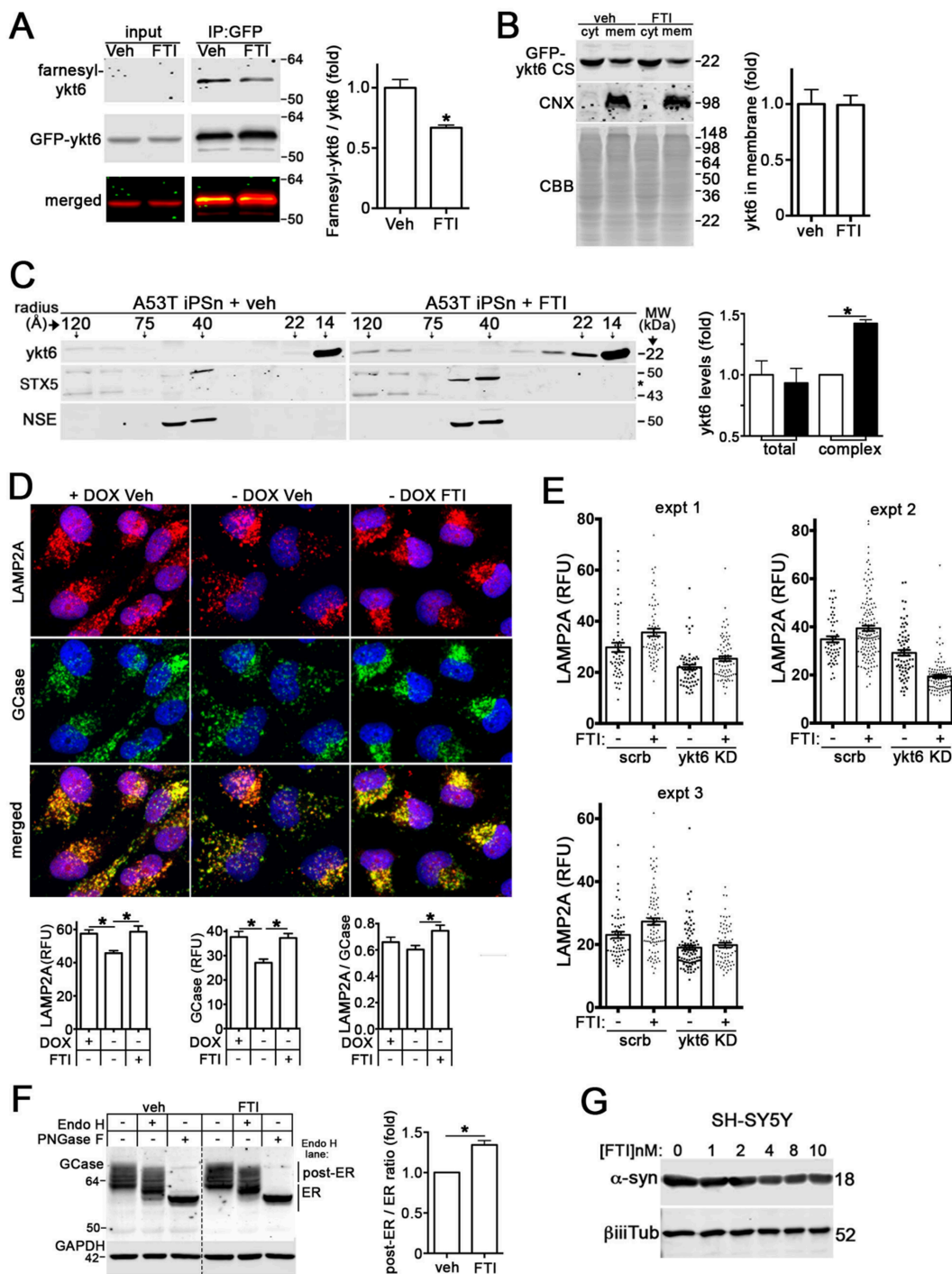
Fig. S1-4: The effects of FTI treatment on ykt6 and lysosomes.

A) Farnesylation of ykt6 was measured in SH-SY5Y cells expressing GFP-ykt6. Cells treated with or without FTI (LNK754) were cultured with farnesyl-azide to label farnesyl-modified proteins, immunoprecipitated with GFPaffinity beads, and then conjugated with phosphine-biotin. Biotin

was detected with streptavidin-conjugated IRDye800, and normalized to total levels of GFP-ykt6. See methods for details. The merged blot image shows total ykt6 (red) and farnesylated forms (green) (n=3). **B)** Membrane shift analysis of SH-SY5Y cells stably expressing GFP-ykt6-CS, treated with 5nM FTI. Calnexin (CNX) and Coomassie blue (CBB) were used as a loading controls. **C)** Gel filtration / western blot analysis of FTI treated A53T iPSn. Ykt6 complex levels eluting at ca. 120A were quantified on the right (n=2). **D)** Analysis of GCase localization in H4 cells treated with 5nM FTI demonstrates an increase in the levels of lysosomal marker LAMP2A and GCase (n=3). **E)** Raw quantification data of LAMP2A immunofluorescence intensity of individual cells from H4 cells treated with FTI, +/- ykt6 KD. Each data point represents LAMP2A intensity from individual cells, from 3 different culture wells. **F)** Analysis of ER-Golgi trafficking of GCase by endo H resistance after treatment with FTI in SH-SY5Y cells overexpressing wt a-syn (n=3). **G)** Western blot analysis of Triton X-100 soluble a-syn in SH-SY5Y wt a-syn cells after treatment with various concentrations of FTI for 5 days. For all quantifications, values are the mean +/- SEM, *p

2. Pathological α-syn aggregation is mediated by glycosphingolipid chain length and the physiological state of α-syn in vivo.

ABSTRACT

GBA1 mutations that encode lysosomal β-glucocerebrosidase (GCase) cause the lysosomal storage disorder Gaucher disease (GD) and are strong risk factors for synucleinopathies, including Parkinson's disease and Lewy body dementia. Only a subset of subjects with *GBA1* mutations exhibit neurodegeneration, and the factors that influence neurological phenotypes are unknown. We find that α-synuclein (α-syn) neuropathology induced by GCase depletion depends on neuronal maturity, the physiological state of α-syn, and specific accumulation of long-chain glycosphingolipid (GSL) GCase substrates. Reduced GCase activity does not initiate α-syn aggregation in neonatal mice or immature human midbrain cultures; however, adult mice or mature midbrain cultures that express physiological α-syn oligomers are aggregation prone. Accumulation of long-chain GSLs (≥C22), but not short-chain species, induced α-syn pathology and neurological dysfunction. Selective reduction of long-chain GSLs ameliorated α-syn pathology through lysosomal cathepsins. We identify specific requirements that dictate synuclein pathology in GD models, providing possible explanations for the phenotypic variability in subjects with GCase deficiency.

CONTRIBUTION

- Contributed by performing the leupeptin solubility shift experiment shown in Supplemental Figure 4A-C (here termed Fig. S2-1). This showed that lysosomal inhibition shifts a-syn, LC3, and p62 into the triton insoluble fraction of healthy control neurons. Prepared the figure and wrote the methods section for this experiment.

FIGURES
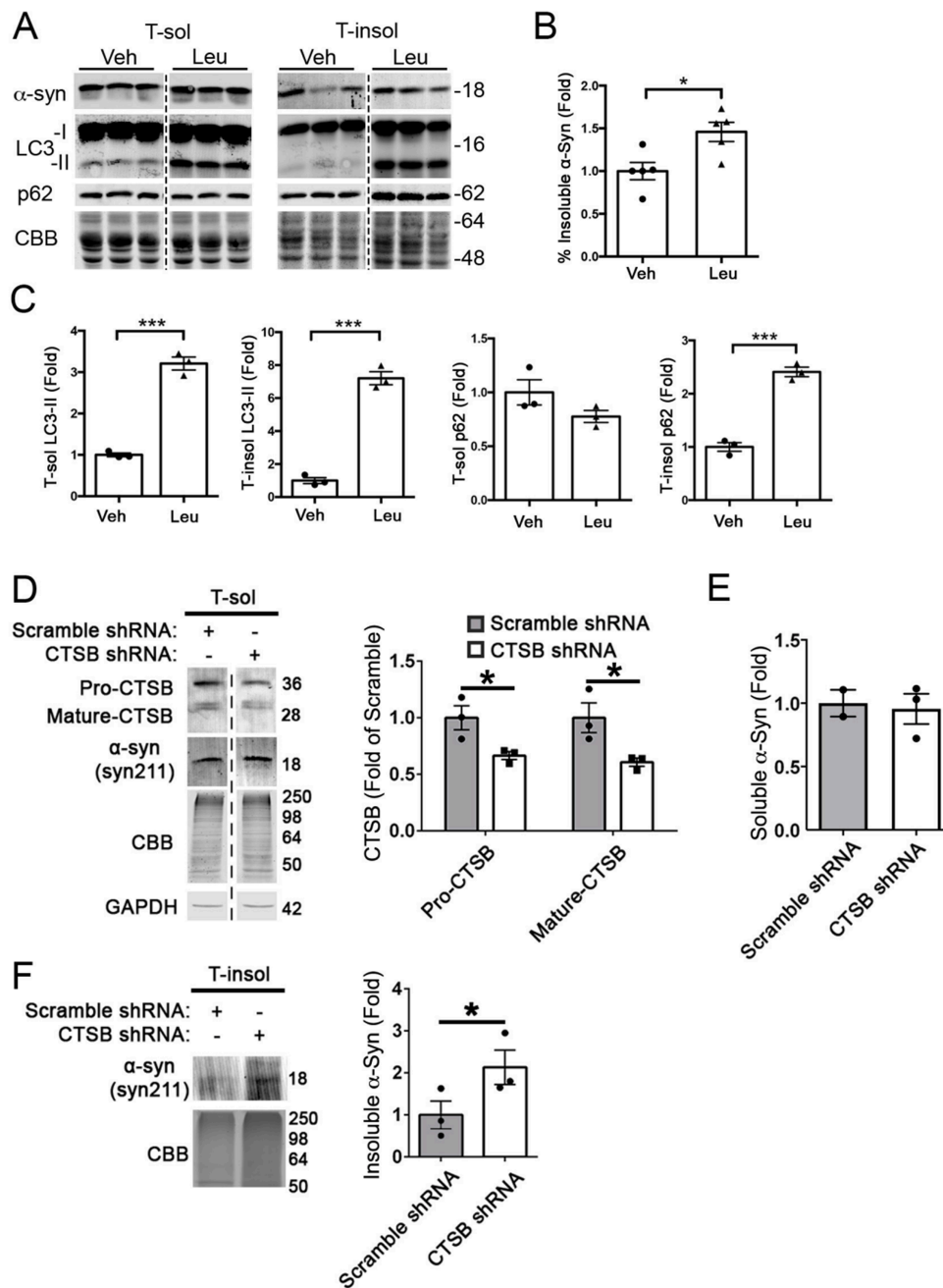
Fig. S2-1: Insoluble a-Synuclein increases upon lysosomal inhibition.

A) Wild-type midbrain neurons from a healthy control were treated with 3-methyladenine (3-MA), (10mM, 24 hr) or 17 leupeptin (Leu) (100μM,24 hr) then analyzed by sequential extraction / western blot of asynuclein. LC3 and p62 are autophagy proteins that are lysosomal substrates, and used to determine effective inhibition of the autophagic-lysosomal pathway. Coomassie blue (CBB) was used as a loading control. **B)** Quantification of % insoluble a-syn (n=5). A-Syn levels

from each fraction were normalized to CBB, and % insoluble a-syn was calculated (T-insol / (T-sol+Tinsol)*100) then expressed as fold change of vehicle (veh) treated cultures. **C)** Quantification of P62 and LC3 in each fraction normalized to CBB (n=3). **D)** Wild-type midbrain cultures were infected with lentiviral particles to express either scrambled or CTSB shRNA constructs. CTSB and a-syn levels were measured five days after lentiviral transduction by western blot from (MOI = 5; n = 3 culture wells). **E)** Quantification of soluble a-syn normalized to CBB. **F)** Quantification of insoluble a-syn normalized to CBB (n=2-3). Values are the mean +/- SEM, *p<0.05, ***p<0.001, ANOVA with Tukey's post hoc test (Panels B, C) or unpaired two-tailed student's t-test (panels E, F).

REFERENCES

Abounit, K., Scarabelli, T.M., and McCauley, R.B. (2012). Autophagy in mammalian cells. World journal of biological chemistry *3*, 1-6.

Adjei, A.A., Davis, J.N., Erlichman, C., Svingen, P.A., and Kaufmann, S.H. (2000). Comparison of potential markers of farnesyltransferase inhibition. Clin Cancer Res *6*, 2318-2325.

Aflaki, E., Westbroek, W., and Sidransky, E. (2017). The Complicated Relationship between Gaucher Disease and Parkinsonism: Insights from a Rare Disease. Neuron *93*, 737-746.

Alcalay, R.N., Levy, O.A., Waters, C.C., Fahn, S., Ford, B., Kuo, S.H., Mazzoni, P., Pauciulo, M.W., Nichols, W.C., Gan-Or, Z*., et al.* (2015). Glucocerebrosidase activity in Parkinson's disease with and without GBA mutations. Brain *138*, 2648-2658.

Alvarez-Erviti, L., Rodriguez-Oroz, M.C., Cooper, J.M., Caballero, C., Ferrer, I., Obeso, J.A., and Schapira, A.H.V. (2010). Chaperone-Mediated Autophagy Markers in Parkinson Disease Brains. Archives of Neurology *67*, 16-25.

Appenzeller-Herzog, C., and Hall, M.N. (2012). Bidirectional crosstalk between endoplasmic reticulum stress and mTOR signaling. Trends in Cell Biology *22*, 274-282.

Baba, M., Nakajo, S., Tu, P.H., Tomita, T., Nakaya, K., Lee, V.M., Trojanowski, J.Q., and Iwatsubo, T. (1998). Aggregation of alpha-synuclein in Lewy bodies of sporadic Parkinson's disease and dementia with Lewy bodies. The American journal of pathology *152*, 879-884.

Barbour, R., Kling, K., Anderson, J.P., Banducci, K., Cole, T., Diep, L., Fox, M., Goldstein, J.M., Soriano, F., Seubert, P*., et al.* (2008). Red blood cells are the major source of alpha-synuclein in blood. Neurodegener Dis *5*, 55-59.

Bas, L., Papinski, D., Licheva, M., Torggler, R., Rohringer, S., Schuschnig, M., and Kraft, C. (2018). Reconstitution reveals Ykt6 as the autophagosomal SNARE in autophagosome-vacuole fusion. J Cell Biol *217*, 3656-3669.

Benito-Cuesta, I., Diez, H., Ordonez, L., and Wandosell, F. (2017). Assessment of Autophagy in Neurons and Brain Tissue. Cells *6*.

Beutler, E. (1992). Gaucher disease: new molecular approaches to diagnosis and treatment. Science (New York, NY) *256*, 794-799.

Beyer, K., Domingo-Sabat, M., and Ariza, A. (2009). Molecular pathology of Lewy body diseases. Int J Mol Sci *10*, 724-745.

Burbidge, K., Rademacher, D.J., Mattick, J., Zack, S., Grillini, A., Bousset, L., Kwon, O., Kubicki, K., Simon, A., Melki, R*., et al.* (2021). LGALS3 (galectin 3) mediates an unconventional secretion of SNCA/alpha-synuclein in response to lysosomal membrane damage by the autophagic-lysosomal pathway in human midbrain dopamine neurons. Autophagy, 1-29.

Burre, J., Sharma, M., Tsetsenis, T., Buchman, V., Etherton, M.R., and Sudhof, T.C. (2010). Alpha-synuclein promotes SNARE-complex assembly in vivo and in vitro. Science *329*, 1663-1667.

Cao, K., Graziotto, J.J., Blair, C.D., Mazzulli, J.R., Erdos, M.R., Krainc, D., and Collins, F.S. (2011). Rapamycin reverses cellular phenotypes and enhances mutant protein clearance in Hutchinson-Gilford progeria syndrome cells. Sci Transl Med *3*, 89ra58.

Capell, B.C., Olive, M., Erdos, M.R., Cao, K., Faddah, D.A., Tavarez, U.L., Conneely, K.N., Qu, X., San, H., Ganesh, S.K.*, et al.* (2008). A farnesyltransferase inhibitor prevents both the onset and late progression of cardiovascular disease in a progeria mouse model. Proc Natl Acad Sci U S A *105*, 15902-15907.

Casey, P.J., and Seabra, M.C. (1996). Protein prenyltransferases. J Biol Chem *271*, 5289-5292.

Cassidy, P.B., Dolence, J.M., and Poulter, C.D. (1995). Continuous fluorescence assay for protein prenyltransferases. Methods Enzymol *250*, 30-43.

Cavallo-Medved, D., Moin, K., and Sloane, B. (2011). Cathepsin B: Basis Sequence: Mouse. AFCS Nat Mol Pages *2011*.

Chang, D., Nalls, M.A., Hallgrimsdottir, I.B., Hunkapiller, J., van der Brug, M., Cai, F., Kerchner, G.A., Ayalon, G., Bingol, B., Sheng, M.*, et al.* (2017a). A meta-analysis of genome-wide association studies identifies 17 new Parkinson's disease risk loci. Nat Genet *49*, 1511-1516.

Chang, J.T., Kumsta, C., Hellman, A.B., Adams, L.M., and Hansen, M. (2017b). Spatiotemporal regulation of autophagy during Caenorhabditis elegans aging. eLife *6*.

Chen, L., Xie, Z., Turkson, S., and Zhuang, X. (2015). A53T Human -Synuclein Overexpression in Transgenic Mice Induces Pervasive Mitochondria Macroautophagy Defects Preceding Dopamine Neuron Degeneration. Journal of Neuroscience *35*, 890-905.

Choi, B.K., Choi, M.G., Kim, J.Y., Yang, Y., Lai, Y., Kweon, D.H., Lee, N.K., and Shin, Y.K. (2013). Large alpha-synuclein oligomers inhibit neuronal SNARE-mediated vesicle docking. Proc Natl Acad Sci U S A *110*, 4087-4092.

Choubey, V., Safiulina, D., Vaarmann, A., Cagalinec, M., Wareski, P., Kuum, M., Zharkovsky, A., and Kaasik, A. (2011). Mutant A53T α-Synuclein Induces Neuronal Death by Increasing Mitochondrial Autophagy. Journal of Biological Chemistry *286*, 10814-10824.

Chung, Sun Y., Kishinevsky, S., Mazzulli, Joseph R., Graziotto, J., Mrejeru, A., Mosharov, Eugene V., Puspita, L., Valiulahi, P., Sulzer, D., Milner, Teresa A.*, et al.* (2016). Parkin and PINK1 Patient iPSC-Derived Midbrain Dopamine Neurons Exhibit Mitochondrial Dysfunction and α-Synuclein Accumulation. Stem Cell Reports *7*, 664-677.

Clark, L.N., Ross, B.M., Wang, Y., Mejia-Santana, H., Harris, J., Louis, E.D., Cote, L.J., Andrews, H., Fahn, S., Waters, C.*, et al.* (2007). Mutations in the glucocerebrosidase gene are associated with early-onset Parkinson disease. Neurology *69*, 1270-1277.

Cleeter, M.W.J., Chau, K.-Y., Gluck, C., Mehta, A., Hughes, D.A., Duchen, M., Wood, N.W., Hardy, J., Mark Cooper, J., and Schapira, A.H. (2013). Glucocerebrosidase inhibition causes mitochondrial dysfunction and free radical damage. Neurochemistry international *62*, 1-7.

Collier, J.J., Guissart, C., Olahova, M., Sasorith, S., Piron-Prunier, F., Suomi, F., Zhang, D., Martinez-Lopez, N., Leboucq, N., Bahr, A.*, et al.* (2021). Developmental Consequences of Defective ATG7-Mediated Autophagy in Humans. N Engl J Med *384*, 2406-2417.

Conway, K.A., Harper, J.D., and Lansbury, P.T. (1998). Accelerated in vitro fibril formation by a mutant alpha-synuclein linked to early-onset Parkinson disease. Nat Med *4*, 1318-1320.

Cooper, A.A., Gitler, A.D., Cashikar, A., Haynes, C.M., Hill, K.J., Bhullar, B., Liu, K., Xu, K., Strathearn, K.E., Liu, F.*, et al.* (2006). Alpha-synuclein blocks ER-Golgi traffic and Rab1 rescues neuron loss in Parkinson's models. Science *313*, 324-328.

Cuddy, L.K., Wani, W.Y., Morella, M.L., Pitcairn, C., Tsutsumi, K., Fredriksen, K., Justman, C.J., Grammatopoulos, T.N., Belur, N.R., Zunke, F.*, et al.* (2019). Stress-Induced Cellular Clearance Is

Mediated by the SNARE Protein ykt6 and Disrupted by alpha-Synuclein. LID - S0896-6273(19)30774-3 [pii] LID - 10.1016/j.neuron.2019.09.001 [doi].

Cuervo, A.M., Stefanis, L., Fredenburg, R., Lansbury, P.T., and Sulzer, D. (2004). Impaired degradation of mutant alpha-synuclein by chaperone-mediated autophagy. Science *305*, 1292-1295.

Dandana, A., Ben Khelifa, S., Chahed, H., Miled, A., and Ferchichi, S. (2016). Gaucher Disease: Clinical, Biological and Therapeutic Aspects. Pathobiology : journal of immunopathology, molecular and cellular biology *83*, 13-23.

Daniele, S., Frosini, D., Pietrobono, D., Petrozzi, L., Lo Gerfo, A., Baldacci, F., Fusi, J., Giacomelli, C., Siciliano, G., Trincavelli, M.L.*, et al.* (2018). alpha-Synuclein Heterocomplexes with beta-Amyloid Are Increased in Red Blood Cells of Parkinson's Disease Patients and Correlate with Disease Severity. Front Mol Neurosci *11*, 53.

Daste, F., Galli, T., and Tareste, D. (2015). Structure and function of longin SNAREs. Journal of Cell Science *128*.

De Sandre-Giovannoli, A., Bernard, R., Cau, P., Navarro, C., Amiel, J., Boccaccio, I., Lyonnet, S., Stewart, C.L., Munnich, A., Le Merrer, M.*, et al.* (2003). Lamin a truncation in Hutchinson-Gilford progeria. Science *300*, 2055.

Decressac, M., Mattsson, B., Weikop, P., Lundblad, M., Jakobsson, J., and Bjorklund, A. (2013). TFEB-mediated autophagy rescues midbrain dopamine neurons from -synuclein toxicity. Proceedings of the National Academy of Sciences *110*, E1817-E1826.

Dehay, B., Bove J Fau - Rodriguez-Muela, N., Rodriguez-Muela N Fau - Perier, C., Perier C Fau - Recasens, A., Recasens A Fau - Boya, P., Boya P Fau - Vila, M., and Vila, M. (2010). Pathogenic lysosomal depletion in Parkinson's disease.

Dhillon, S. (2021). Lonafarnib: First Approval. Drugs *81*, 283-289.

Ebrahimi-Fakhari, D., Cantuti-Castelvetri, I., Fan, Z., Rockenstein, E., Masliah, E., Hyman, B.T., McLean, P.J., and Unni, V.K. (2011). Distinct roles in vivo for the ubiquitin-proteasome system and the autophagy-lysosomal pathway in the degradation of alpha-synuclein. J Neurosci *31*, 14508-14520.

Emamzadeh, F.N. (2016). Alpha-synuclein structure, functions, and interactions. Journal of Research in Medical Sciences : The Official Journal of Isfahan University of Medical Sciences *21*, 29.

Farfel-Becker, T., Vitner, E.B., Kelly, S.L., Bame, J.R., Duan, J., Shinder, V., Merrill, A.H., Dobrenis, K., and Futerman, A.H. (2014). Neuronal accumulation of glucosylceramide in a mouse model of neuronopathic Gaucher disease leads to neurodegeneration. Human Molecular Genetics *23*, 843-854.

Fasshauer, D., Sutton, R.B., Brunger, A.T., and Jahn, R. (1998). Conserved structural features of the synaptic fusion complex: SNARE proteins reclassified as Q- and R-SNAREs. Proc Natl Acad Sci U S A *95*, 15781-15786.

Fernandez, A.F., Sebti, S., Wei, Y., Zou, Z., Shi, M., McMillan, K.L., He, C., Ting, T., Liu, Y., Chiang, W.C.*, et al.* (2018). Disruption of the beclin 1-BCL2 autophagy regulatory complex promotes longevity in mice. Nature *558*, 136-140.

Freeman, D., Cedillos, R., Choyke, S., Lukic, Z., McGuire, K., Marvin, S., Burrage, A.M., Sudholt, S., Rana, A., O'Connor, C., *et al.* (2013). Alpha-synuclein induces lysosomal rupture and cathepsin dependent reactive oxygen species following endocytosis. PloS one *8*, e62143.

Friedman, L.G., Lachenmayer, M.L., Wang, J., He, L., Poulose, S.M., Komatsu, M., Holstein, G.R., and Yue, Z. (2012). Disrupted Autophagy Leads to Dopaminergic Axon and Dendrite Degeneration and Promotes Presynaptic Accumulation of -Synuclein and LRRK2 in the Brain. Journal of Neuroscience *32*, 7585-7593.

Fukasawa, M., Varlamov, O., Eng, W.S., Söllner, T.H., and Rothman, J.E. (2004). Localization and activity of the SNARE Ykt6 determined by its regulatory domain and palmitoylation. Proceedings of the National Academy of Sciences of the United States of America *101*, 4815-4820.

Gan-Or, Z., Dion, P.A., and Rouleau, G.A. (2015). Genetic perspective on the role of the autophagy-lysosome pathway in Parkinson disease. Autophagy *11*, 1443-1457.

Gao, J., Reggiori, F., and Ungermann, C. (2018). A novel in vitro assay reveals SNARE topology and the role of Ykt6 in autophagosome fusion with vacuoles. J Cell Biol *217*, 3670-3682.

Gegg, M.E., Burke, D., Heales, S.J.R., Cooper, J.M., Hardy, J., Wood, N.W., and Schapira, A.H.V. (2012). Glucocerebrosidase deficiency in substantia nigra of parkinson disease brains. Annals of Neurology *72*, 455-463.

Geisler, S., Holmstrom, K.M., Skujat, D., Fiesel, F.C., Rothfuss, O.C., Kahle, P.J., and Springer, W. (2010). PINK1/Parkin-mediated mitophagy is dependent on VDAC1 and p62/SQSTM1. Nature cell biology *12*, 119-131.

Goker-Alpan, O., Giasson, B.I., Eblan, M.J., Nguyen, J., Hurtig, H.I., Lee, V.M.Y., Trojanowski, J.Q., and Sidransky, E. (2006). Glucocerebrosidase mutations are an important risk factor for Lewy body disorders. Neurology *67*, 908-910.

Goker-Alpan, O., Schiffmann, R., LaMarca, M.E., Nussbaum, R.L., McInerney-Leo, A., and Sidransky, E. (2004). Parkinsonism among Gaucher disease carriers. Journal of medical genetics *41*, 937-940.

Gonzalo, S., Kreienkamp, R., and Askjaer, P. (2017). Hutchinson-Gilford Progeria Syndrome: A premature aging disease caused by LMNA gene mutations. Ageing Res Rev *33*, 18-29.

Gordon, L.B., Kleinman, M.E., Massaro, J., D'Agostino, R.B., Sr., Shappell, H., Gerhard-Herman, M., Smoot, L.B., Gordon, C.M., Cleveland, R.H., Nazarian, A., *et al.* (2016). Clinical Trial of the Protein Farnesylation Inhibitors Lonafarnib, Pravastatin, and Zoledronic Acid in Children With Hutchinson-Gilford Progeria Syndrome. Circulation *134*, 114-125.

Gordon, L.B., Kleinman, M.E., Miller, D.T., Neuberg, D.S., Giobbie-Hurder, A., Gerhard-Herman, M., Smoot, L.B., Gordon, C.M., Cleveland, R., Snyder, B.D., *et al.* (2012). Clinical trial of a farnesyltransferase inhibitor in children with Hutchinson-Gilford progeria syndrome. Proc Natl Acad Sci U S A *109*, 16666-16671.

Gordon, L.B., Shappell, H., Massaro, J., D'Agostino, R.B., Sr., Brazier, J., Campbell, S.E., Kleinman, M.E., and Kieran, M.W. (2018). Association of Lonafarnib Treatment vs No Treatment With Mortality Rate in Patients With Hutchinson-Gilford Progeria Syndrome. JAMA *319*, 1687-1695.

Halperin, A., Elstein, D., and Zimran, A. (2006). Increased incidence of Parkinson disease among relatives of patients with Gaucher disease. Blood cells, molecules & diseases *36*, 426-428.

Hara, T., Nakamura, K., Matsui, M., Yamamoto, A., Nakahara, Y., Suzuki-Migishima, R., Yokoyama, M., Mishima, K., Saito, I., Okano, H.*, et al.* (2006). Suppression of basal autophagy in neural cells causes neurodegenerative disease in mice. Nature *441*, 885-889.

Hasegawa, H., Zinsser, S., Rhee, Y., Vik-Mo, E.O., Davanger, S., and Hay, J.C. (2003). Mammalian ykt6 is a neuronal SNARE targeted to a specialized compartment by its profilin-like amino terminal domain. Molecular biology of the cell *14*, 698-720.

Hay, J.C., Chao, D.S., Kuo, C.S., and Scheller, R.H. (1997). Protein interactions regulating vesicle transport between the endoplasmic reticulum and Golgi apparatus in mammalian cells. Cell *89*, 149-158.

Hernandez, I., Luna, G., Rauch, J.N., Reis, S.A., Giroux, M., Karch, C.M., Boctor, D., Sibih, Y.E., Storm, N.J., Diaz, A.*, et al.* (2019). A farnesyltransferase inhibitor activates lysosomes and reduces tau pathology in mice with tauopathy. Sci Transl Med *11*.

Hornykiewicz, O. (2006). The discovery of dopamine deficiency in the parkinsonian brain. J Neural Transm Suppl, 9-15.

Hou, X., Fiesel, F.C., Truban, D., Castanedes Casey, M., Lin, W.L., Soto, A.I., Tacik, P., Rousseau, L.G., Diehl, N.N., Heckman, M.G.*, et al.* (2018). Age- and disease-dependent increase of the mitophagy marker phospho-ubiquitin in normal aging and Lewy body disease.

Hougland, J.L., Hicks, K.A., Hartman, H.L., Kelly, R.A., Watt, T.J., and Fierke, C.A. (2010). Identification of novel peptide substrates for protein farnesyltransferase reveals two substrate classes with distinct sequence selectivities. J Mol Biol *395*, 176-190.

Iranzo, A., Tolosa, E., Gelpi, E., Molinuevo, J.L., Valldeoriola, F., Serradell, M., Sanchez-Valle, R., Vilaseca, I., Lomena, F., Vilas, D.*, et al.* (2013). Neurodegenerative disease status and post-mortem pathology in idiopathic rapid-eye-movement sleep behaviour disorder: an observational cohort study. Lancet Neurol *12*, 443-453.

Itakura, E., Kishi-Itakura, C., and Mizushima, N. (2012). The hairpin-type tail-anchored SNARE syntaxin 17 targets to autophagosomes for fusion with endosomes/lysosomes. Cell *151*, 1256-1269.

Jeong, A., Cheng, S., Zhong, R., Bennett, D.A., Bergo, M.O., and Li, L. (2021). Protein farnesylation is upregulated in Alzheimer's human brains and neuron-specific suppression of farnesyltransferase mitigates pathogenic processes in Alzheimer's model mice. Acta Neuropathol Commun *9*, 129.

Jinn, S., Drolet, R.E., Cramer, P.E., Wong, A.H., Toolan, D.M., Gretzula, C.A., Voleti, B., Vassileva, G., Disa, J., Tadin-Strapps, M.*, et al.* (2017). TMEM175 deficiency impairs lysosomal and mitochondrial function and increases alpha-synuclein aggregation. Proc Natl Acad Sci U S A *114*, 2389-2394.

Jo, A., Lee, Y., Kam, T.I., Kang, S.U., Neifert, S., Karuppagounder, S.S., Khang, R., Kang, H., Park, H., Chou, S.C.*, et al.* (2021). PARIS farnesylation prevents neurodegeneration in models of Parkinson's disease. Sci Transl Med *13*.

Jozwiak, N., Postuma, R.B., Montplaisir, J., Latreille, V., Panisset, M., Chouinard, S., Bourgouin, P.A., and Gagnon, J.F. (2017). REM Sleep Behavior Disorder and Cognitive Impairment in Parkinson's Disease. Sleep *40*.

Jung, M., Choi, H., and Mun, J.Y. (2019). The autophagy research in electron microscopy. Appl Microsc *49*, 11.

Kalia, L.V., and Lang, A.E. (2015). Parkinson's disease. Lancet *386*, 896-912.

Kapuy, O., Vinod, P.K., and Bánhegyi, G. (2014). mTOR inhibition increases cell viability via autophagy induction during endoplasmic reticulum stress – An experimental and modeling study. FEBS Open Bio *4*, 704-713.

Karuna, M.P., Witte, L., Linnemannstoens, K., Choezom, D., Danieli-Mackay, A., Honemann-Capito, M., and Gross, J.C. (2020). Phosphorylation of Ykt6 SNARE Domain Regulates Its Membrane Recruitment and Activity. Biomolecules *10*.

Khuri, F.R., Glisson, B.S., Kim, E.S., Statkevich, P., Thall, P.F., Meyers, M.L., Herbst, R.S., Munden, R.F., Tendler, C., Zhu, Y.*, et al.* (2004). Phase I study of the farnesyltransferase inhibitor lonafarnib with paclitaxel in solid tumors. Clin Cancer Res *10*, 2968-2976.

Kieran, M.W., Packer, R.J., Onar, A., Blaney, S.M., Phillips, P., Pollack, I.F., Geyer, J.R., Gururangan, S., Banerjee, A., Goldman, S.*, et al.* (2007). Phase I and pharmacokinetic study of the oral farnesyltransferase inhibitor lonafarnib administered twice daily to pediatric patients with advanced central nervous system tumors using a modified continuous reassessment method: a Pediatric Brain Tumor Consortium Study. J Clin Oncol *25*, 3137-3143.

Kilpatrick, K., Zeng, Y., Hancock, T., and Segatori, L. (2015). Genetic and chemical activation of TFEB mediates clearance of aggregated alpha-synuclein. PLoS One *10*, e0120819.

Kim, M., Sandford, E., Gatica, D., Qiu, Y., Liu, X., Zheng, Y., Schulman, B.A., Xu, J., Semple, I., Ro, S.H.*, et al.* (2016). Mutation in ATG5 reduces autophagy and leads to ataxia with developmental delay. Elife *5*.

Kinghorn, K.J., Grönke, S., Castillo-Quan, J.I., Woodling, N.S., Li, L., Sirka, E., Gegg, M., Mills, K., Hardy, J., Bjedov, I.*, et al.* (2016). A Drosophila Model of Neuronopathic Gaucher Disease Demonstrates Lysosomal-Autophagic Defects and Altered mTOR Signalling and Is Functionally Rescued by Rapamycin. The Journal of neuroscience : the official journal of the Society for Neuroscience *36*, 11654-11670.

Kirkin, V., and Rogov, V.V. (2019). A Diversity of Selective Autophagy Receptors Determines the Specificity of the Autophagy Pathway. Molecular cell *76*, 268-285.

Klionsky, D.J., Abdel-Aziz, A.K., Abdelfatah, S., Abdellatif, M., Abdoli, A., Abel, S., Abeliovich, H., Abildgaard, M.H., Abudu, Y.P., Acevedo-Arozena, A.*, et al.* (2021). Guidelines for the use and interpretation of assays for monitoring autophagy (4th edition)(1). Autophagy *17*, 1-382.

Klucken, J., Poehler, A.-M., Ebrahimi-Fakhari, D., Schneider, J., Nuber, S., Rockenstein, E., Schlötzer-Schrehardt, U., Hyman, B.T., McLean, P.J., Masliah, E.*, et al.* (2012). Alpha-synuclein aggregation involves a bafilomycin A 1-sensitive autophagy pathway. Autophagy *8*, 754-766.

Komatsu, M., Waguri, S., Chiba, T., Murata, S., Iwata, J., Tanida, I., Ueno, T., Koike, M., Uchiyama, Y., Kominami, E.*, et al.* (2006). Loss of autophagy in the central nervous system causes neurodegeneration in mice. Nature *441*, 880-884.

Komatsu, M., Waguri, S., Koike, M., Sou, Y.S., Ueno, T., Hara, T., Mizushima, N., Iwata, J., Ezaki, J., Murata, S.*, et al.* (2007). Homeostatic levels of p62 control cytoplasmic inclusion body formation in autophagy-deficient mice. Cell *131*, 1149-1163.

Kriks, S., Shim, J.W., Piao, J., Ganat, Y.M., Wakeman, D.R., Xie, Z., Carrillo-Reid, L., Auyeung, G., Antonacci, C., Buch, A.*, et al.* (2011). Dopamine neurons derived from human ES cells efficiently engraft in animal models of Parkinson's disease. Nature *480*, 547-551.

Larsen, K.E., and Sulzer, D. (2002). Autophagy in neurons: a review. Histology and histopathology *17*, 897-908.

Li, J., Uversky, V.N., and Fink, A.L. (2001). Effect of familial Parkinson's disease point mutations A30P and A53T on the structural properties, aggregation, and fibrillation of human alpha-synuclein. Biochemistry *40*, 11604-11613.

Li, T., and Le, W. (2020). Biomarkers for Parkinson's Disease: How Good Are They? Neurosci Bull *36*, 183-194.

Li, W., Lesuisse, C., Xu, Y., Troncoso, J.C., Price, D.L., and Lee, M.K. (2004). Stabilization of alpha-synuclein protein with aging and familial parkinson's disease-linked A53T mutation. The Journal of neuroscience : the official journal of the Society for Neuroscience *24*, 7400-7409.

Liao, Z., Wang, B., Liu, W., Xu, Q., Hou, L., Song, J., Guo, Q., and Li, N. (2021). Dysfunction of chaperone-mediated autophagy in human diseases. Mol Cell Biochem *476*, 1439-1454.

Lipinski, M.M., Zheng, B., Lu, T., Yan, Z., Py, B.F., Ng, A., Xavier, R.J., Li, C., Yankner, B.A., Scherzer, C.R.*, et al.* (2010). Genome-wide analysis reveals mechanisms modulating autophagy in normal brain aging and in Alzheimer's disease. Proc Natl Acad Sci U S A *107*, 14164-14169.

Liu, Y., and Barlowe, C. (2002). Analysis of Sec22p in Endoplasmic Reticulum/Golgi Transport Reveals Cellular Redundancy in SNARE Protein Function. Molecular Biology of the Cell *13*, 3314-3324.

Lorincz, P., and Juhasz, G. (2020). Autophagosome-Lysosome Fusion. J Mol Biol *432*, 2462-2482.

Lotankar, S., Prabhavalkar, K.S., and Bhatt, L.K. (2017). Biomarkers for Parkinson's Disease: Recent Advancement. Neurosci Bull *33*, 585-597.

Maday, S., and Holzbaur, E.L. (2016). Compartment-Specific Regulation of Autophagy in Primary Neurons. J Neurosci *36*, 5933-5945.

Magalhaes, J., Gegg, M.E., Migdalska-Richards, A., Doherty, M.K., Whitfield, P.D., and Schapira, A.H.V. (2016). Autophagic lysosome reformation dysfunction in glucocerebrosidase deficient cells: relevance to Parkinson disease. Human Molecular Genetics *25*, 3432-3445.

Mamais, A., Manzoni, C., Nazish, I., Arber, C., Sonustun, B., Wray, S., Warner, T.T., Cookson, M.R., Lewis, P.A., and Bandopadhyay, R. (2018). Analysis of macroautophagy related proteins in G2019S LRRK2 Parkinson's disease brains with Lewy body pathology.

Manning-Boğ, A.B., Schüle, B., and Langston, J.W. (2009). Alpha-synuclein-glucocerebrosidase interactions in pharmacological Gaucher models: A biological link between Gaucher disease and parkinsonism. NeuroToxicology *30*, 1127-1132.

Mari, M., Griffith, J., Rieter, E., Krishnappa, L., Klionsky, D.J., and Reggiori, F. (2010). An Atg9-containing compartment that functions in the early steps of autophagosome biogenesis. J Cell Biol *190*, 1005-1022.

Martinez-Vicente, M., Talloczy, Z., Kaushik, S., Massey, A.C., Mazzulli, J., Mosharov, E.V., Hodara, R., Fredenburg, R., Wu, D.C., Follenzi, A.*, et al.* (2008). Dopamine-modified alpha-synuclein blocks chaperone-mediated autophagy. J Clin Invest *118*, 777-788.

Martini-Stoica, H., Xu, Y., Ballabio, A., and Zheng, H. (2016). The Autophagy-Lysosomal Pathway in Neurodegeneration: A TFEB Perspective. Trends Neurosci *39*, 221-234.

Matsui, T., Jiang, P., Nakano, S., Sakamaki, Y., Yamamoto, H., and Mizushima, N. (2018). Autophagosomal YKT6 is required for fusion with lysosomes independently of syntaxin 17. The Journal of Cell Biology.

Mazzulli, J.R., Xu, Y.H., Sun, Y., Knight, A.L., McLean, P.J., Caldwell, G.A., Sidransky, E., Grabowski, G.A., and Krainc, D. (2011). Gaucher disease glucocerebrosidase and alpha-synuclein form a bidirectional pathogenic loop in synucleinopathies. Cell *146*, 37-52.

Mazzulli, J.R., Zunke, F., Isacson, O., Studer, L., and Krainc, D. (2016). alpha-Synuclein-induced lysosomal dysfunction occurs through disruptions in protein trafficking in human midbrain synucleinopathy models. Proc Natl Acad Sci U S A *113*, 1931-1936.

McGrath, K., Agarwal, S., Tonelli, M., Dergai, M., Gaeta, A.L., Shum, A.K., Lacoste, J., Zhang, Y., Wen, W., Chung, D.*, et al.* (2021). A conformational switch driven by phosphorylation regulates the activity of the evolutionarily conserved SNARE Ykt6. Proc Natl Acad Sci U S A *118*.

McNew, J.A., Søgaard, M., Lampen, N.M., Machida, S., Ye, R.R., Lacomis, L., Tempst, P., Rothman, J.E., and Söllner, T.H. (1997). Ykt6p, a Prenylated SNARE Essential for Endoplasmic Reticulum-Golgi Transport*. Journal of Biological Chemistry *272*, 17776-17783.

Medina, D.L., Di Paola, S., Peluso, I., Armani, A., De Stefani, D., Venditti, R., Montefusco, S., Scotto-Rosato, A., Prezioso, C., Forrester, A.*, et al.* (2015). Lysosomal calcium signalling regulates autophagy through calcineurin and TFEB. Nature cell biology *17*, 288-299.

Migdalska-Richards, A., and Schapira, A.H.V. (2016). The relationship between glucocerebrosidase mutations and Parkinson disease. Journal of neurochemistry *139 Suppl 1*, 77-90.

Molina, J.R., and Adjei, A.A. (2006). The Ras/Raf/MAPK pathway. J Thorac Oncol *1*, 7-9.

Moore, A.R., Rosenberg, S.C., McCormick, F., and Malek, S. (2020). RAS-targeted therapies: is the undruggable drugged? Nat Rev Drug Discov *19*, 533-552.

Moras, M., Lefevre, S.D., and Ostuni, M.A. (2017). From Erythroblasts to Mature Red Blood Cells: Organelle Clearance in Mammals. Front Physiol *8*, 1076.

Moulder, S.L., Mahany, J.J., Lush, R., Rocha-Lima, C., Langevin, M., Ferrante, K.J., Bartkowski, L.M., Kajiji, S.M., Noe, D.A., Paillet, S.*, et al.* (2004). A phase I open label study of the farnesyltransferase inhibitor CP-609,754 in patients with advanced malignant tumors. Clin Cancer Res *10*, 7127-7135.

Mullin, S., and Schapira, A.H.V. (2015). Pathogenic Mechanisms of Neurodegeneration in Parkinson Disease. Neurologic Clinics *33*, 1-17.

Murphy, K.E., Gysbers, A.M., Abbott, S.K., Tayebi, N., Kim, W.S., Sidransky, E., Cooper, A., Garner, B., and Halliday, G.M. (2014). Reduced glucocerebrosidase is associated with increased α-synuclein in sporadic Parkinson's disease. Brain *137*, 834-848.

Murphy, K.E., and Halliday, G.M. (2014). Glucocerebrosidase deficits in sporadic Parkinson disease. Autophagy *10*, 1350-1351.

Murray, G.J., and Jin, F.S. (1995). Immunoelectron microscopic localization of mannose-terminal glucocerebrosidase in lysosomes of rat liver Kupffer cells. The journal of histochemistry and cytochemistry : official journal of the Histochemistry Society *43*, 149-158.

Nair, U., Jotwani, A., Geng, J., Gammoh, N., Richerson, D., Yen, W.-L., Griffith, J., Nag, S., Wang, K., Moss, T.*, et al.* (2011). SNARE Proteins Are Required for Macroautophagy. Cell *146*, 290-302.

Nakatogawa, H. (2020). Mechanisms governing autophagosome biogenesis. Nat Rev Mol Cell Biol *21*, 439-458.

Nalls, M.A., Pankratz, N., Lill, C.M., Do, C.B., Hernandez, D.G., Saad, M., DeStefano, A.L., Kara, E., Bras, J., Sharma, M.*, et al.* (2014). Large-scale meta-analysis of genome-wide association data identifies six new risk loci for Parkinson's disease. Nature Genetics *46*, 989-993.

Napolitano, G., and Ballabio, A. (2016). TFEB at a glance. J Cell Sci *129*, 2475-2481.

Neudorfer, O., Giladi, N., Elstein, D., Abrahamov, A., Turezkite, T., Aghai, E., Reches, A., Bembi, B., and Zimran, A. (1996). Occurrence of Parkinson's syndrome in type 1 Gaucher disease. QJM *89*, 691-694.

Ogata, M., Hino, S.-i., Saito, A., Morikawa, K., Kondo, S., Kanemoto, S., Murakami, T., Taniguchi, M., Tanii, I., Yoshinaga, K.*, et al.* (2006). Autophagy Is Activated for Cell Survival after Endoplasmic Reticulum Stress. Molecular and Cellular Biology *26*, 9220-9231.

Ohashi, Y., and Munro, S. (2010). Membrane delivery to the yeast autophagosome from the Golgi-endosomal system. Mol Biol Cell *21*, 3998-4008.

Oliveira, L.M., Falomir-Lockhart, L.J., Botelho, M.G., Lin, K.H., Wales, P., Koch, J.C., Gerhardt, E., Taschenberger, H., Outeiro, T.F., Lingor, P.*, et al.* (2015). Elevated alpha-synuclein caused by SNCA gene triplication impairs neuronal differentiation and maturation in Parkinson's patient-derived induced pluripotent stem cells. Cell Death Dis *6*, e1994.

Orenstein, S.J., Kuo, S.-H., Tasset, I., Arias, E., Koga, H., Fernandez-Carasa, I., Cortes, E., Honig, L.S., Dauer, W., Consiglio, A.*, et al.* (2013). Interplay of LRRK2 with chaperone-mediated autophagy. Nature Neuroscience *16*, 394-406.

Osellame, Laura D., Rahim, Ahad A., Hargreaves, Iain P., Gegg, Matthew E., Richard-Londt, A., Brandner, S., Waddington, Simon N., Schapira, Anthony H.V., and Duchen, Michael R. (2013). Mitochondria and Quality Control Defects in a Mouse Model of Gaucher Disease—Links to Parkinson's Disease. Cell Metabolism *17*, 941-953.

Ossig, R., Schmitt, H.D., de Groot, B., Riedel, D., Keranen, S., Ronne, H., Grubmuller, H., and Jahn, R. (2000). Exocytosis requires asymmetry in the central layer of the SNARE complex. EMBO J *19*, 6000-6010.

Pan, J., Chen, B., Su, C.H., Zhao, R., Xu, Z.X., Sun, L., Lee, M.H., and Yeung, S.C. (2008). Autophagy induced by farnesyltransferase inhibitors in cancer cells. Cancer Biol Ther *7*, 1679-1684.

Pan, P.Y., and Yue, Z. (2014). Genetic causes of Parkinson's disease and their links to autophagy regulation.

Pandey, M.K., Burrow, T.A., Rani, R., Martin, L.J., Witte, D., Setchell, K.D., McKay, M.A., Magnusen, A.F., Zhang, W., Liou, B.*, et al.* (2017). Complement drives glucosylceramide accumulation and tissue inflammation in Gaucher disease. Nature *543*, 108-112.

Park, J.-S., Mehta, P., Cooper, A.A., Veivers, D., Heimbach, A., Stiller, B., Kubisch, C., Fung, V.S., Krainc, D., Mackay-Sim, A.*, et al.* (2011). Pathogenic effects of novel mutations in the P-type ATPase ATP13A2 (PARK9) causing Kufor-Rakeb syndrome, a form of early-onset parkinsonism. Human mutation *32*, 956-964.

Parnetti, L., Gaetani, L., Eusebi, P., Paciotti, S., Hansson, O., El-Agnaf, O., Mollenhauer, B., Blennow, K., and Calabresi, P. (2019). CSF and blood biomarkers for Parkinson's disease. Lancet Neurol *18*, 573-586.

Parnetti, L., Paciotti, S., Eusebi, P., Dardis, A., Zampieri, S., Chiasserini, D., Tasegian, A., Tambasco, N., Bembi, B., Calabresi, P.*, et al.* (2017). Cerebrospinal fluid beta-

glucocerebrosidase activity is reduced in parkinson's disease patients. Movement disorders : official journal of the Movement Disorder Society *32*, 1423-1431.

Pfefferkorn, C.M., Jiang, Z., and Lee, J.C. (2012). Biophysics of alpha-synuclein membrane interactions. Biochim Biophys Acta *1818*, 162-171.

Pickrell, A.M., and Youle, R.J. (2015). The roles of PINK1, parkin, and mitochondrial fidelity in Parkinson's disease. Neuron *85*, 257-273.

Plowey, E.D., Cherra, S.J., Liu, Y.-J., and Chu, C.T. (2008). Role of autophagy in G2019S-LRRK2-associated neurite shortening in differentiated SH-SY5Y cells. Journal of neurochemistry *105*, 1048-1056.

Pokrywka, N.J., Bush, S., and Nick, S.E. (2022). The R-SNARE Ykt6 is required for multiple events during oogenesis in Drosophila. Cells Dev *169*, 203759.

Polymeropoulos, M.H., Lavedan, C., Leroy, E., Ide, S.E., Dehejia, A., Dutra, A., Pike, B., Root, H., Rubenstein, J., Boyer, R*., et al.* (1997). Mutation in the alpha-synuclein gene identified in families with Parkinson's disease. Science *276*, 2045-2047.

Porritt, M., Stanic, D., Finkelstein, D., Batchelor, P., Lockhart, S., Hughes, A., Kalnins, R., and Howells, D. (2005). Dopaminergic innervation of the human striatum in Parkinson's disease. Movement disorders : official journal of the Movement Disorder Society *20*, 810-818.

Postuma, R.B., Gagnon, J.F., Vendette, M., Fantini, M.L., Massicotte-Marquez, J., and Montplaisir, J. (2009). Quantifying the risk of neurodegenerative disease in idiopathic REM sleep behavior disorder. Neurology *72*, 1296-1300.

Potter, W.Z. (2015). Optimizing early Go/No Go decisions in CNS drug development. Expert Rev Clin Pharmacol *8*, 155-157.

Prior, I.A., Hood, F.E., and Hartley, J.L. (2020). The Frequency of Ras Mutations in Cancer. Cancer Res *80*, 2969-2974.

Ramirez, A., Heimbach, A., Gründemann, J., Stiller, B., Hampshire, D., Cid, L.P., Goebel, I., Mubaidin, A.F., Wriekat, A.-L., Roeper, J*., et al.* (2006). Hereditary parkinsonism with dementia is caused by mutations in ATP13A2, encoding a lysosomal type 5 P-type ATPase. Nature Genetics *38*, 1184.

Roosen, D.A., and Cookson, M.R. (2016). LRRK2 at the interface of autophagosomes, endosomes and lysosomes. Mol Neurodegener *11*, 73.

Sancak, Y., Bar-Peled, L., Zoncu, R., Markhard, A.L., Nada, S., and Sabatini, D.M. (2010). Ragulator-Rag complex targets mTORC1 to the lysosomal surface and is necessary for its activation by amino acids. Cell *141*, 290-303.

Sanchez-Danes, A., Richaud-Patin, Y., Carballo-Carbajal, I., Jimenez-Delgado, S., Caig, C., Mora, S., Di Guglielmo, C., Ezquerra, M., Patel, B., Giralt, A*., et al.* (2012). Disease-specific phenotypes in dopamine neurons from human iPS-based models of genetic and sporadic Parkinson's disease. EMBO Mol Med *4*, 380-395.

Sardi, S.P., Clarke, J., Viel, C., Chan, M., Tamsett, T.J., Treleaven, C.M., Bu, J., Sweet, L., Passini, M.A., Dodge, J.C*., et al.* (2013). Augmenting CNS glucocerebrosidase activity as a therapeutic strategy for parkinsonism and other Gaucher-related synucleinopathies. Proceedings of the National Academy of Sciences *110*, 3537-3542.

Sardiello, M., Palmieri, M., di Ronza, A., Medina, D.L., Valenza, M., Gennarino, V.A., Di Malta, C., Donaudy, F., Embrione, V., Polishchuk, R.S*., et al.* (2009). A gene network regulating lysosomal biogenesis and function. Science *325*, 473-477.

Sato, S., Uchihara, T., Fukuda, T., Noda, S., Kondo, H., Saiki, S., Komatsu, M., Uchiyama, Y., Tanaka, K., and Hattori, N. (2018). Loss of autophagy in dopaminergic neurons causes Lewy pathology and motor dysfunction in aged mice. Scientific reports *8*, 2813-2813.

Savitt, I.A., Yideng, L., Sabitha, S., Valina, L.D., Ted, M.D., and Joseph, M. (2012). Development and Characterization of a New Parkinson's Disease Model Resulting from Impaired Autophagy.

Sawa-Makarska, J., Baumann, V., Coudevylle, N., von Bulow, S., Nogellova, V., Abert, C., Schuschnig, M., Graef, M., Hummer, G., and Martens, S. (2020). Reconstitution of autophagosome nucleation defines Atg9 vesicles as seeds for membrane formation. Science *369*.

Sengupta, S., Peterson, T.R., and Sabatini, D.M. (2010). Regulation of the mTOR complex 1 pathway by nutrients, growth factors, and stress. Molecular cell *40*, 310-322.

Settembre, C., Di Malta, C., Polito, V.A., Garcia Arencibia, M., Vetrini, F., Erdin, S., Erdin, S.U., Huynh, T., Medina, D., Colella, P*., et al.* (2011). TFEB links autophagy to lysosomal biogenesis. Science *332*, 1429-1433.

Shahnawaz, M., Tokuda, T., Waragai, M., Mendez, N., Ishii, R., Trenkwalder, C., Mollenhauer, B., and Soto, C. (2017). Development of a Biochemical Diagnosis of Parkinson Disease by Detection of alpha-Synuclein Misfolded Aggregates in Cerebrospinal Fluid. JAMA Neurol *74*, 163-172.

Shen, M., Pan, P., Li, Y., Li, D., Yu, H., and Hou, T. (2015). Farnesyltransferase and geranylgeranyltransferase I: structures, mechanism, inhibitors and molecular modeling. Drug Discov Today *20*, 267-276.

Sidransky, E., Nalls, M.A., Aasly, J.O., Aharon-Peretz, J., Annesi, G., Barbosa, E.R., Bar-Shira, A., Berg, D., Bras, J., Brice, A*., et al.* (2009). Multicenter Analysis of Glucocerebrosidase Mutations in Parkinson's Disease. New England Journal of Medicine *361*, 1651-1661.

Singleton, A.B., Farrer, M., Johnson, J., Singleton, A., Hague, S., Kachergus, J., Hulihan, M., Peuralinna, T., Dutra, A., Nussbaum, R*., et al.* (2003). α-Synuclein Locus Triplication Causes Parkinson's Disease. Science *302*, 841-841.

Singleton, A.B., Farrer, M.J., and Bonifati, V. (2013). The genetics of Parkinson's disease: progress and therapeutic implications. Movement disorders : official journal of the Movement Disorder Society *28*, 14-23.

Song, W., Wang, F., Savini, M., Ake, A., di Ronza, A., Sardiello, M., and Segatori, L. (2013). TFEB regulates lysosomal proteostasis. Hum Mol Genet *22*, 1994-2009.

Spillantini, M.G., Schmidt, M.L., Lee, V.M.Y., Trojanowski, J.Q., Jakes, R., and Goedert, M. (1997). α-Synuclein in Lewy bodies. Nature *388*, 839-840.

St Louis, E.K., and Boeve, B.F. (2017). REM Sleep Behavior Disorder: Diagnosis, Clinical Implications, and Future Directions. Mayo Clin Proc *92*, 1723-1736.

Stauffer, W., Sheng, H., and Lim, H.N. (2018). EzColocalization: An ImageJ plugin for visualizing and measuring colocalization in cells and organisms. Sci Rep *8*, 15764.

Steger, M., Tonelli, F., Ito, G., Davies, P., Trost, M., Vetter, M., Wachter, S., Lorentzen, E., Duddy, G., Wilson, S*., et al.* (2016). Phosphoproteomics reveals that Parkinson's disease kinase LRRK2 regulates a subset of Rab GTPases. Elife *5*.

Stojkovska, I., Wani, W.Y., Zunke, F., Belur, N.R., Pavlenko, E.A., Mwenda, N., Sharma, K., Francelle, L., and Mazzulli, J.R. (2021). Rescue of alpha-synuclein aggregation in Parkinson's patient neurons by synergistic enhancement of ER proteostasis and protein trafficking. Neuron.

Stojkovska, I., Wani, W.Y., Zunke, F., Belur, N.R., Pavlenko, E.A., Mwenda, N., Sharma, K., Francelle, L., and Mazzulli, J.R. (2022). Rescue of alpha-synuclein aggregation in Parkinson's patient neurons by synergistic enhancement of ER proteostasis and protein trafficking. Neuron *110*, 436-451 e411.

Su, Y.-C., and Qi, X. (2013). Inhibition of excessive mitochondrial fission reduced aberrant autophagy and neuronal damage caused by LRRK2 G2019S mutation. Human Molecular Genetics *22*, 4545-4561.

Szwed, A., Kim, E., and Jacinto, E. (2021). Regulation and metabolic functions of mTORC1 and mTORC2. Physiol Rev *101*, 1371-1426.

Takáts, S., Glatz, G., Szenci, G., Boda, A., Horváth, G.V., Hegedűs, K., Kovács, A.L., and Juhász, G. (2018). Non-canonical role of the SNARE protein Ykt6 in autophagosome-lysosome fusion. PLoS Genetics *14*, e1007359.

Tambasco, N., Nigro, P., Romoli, M., Prontera, P., Simoni, S., and Calabresi, P. (2016). A53T in a parkinsonian family: a clinical update of the SNCA phenotypes. J Neural Transm (Vienna) *123*, 1301-1307.

Tang, F.-L., Liu, W., Hu, J.-X., Erion, J.R., Ye, J., Mei, L., and Xiong, W.-C. (2015a). VPS35 deficiency or mutation causes dopaminergic neuronal loss by impairing mitochondrial fusion and function. Cell reports *12*, 1631-1643.

Tang, F.L., Erion, J.R., Tian, Y., Liu, W., Yin, D.M., Ye, J., Tang, B., Mei, L., and Xiong, W.C. (2015b). VPS35 in Dopamine Neurons Is Required for Endosome-to-Golgi Retrieval of Lamp2a, a Receptor of Chaperone-Mediated Autophagy That Is Critical for -Synuclein Degradation and Prevention of Pathogenesis of Parkinson's Disease. Journal of Neuroscience *35*, 10613-10628.

Tang, Q., Gao, P., Arzberger, T., Höllerhage, M., Herms, J., Höglinger, G., and Koeglsperger, T. (2021). Alpha-Synuclein defects autophagy by impairing SNAP29-mediated autophagosome-lysosome fusion. Cell Death Dis *12*, 854-854.

Tanida, I., Ueno, T., and Kominami, E. (2004). LC3 conjugation system in mammalian autophagy. Int J Biochem Cell Biol *36*, 2503-2518.

Tanida, I., Ueno, T., and Kominami, E. (2008). LC3 and Autophagy. In, pp. 77-88.

Tanik, S.A., Schultheiss, C.E., Volpicelli-Daley, L.A., Brunden, K.R., and Lee, V.M.Y. (2013). Lewy Body-like α-Synuclein Aggregates Resist Degradation and Impair Macroautophagy. Journal of Biological Chemistry *288*, 15194-15210.

Tanji, K., Odagiri, S., Miki, Y., Maruyama, A., Nikaido, Y., Mimura, J., Mori, F., Warabi, E., Yanagawa, T., Ueno, S.*, et al.* (2015). p62 Deficiency Enhances alpha-Synuclein Pathology in Mice. Brain Pathol *25*, 552-564.

Tayebi, N., Callahan, M., Madike, V., Stubblefield, B.K., Orvisky, E., Krasnewich, D., Fillano, J.J., and Sidransky, E. (2001). Gaucher disease and parkinsonism: a phenotypic and genotypic characterization. Mol Genet Metab *73*, 313-321.

Taylor, S.A., Marrinan, C.H., Liu, G., Nale, L., Bishop, W.R., Kirschmeier, P., Liu, M., and Long, B.J. (2008). Combining the farnesyltransferase inhibitor lonafarnib with paclitaxel results in

enhanced growth inhibitory effects on human ovarian cancer models in vitro and in vivo. Gynecol Oncol *109*, 97-106.

Thayanidhi, N., Helm, J.R., Nycz, D.C., Bentley, M., Liang, Y., and Hay, J.C. (2010). Alpha-synuclein delays endoplasmic reticulum (ER)-to-Golgi transport in mammalian cells by antagonizing ER/Golgi SNAREs. Molecular biology of the cell *21*, 1850-1863.

Tochio, H., Tsui, M.M., Banfield, D.K., and Zhang, M. (2001). An autoinhibitory mechanism for nonsyntaxin SNARE proteins revealed by the structure of Ykt6p. Science *293*, 698-702.

Ullrich, N.J., Kieran, M.W., Miller, D.T., Gordon, L.B., Cho, Y.J., Silvera, V.M., Giobbie-Hurder, A., Neuberg, D., and Kleinman, M.E. (2013). Neurologic features of Hutchinson-Gilford progeria syndrome after lonafarnib treatment. Neurology *81*, 427-430.

Usenovic, M., Tresse, E., Mazzulli, J.R., Taylor, J.P., and Krainc, D. (2012). Deficiency of ATP13A2 leads to lysosomal dysfunction, α-synuclein accumulation and neurotoxicity. The Journal of neuroscience : the official journal of the Society for Neuroscience *32*, 4240-4246.

Villar-Pique, A., Lopes da Fonseca, T., and Outeiro, T.F. (2016). Structure, function and toxicity of alpha-synuclein: the Bermuda triangle in synucleinopathies. J Neurochem *139 Suppl 1*, 240-255.

Vogiatzi, T., Xilouri, M., Vekrellis, K., and Stefanis, L. (2008). Wild Type α-Synuclein Is Degraded by Chaperone-mediated Autophagy and Macroautophagy in Neuronal Cells. Journal of Biological Chemistry *283*, 23542-23556.

Wang, G.F., Li, C., and Pielak, G.J. (2010). 19F NMR studies of alpha-synuclein-membrane interactions. Protein Sci *19*, 1686-1691.

Wang, J., Yao, X., and Huang, J. (2017). New tricks for human farnesyltransferase inhibitor: cancer and beyond. Medchemcomm *8*, 841-854.

Wang, W., Wang, X., Fujioka, H., Hoppel, C., Whone, A.L., Caldwell, M.A., Cullen, P.J., Liu, J., and Zhu, X. (2016a). Parkinson's disease-associated mutant VPS35 causes mitochondrial dysfunction by recycling DLP1 complexes. Nature medicine *22*, 54-63.

Wang, Y., Li, L., Hou, C., Lai, Y., Long, J., Liu, J., Zhong, Q., and Diao, J. (2016b). SNARE-mediated membrane fusion in autophagy. Seminars in Cell & Developmental Biology *60*, 97-104.

Webb, J.L., Ravikumar, B., Atkins, J., Skepper, J.N., and Rubinsztein, D.C. (2003). α-Synuclein Is Degraded by Both Autophagy and the Proteasome. Journal of Biological Chemistry *278*, 25009-25013.

Wen, W., Yu, J., Pan, L., Wei, Z., Weng, J., Wang, W., Ong, Y.S., Tran, T.H., Hong, W., and Zhang, M. (2010). Lipid-Induced conformational switch controls fusion activity of longin domain SNARE Ykt6. Molecular cell *37*, 383-395.

Westbroek, W., Gustafson, A.M., and Sidransky, E. (2011). Exploring the link between glucocerebrosidase mutations and parkinsonism. Trends in Molecular Medicine *17*, 485-493.

Willemsen, R., van Dongen, J.M., Aerts, J.M., Schram, A.W., Tager, J.M., Goudsmit, R., and Reuser, A.J. (1988). An immunoelectron microscopic study of glucocerebrosidase in type 1 Gaucher's disease spleen. Ultrastructural pathology *12*, 471-478.

Winslow, A.R., Chen, C.-W., Corrochano, S., Acevedo-Arozena, A., Gordon, D.E., Peden, A.A., Lichtenberg, M., Menzies, F.M., Ravikumar, B., Imarisio, S*., et al.* (2010). α-Synuclein impairs macroautophagy: implications for Parkinson's disease. The Journal of cell biology *190*, 1023-1037.

Wong, K., Sidransky, E., Verma, A., Mixon, T., Sandberg, G.D., Wakefield, L.K., Morrison, A., Lwin, A., Colegial, C., Allman, J.M.*, et al.* (2004). Neuropathology provides clues to the pathophysiology of Gaucher disease. Molecular genetics and metabolism *82*, 192-207.

Wu, H., Chen, S., Ammar, A.-B., Xu, J., Wu, Q., Pan, K., Zhang, J., and Hong, Y. (2015). Crosstalk Between Macroautophagy and Chaperone-Mediated Autophagy: Implications for the Treatment of Neurological Diseases. Molecular neurobiology *52*, 1284-1296.

Xilouri, M., Brekk, O.R., and Stefanis, L. (2016). Autophagy and Alpha-Synuclein: Relevance to Parkinson's Disease and Related Synucleopathies. Movement Disorders *31*, 178-192.

Xilouri, M., Vogiatzi, T., Vekrellis, K., Park, D., and Stefanis, L. (2009). Abberant alpha-synuclein confers toxicity to neurons in part through inhibition of chaperone-mediated autophagy. PLoS One *4*, e5515.

Yap, T.L., Velayati, A., Sidransky, E., and Lee, J.C. (2013). Membrane-bound alpha-synuclein interacts with glucocerebrosidase and inhibits enzyme activity. Mol Genet Metab *108*, 56-64.

Young, J.E., Martinez, R.A., and La Spada, A.R. (2009). Nutrient Deprivation Induces Neuronal Autophagy and Implicates Reduced Insulin Signaling in Neuroprotective Autophagy Activation. Journal of Biological Chemistry *284*, 2363-2373.

Zhang, H., Duan, C., and Yang, H. (2015). Defective Autophagy in Parkinson's Disease: Lessons from Genetics. Molecular Neurobiology *51*, 89-104.

Zhang, T., and Hong, W. (2001). Ykt6 forms a SNARE complex with syntaxin 5, GS28, and Bet1 and participates in a late stage in endoplasmic reticulum-Golgi transport. J Biol Chem *276*, 27480-27487.

Zhou, Y.-F., Wang, Q.-X., Zhou, H.-Y., and Chen, G. (2016). Autophagy activation prevents sevoflurane-induced neurotoxicity in H4 human neuroglioma cells. Acta pharmacologica Sinica *37*, 580-588.